The ring laser gyro

W. W. Chow, J. Gea-Banacloche, and L. M. Pedrotti

Institute for Modern Optics, University of New Mexico, Albuquerque, New Mexico 87131

V. E. Sanders

Rockwell International Autonetics Marine Systems Division, P.O. Box 49211, Anaheim, California 92803

W. Schleich

Max-Planck-Institut für Quantenoptik, D-8046 Garching bei München, West Germany

M. O. Scully

Institute for Modern Optics, University of New Mexico, Albuquerque, New Mexico 87131
and Max-Planck-Institut für Quantenoptik, D-8046 Garching bei München, West Germany

This paper presents a review of both active and passive ring laser devices. The operating principles of the ring laser are developed and discussed, with special emphasis given to the problems associated with the achievement of greater sensitivity and stability. First-principle treatments of the nature of quantum noise in the ring laser gyro and various methods designed to avoid low-rotation-rate lock-in are presented. Descriptions of state-of-the-art devices and current and proposed applications (including a proposed test of metric theories of gravity using a passive cavity ring laser) are given.

CONTENTS

INTRODUCTION

The development of the laser in the early 1960s moved optical physics into a new regime of precision and commercial applicability. One of the more interesting devices that the laser has made possible is the ring laser gyroscope. (See Gyorffi and Lamb, 1965; Menegozzi and Lamb, 1973; and Aronowitz, 1965, for the general theory of a ring laser.) This consists basically of a ring cavity around which two laser light beams travel in opposite directions. An examination of the interference pattern formed by extracting and heterodyning portions of the two counterpropagating beams provides information about the rotation rate of the ring cavity relative to an inertial frame.

The idea of using a ring interferometer as a rotation rate sensor was introduced by Sagnac (1913a) but, until the development of the laser, the Sagnac interferometer was not even considered as an alternative to conventional

mechanical gyroscopes. With current laser technology, however, this is no longer the case. Ring laser gyros are presently used for navigation of some commercial aircraft and are being considered for use in a variety of military applications. The inherent advantage of the ring laser gyro as a rotation sensing device is that it has no moving parts and so would seem, potentially, to have a longer repair lifetime than a mechanical gryoscope.

The initial optimism surrounding the ring laser gyro's development eventually proved to be justified; however, during the last twenty years many obstacles, most notably the so-called lock-in effect, have been encountered and for the most part overcome. It is just these obstacles that make the ring laser gyro a doubly interesting device. Not surprisingly, the struggle to produce a commercially competitive optical gyro has uncovered new physics which has its own inherent interest. The development of the ring laser gyro evinces particularly well the way in which physics characteristically benefits from the interplay of the applied and "pure" spheres.

In this paper we first explain the basic operating principle of the ring laser gyro (Sec. I) and then proceed to the schemes devised to maximize the stability and sensitivity of these devices. It is with this last task that we are primarily concerned, and we discuss at length the two basic types of optical rotation sensors—passive ring resonators and active ring laser gyros. In Sec. II passive ring resonator gyros, in which the lasing medium is outside the ring cavity, are discussed. Section III is an overview of the more important active ring laser gyro, so called because in this variation the active laser medium is within the resonator and forms part of the optical path. Section IV deals with variants of the active devices which use multiple modes of the resonator to overcome the lock-in effect. In Sec. V the important topic of noise in optical rotation rate sensors is considered, with special emphasis given to the origin and nature of quantum noise in active ring laser gyros. Finally, in Sec. VI we conclude this paper with a short overview of the applications of optical rotation sensors in which we discuss conventional gyro applications (such as navigation) and a more esoteric scheme proposing the use of a ring laser gyroscope to distinguish between various metric theories of gravitation.

I. SAGNAC EFFECT

A. Elementary derivation of the Sagnac effect

The basis for understanding the operation of ring laser gyros is the so-called Sagnac effect, first discussed by Sagnac in 1913 when he demonstrated the feasibility of the use of an interferometer to sense rotation. In this section a simple classical derivation (Aronowitz, 1971) of the Sagnac effect is presented.

An understanding of the Sagnac effect can be gained by considering a circular ring interferometer like the one shown in Fig. 1. Laser light enters the interferometer at point A and is split into clockwise (CW) and counterclockwise (CCW) propagating beams by a beam splitter. If the interferometer is not rotating, the CW and CCW propagating beams recombine at point A after a time given by

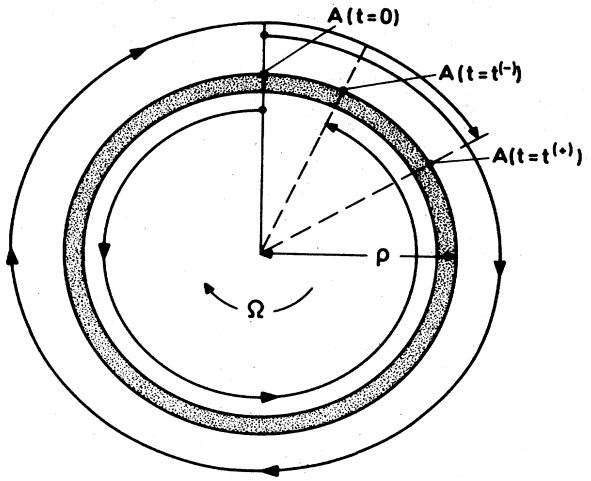

FIG. 1. Passive ring interferometer.

$$t=\frac{2\pi\rho}{c}\ , \tag{1.1}$$

where ρ is the radius of the circular beam path. However, if the interferometer is rotating, with angular velocity Ω, about an axis through the center and perpendicular to the plane of the interferometer, then the beams reencounter the beam splitter at different times because the CW (codirectional with Ω) propagating beam must traverse a path length of slightly more than $2\pi\rho$ in order to complete one round trip, since the interferometer rotates through a small angle during the round-trip transit time. Similarly, the CCW propagating beam traverses a path length slightly less than $2\pi\rho$ during one round trip. If we denote the round-trip transit time of the CW beam by t^+ and that of the CCW beam by t^-, then t^+ is given by

$$t^+=\frac{2\pi\rho+\rho\Omega t^+}{c}\ , \tag{1.2}$$

where $\rho\Omega t^+$ is the arc length the interferometer rotates through before the CW beam arrives back at the beam splitter, and c is the speed of light. Similarly,

$$t^-=\frac{2\pi\rho-\rho\Omega t^-}{c}\ . \tag{1.3}$$

Solving Eqs. (1.2) and (1.3) for t^+ and t^- and then taking the difference gives

$$\Delta t=t^+-t^-=\frac{4\pi\rho^2\Omega}{c^2-\rho^2\Omega^2}\ . \tag{1.4}$$

For reasonable values of ρ and Ω, $(\rho\Omega)^2\ll c^2$, so that

$$\Delta t\cong\frac{4\pi\rho^2\Omega}{c^2}\ ; \tag{1.5}$$

the round-trip optical path difference, ΔL, is given by

$$\Delta L = c\Delta t = \frac{4\pi\rho^2\Omega}{c} . \tag{1.6}$$

From Eq. (1.6) we see that the round-trip optical path difference, according to this analysis, is directly proportional to the rotation rate of the interferometer. A more general approach valid for an arbitrary interferometer shape (see Post, 1967; Schleich and Scully, 1984; and Jacobs and Zamoni, 1982) leads to the result

$$\Delta L = \frac{4\boldsymbol{\Omega}\cdot\hat{Z}A}{c} , \tag{1.7}$$

where A is the area enclosed by the light path and $\hat{Z}$ is a unit vector normal to the surface of the interferometer.

The effectiveness of the Sagnac interferometer is limited by the fact that the optical path difference given by Eq. (1.6) is much less than a wavelength. (For instance, if $\rho=1$ m and $\Omega=10$ deg/h, then $\Delta L \cong 4.1\times10^{-12}$ m.) At first glance this would seem to make the use of ring laser gyros impractical as rotation sensing devices, since sensitivities of 10^{-3} deg/h or less are desirable. However, there are two different schemes used to greatly increase the sensitivity of ring laser gyros.

The first of these is to increase the total round-trip path length of the light by the use of a kilometer-long optical fiber as the interferometer cavity. To see why this increases the sensitivity of the gyroscope, we shall recast Eq. (1.6) into a more general form. From Eq. (1.6) we see that the phase difference, φ, between the counterpropagating beams after one round trip is given by

$$\varphi = \frac{2\pi\Delta L}{\lambda} = \frac{8\pi^2\rho^2\Omega}{c\lambda} = \frac{4A\Omega}{c\lambda} , \tag{1.8}$$

where λ is the reduced wavelength of the laser light and $A=\pi\rho^2$ the area enclosed by the light beams. Equation (1.8) is valid for a one loop circular light path. If an optical fiber is used, the light path typically consists of a fiber coil of radius ρ and many turns. In particular, in such a fiber coil with n turns Eq. (1.8) becomes

$$\varphi = \frac{8\pi^2\rho^2 n\Omega}{c\lambda} . \tag{1.9}$$

Or, in terms of the total length, L, of the optical fiber,

$$\varphi = \frac{4\pi L\rho\Omega}{c\lambda} . \tag{1.10}$$

Equation (1.10) represents the important result that the phase shift induced by rotation of a Sagnac fiber ring interferometer increases linearly with the total length of the optical fiber. A detailed analysis of rotation sensors which utilize this fact is presented in Sec. II of this paper.

The second scheme devised to increase the sensitivity of ring laser gyroscopes is the introduction of an active laser medium into the ring cavity. This arrangement is illustrated by Fig. 2. For convenience, throughout the rest of this paper, such an arrangement will be called an active ring laser gyro. Then the CW and CCW ring laser modes have different frequencies because of the difference in effective round-trip optical path lengths caused by the rotation of the cavity. In particular, only oscillations with wavelengths satisfying the resonance condition

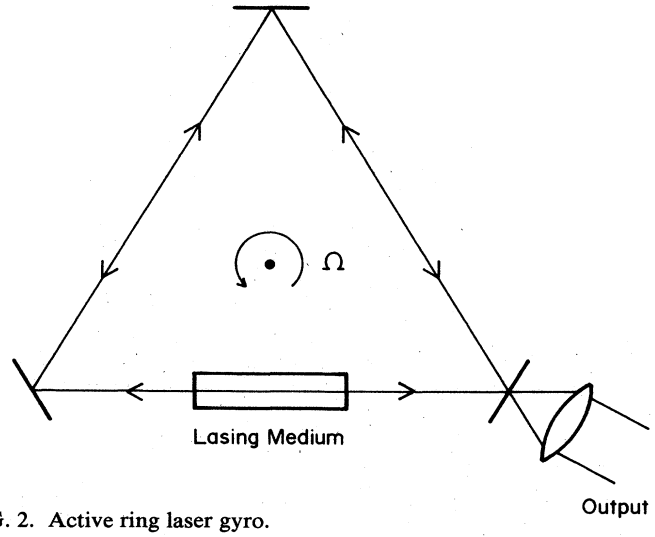

FIG. 2. Active ring laser gyro.

$$m\lambda_\pm = L_\pm \tag{1.11}$$

can be sustained in the cavity. Here, m is an integer, $\lambda_\pm$ and $L_\pm$ correspond to the wavelengths of and effective cavity lengths seen by the CW and CCW propagating beams, respectively. Equation (1.11) can be rewritten in terms of the resonant frequencies as

$$\omega_\pm = \frac{mc}{L_\pm} . \tag{1.12}$$

Using Eq. (1.12) the frequency difference between the CW and CCW propagating beams can be approximated by

$$\Delta\omega = \omega_- - \omega_+ = \frac{mc}{L_-} - \frac{mc}{L_+} \cong \frac{mc\Delta L}{L^2} = \omega\frac{\Delta L}{L} . \tag{1.13}$$

The approximation arises out of setting $L_+L_- \cong L^2$.

Now, a couple of important points need to be made. The first of these is that when using an active ring laser gyro it is the frequency difference (not the optical path difference) between the counterpropagating beams which is measured. This frequency difference is generally measured by heterodyning the two output beams (see Aronowitz, 1971 or Sec. III of this paper). Also note that the frequency difference given by Eq. (1.13) is a factor of ω/L larger than the optical path length difference given by Eq. (1.6). This increased scale factor together with the relative experimental ease associated with small frequency difference measurements makes the active ring laser gyro the most common and, currently, the most sensitive interferometer rotation sensor.

Inserting Eq. (1.6) into Eq. (1.13) gives (for a circular ring),

$$\Delta\omega = \frac{2\omega\rho\Omega}{c} = \frac{2\rho\Omega}{\lambda} . \tag{1.14}$$

For small Ω Eq. (1.14) becomes inaccurate due to problems such as lock-in, scale factor variation, etc., to be discussed throughout the remainder of this paper. Note that

$\Delta\omega$ does not depend on the total length of the cavity so an increased scale factor is not achieved by using long fiber optic coils in active ring laser gyros. For an arbitrary cavity geometry we see from Eq. (1.28) (see also Post, 1967; Schleich and Scully, 1984; Jacobs and Zamoni, 1982) that Eq. (1.14) becomes

$$\Delta\omega=\frac{4A\Omega}{P\lambda}\ , \tag{1.15}$$

where A is the area enclosed by the light path and P is the perimeter of the light path. The constant of proportionality, $4A/\lambda P$ between $\Delta\omega$ and Ω is often called the scale factor which we will later represent by the symbol S.

In passing let us note that Eqs. (1.14) and (1.15) ignore the effects of a refractive medium in the light path. These effects are treated extensively in a review article by Post (1967).

B. The Sagnac effect in general relativity

1. Wave equation for electric field in ring laser

In this section we are going to consider the Sagnac effect in the framework of general relativity. This may be achieved by deriving a wave equation for the electric field in the ring laser in the presence of a gravitational field and solving it. However, due to the presence of a gravitational field we cannot use Maxwell's equations from special relativity. The starting point must be Maxwell's equations in curved spacetime (see Misner *et al.*, 1973). However, these equations are difficult to handle, because they contain covariant derivatives and Christoffel symbols, etc. But there is a way around this complication. Plebanski (1960) showed that it is possible to write Maxwell's equations in an arbitrary gravitational field in a form in which they resemble electrodynamic equations in a dielectric medium. Therefore, the gravitational field is in some sense equivalent to a dielectric medium. From these equations we can then use the standard techniques to derive the wave equation.

The gravitational field, represented by the metric $g_{\mu\nu}=g_{\nu\mu}$, is assumed to be of the form

$$g_{\mu\nu}=\eta_{\mu\nu}+h_{\mu\nu}$$
$$=\begin{bmatrix}1&&&0\\&-1&&\\&&-1&\\0&&&-1\end{bmatrix}+\begin{bmatrix}0&h_{01}&h_{02}&h_{03}\\h_{10}&0&0&0\\h_{20}&0&0&0\\h_{30}&0&0&0\end{bmatrix}\ , \tag{1.16}$$

where $\eta_{\mu\nu}$ is the metric of special relativity and $h_{\mu\nu}$ is a small correction to it. In all that follows we only keep terms linear in $h_{\mu\nu}$.

Maxwell's equations (charge and current free) in Plebanski's notation have the following form (Schleich and Scully, 1984) assuming the metric Eq. (1.16):

$$\nabla\cdot\mathbf{D}=0\ ,\quad \nabla\times\mathbf{E}=-\frac{\partial\mathbf{B}}{\partial t}\ , \tag{1.17}$$

$$\nabla\cdot\mathbf{B}=0\ ,\quad \nabla\times\mathbf{H}=\frac{1}{c^2}\frac{\partial\mathbf{D}}{\partial t}\ , \tag{1.18}$$

together with the material equations

$$\mathbf{D}=\mathbf{E}-c(\mathbf{B}\times\mathbf{h})\ , \tag{1.19}$$

$$\mathbf{B}=\mathbf{H}+\frac{1}{c}(\mathbf{E}\times\mathbf{h})\ , \tag{1.20}$$

where we used the notation

$$\mathbf{h}\equiv(h_{01},h_{02},h_{02})\ .$$

Now we are able to derive a wave equation. The strategy is straightforward and proceeds as follows. Taking as in ordinary electrodynamics $\nabla\times(\nabla\times\mathbf{E})$ and using the material equations (1.19) and (1.20) to eliminate the $\mathbf{D}$ and the $\mathbf{H}$ fields from Maxwell's equations (1.17) and (1.18) we arrive at the following wave equation for the electric field $\mathbf{E}$:

$$\frac{1}{c^2}\frac{\partial^2\mathbf{E}}{\partial t^2}-\Delta\mathbf{E}=-\frac{2}{c}(\mathbf{h}\cdot\nabla)\frac{\partial\mathbf{E}}{\partial t}\ . \tag{1.21}$$

For details of the derivation we refer the reader to the Appendix. In deriving Eq. (1.21) we have neglected all derivatives of $\mathbf{h}$.

2. Derivation of the frequency shift in terms of the metric

In this section we are going to derive the Sagnac effect in a metric field $g_{\mu\nu}$ of the form of Eq. (1.16) for the use of an active and a passive device. To do this we try to solve Eq. (1.21) using the ansatz

$$\mathbf{E}=\mathbf{E}_0e^{iS}$$
$$\equiv\mathbf{E}_0\exp\left[i\left[(\omega+\Delta\omega)t+\int_l d\mathbf{r}'\cdot\mathbf{k}(\mathbf{r}')+\varphi(\mathbf{r})\right]\right]\ .$$

We assume a planar surface of the gyroscope but allow an arbitrary shape. The path of the light may be defined by l. For the sake of simplicity we assume the electric field $\mathbf{E}_0$ to be polarized perpendicular to the direction of the light path and to the area of the gyroscope. This may be achieved by using Brewster windows. Then the electric field vector $\mathbf{E}_0$ is constant along the path of the light. The wave vector $\mathbf{k}$ we assume to be constant in its absolute value but changing its direction due to the shape of the interferometer, therefore

$$\mathbf{k}(\mathbf{r})=\frac{\omega}{c}\mathbf{e}(\mathbf{r})\ , \tag{1.22}$$

where $\mathbf{e}(\mathbf{r})$ denotes a unit vector in the direction of propagation at point $\mathbf{r}$. The effect of the gravitational field $\mathbf{h}$ is fed in by the frequency shift $\Delta\omega$ and the phase shift $\varphi(\mathbf{r})$. Both corrections contain the gravitational field $\mathbf{h}$ at least linearly. To get the passive resonator case results we have to set $\Delta\omega=0$, because the frequencies of the two counterpropagating waves are equal and fixed to be that of the

external light source. To describe the active case we have to fulfill periodic boundary conditions for the phase.

Substituting the ansatz into Eq. (1.21), noting that $\mathbf{E}_0$ is constant we find by standard vector algebra

$$\frac{1}{c^2}(\omega+\Delta\omega)^2-(\mathbf{k}+\nabla\varphi)^2=-2\frac{\omega}{c}\mathbf{h}\cdot\mathbf{k} . \tag{1.23}$$

Note that in deriving the right-hand side we already neglected terms $O(h^2)$. We can simplify this by noting

$$\frac{1}{c^2}(\omega+\Delta\omega)^2-(\mathbf{k}+\nabla\varphi)^2\cong\left[\frac{\omega}{c}\right]^2+2\left[\frac{\omega}{c}\right]\frac{\Delta\omega}{c}-\mathbf{k}^2-2\mathbf{k}\cdot\nabla\varphi$$

$$=2\frac{\omega}{c^2}(\Delta\omega-c\mathbf{e}\cdot\nabla\varphi) ,$$

where we used $\Delta\omega\sim O(h)$ and $\nabla\varphi\sim O(h)$. Equation (1.23) reduces then to

$$\Delta\omega-c\mathbf{e}\cdot\nabla\varphi=-\frac{c}{\lambda\!\!\!^{-}}(\mathbf{h}\cdot\mathbf{e}) ,$$

where we again made use of Eq. (1.22) and defined the reduced wavelength $\lambda\!\!\!^{-}=\lambda/2\pi=c/\omega$. A solution to the above equation is

$$\varphi(\mathbf{r})=\frac{\Delta\omega}{c}\int_{\mathbf{r}_0}^{\mathbf{r}}d\mathbf{r}'\cdot\mathbf{e}(\mathbf{r}')+\frac{1}{\lambda\!\!\!^{-}}\int_{\mathbf{r}_0}^{\mathbf{r}}d\mathbf{r}'\cdot\mathbf{h}(\mathbf{r}') ,$$

where $\mathbf{r}$ denotes a point on the path of the light. The phase shift after one round trip is then simply

$$\varphi=\frac{\Delta\omega}{c}\oint d\mathbf{r}\cdot\mathbf{e}(\mathbf{r})+\frac{1}{\lambda\!\!\!^{-}}\oint d\mathbf{r}\cdot\mathbf{h}(\mathbf{r})$$

$$=\frac{\Delta\omega P}{c}+\frac{1}{\lambda\!\!\!^{-}}\oint d\mathbf{r}\cdot\mathbf{h}(\mathbf{r}) ,$$

where P is the length of the interferometer neglecting gravitational effects.

We first want to consider a passive device with a light source outside of the cavity. In this case the frequencies of the two counterpropagating waves are fixed to be equal to the external frequency ω_0. This means $\Delta\omega=0$. The Sagnac phase shift between the two waves is then simply

$$\varphi=\frac{2}{\lambda\!\!\!^{-}}\oint d\mathbf{r}\cdot\mathbf{h}(\mathbf{r})=\frac{2}{\lambda\!\!\!^{-}}\int\int d\mathbf{A}\cdot(\nabla\times\mathbf{h}) , \tag{1.24}$$

where we have used Stoke's theorem in the last step. The factor of 2 arises from the fact that we consider two counterpropagating waves.

Now we turn to an active cavity, which means the light source is inside the cavity. In such a case the boundary condition is such that the wave after one round trip must interfere with itself in a constructive way, which means

$$2\pi n=\frac{\Delta\omega P}{c}+\frac{1}{\lambda\!\!\!^{-}}\oint d\mathbf{r}\cdot\mathbf{h}(\mathbf{r})+\oint d\mathbf{r}\cdot\mathbf{k}(\mathbf{r}) .$$

From Eq. (1.22) we immediately find

$$\oint d\mathbf{r}\cdot\mathbf{k}(\mathbf{r})=\oint d\mathbf{r}\cdot\mathbf{e}(\mathbf{r})\frac{\omega}{c}=\frac{P\omega}{c}=2\pi n ,$$

and therefore

$$\Delta\omega=-\frac{c}{\lambda\!\!\!^{-}P}\oint d\mathbf{r}\cdot\mathbf{h}(\mathbf{r}) . \tag{1.25}$$

This is the frequency shift for an electromagnetic wave in an active interferometer in a gravitational potential $\mathbf{h}$. Because there are two counterpropagating waves in a ring laser gyroscope we get for the frequency shift between the two waves twice the result of Eq. (1.25), namely

$$\Delta\omega=-\frac{2c}{\lambda\!\!\!^{-}P}\oint d\mathbf{r}\cdot\mathbf{h}(\mathbf{r}) . \tag{1.26}$$

Stoke's theorem can be applied to obtain $\Delta\omega$ in a different form

$$\Delta\omega=-\frac{2c}{\lambda\!\!\!^{-}P}\int\int_A d\mathbf{A}\cdot(\nabla\times\mathbf{h})$$

$$\cong-\frac{2Ac}{\lambda\!\!\!^{-}P}(\nabla\times\mathbf{h})\cdot\mathbf{e}_a . \tag{1.27}$$

This "generalized" Sagnac effect is the main result of this section. In Eq. (1.27) A is the area of the planar surface bounded by the ray path of the interferometer and $\mathbf{e}_a$ is a unit vector normal to the plane of the device. The surface A is bounded by the ray path and the curl is evaluated at the center of the interferometer. In deriving Eq. (1.27) we have retained only the terms linear in $\mathbf{h}$ and neglected derivatives of $\mathbf{h}$.

3. Classical Sagnac effect

In this section we want to make the connection between the classical Sagnac effect discussed in Sec. I.A and the results derived in the previous sections. To do this we need the metric vector $\mathbf{h}$ for a rotating interferometer. We may read this from the line element

$$ds^2=g_{00}(dx^0)^2+2g_{0i}dx^0dx^i+g_{ij}dx^idx^j ,$$

where we sum over double indices.

In the present problem $g_{0i}=h_{0i}$. The simplest example of a metric with off-diagonal elements between space and time is the metric in a rotating frame. This result written in Cartesian coordinates is as follows. In order to transform to a rotating frame the line element

$$ds^2=c^2dt^2-(dx^2+dy^2+dz^2)$$

is transformed (for rotation about the z axis) according to

$$x^0=\bar{x}^0=ct , \quad x^1=x=\bar{x}^1\cos\Omega t-\bar{x}^2\sin\Omega t ,$$

$$x^3=\bar{x}^3=z , \quad x^2=y=\bar{x}^1\sin\Omega t+\bar{x}^2\cos\Omega t ,$$

where we denote the coordinates in the rotating frame by $\bar{x}^\mu=(ct',x',y',z')$. This yields

$$ds^2=\left[1-\frac{\Omega^2(x'^2+y'^2)}{c^2}\right]c^2dt'^2-(dx'^2+dy'^2+dz'^2)$$

$$+2\Omega\frac{y'}{c}c\,dt'dx'-2\Omega\frac{x'}{c}c\,dt'dy'$$

and we see that h_{0i} is given by

$$h_{01}=\frac{\Omega}{c}y' , \quad h_{02}=-\frac{\Omega}{c}x' , \quad h_{03}=0 .$$

This then implies that

$$(\nabla\times\mathbf{h})\cdot\mathbf{e}_z=-2\left[\frac{\Omega}{c}\right] .$$

This yields for the Sagnac phase and frequency shift

$$\Delta\varphi=\frac{4A\Omega}{\lambda c}$$

and

$$\Delta\omega=\frac{4A\Omega}{\lambda P} , \tag{1.28}$$

the well-known results already derived in Sec. I.A. In Sec. VI we use Eq. (1.27) to show how one can test general relativity using ring laser gyroscopes.

II. PASSIVE RING RESONATOR GYROS

The basic characteristic of a passive ring resonator gyro is that the lasing medium is outside of the ring cavity so that the mode structure of the laser light in the interferometer is determined by a cavity external to the ring resonator. This scheme is attractive because it eliminates the problems associated with having the gain medium inside the interferometer itself. For example, in an active gyro, for small rotation rates, the counterpropagating beams tend to lock together so that even for nonzero rotation rates the frequencies of the two beams are degenerate (Aronowitz, 1965). Another problem associated with having the gain medium in the interferometer itself is the variation of the optical length of the light path due to the variation in the index of refraction of the gain medium. These problems are not observed in passive resonator gyros.

There are two basic schemes which make use of the passive ring interferometer. The two approaches differ in that one relates the rotation rate to a fringe shift (Vali and Shorthill, 1976) and the other determines the rotation rate by making a frequency difference measurement (Ezekiel and Balsamo, 1977). As mentioned in Sec. I, determining the rotation rate of the ring by measuring the relative phase shift between the counterpropagating beams has the difficulty that the proportionality constant which relates the relative phase shift between the two beams and the rotation rate of the ring is much smaller than the one which relates the beat note of the two beams and the ring's rotation rate. This problem can be partially overcome by using long optical fibers as the interferometer. In this section we discuss the merits and problems associated with passive ring resonator gyroscopes.

A. Phase-sensitive fiber ring gyros

The first of these approaches, in its most developed form, uses a long single-mode optical fiber as the ring cavity. The basic experimental setup for this approach is shown in Fig. 3. As indicated in the figure, laser light is coupled into the ends of a long single-mode optical fiber. In this way two counter-rotating beams are established in the fiber. When the fiber interferometer is caused to rotate, the two counterpropagating beams travel different effective round-trip path lengths before they exit the fiber and are recombined on the screen. Hence they arrive at the recombination point with a phase difference and so a fringe shift relative to the pattern obtained when the fiber is not rotating is observed. This phase shift for a fiber ring coil is given by Eq. (1.10) as

$$\varphi=\frac{4\pi L\rho\Omega}{c\lambda} , \tag{2.1}$$

where L is the total length of the fiber and R is the radius of each fiber loop. Equation (2.1) illustrates the important point that the observed phase shift is directly proportional to the length of the fiber so that the sensitivity of the fiber ring interferometer can be greatly increased (i.e., the minimum detectable rotation rate can be greatly reduced) by using long fibers.

The sensitivity of this device is fundamentally limited, however, by the minimum distance change that can be detected using an interferometer. The most common experimental technique used to measure the Sagnac fringe shift is to scan the screen for positions of maximum intensity. (For an excellent discussion of measurement techniques, see Schiffner, 1980.) In this case, the minimum distance change is inversely proportional to the square root of the beam power (Ulrich and Johnson, 1979; Lin and Giallorenzi, 1979). (This fundamental limit, often called the shot-noise limit, will be discussed in more detail in Sec. V.) As longer and longer fibers are used, the power coupled out of the fiber ends decreases due to an increase in the amount of light scattered and absorbed by the fiber in accordance with the rule,

$$P_0=P_i e^{-\alpha L} , \tag{2.2}$$

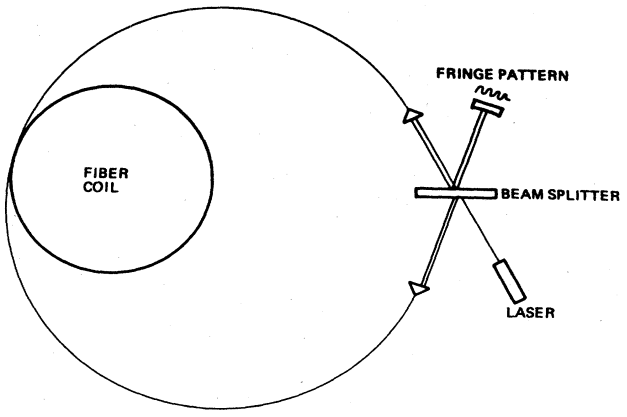

FIG. 3. Fiber ring gyroscope.

where P_i is the power output of the laser, L is the length of the fiber, α is an attenuation coefficient characteristic of the fiber, and P_0 is the power coupled out of the end of the fiber. Typical values of α for existing fibers are a few dB/km. The optimum fiber length for minimizing the detectable rotation rate is determined by balancing the effect that increasing L has on the magnitude of the fringe shift, with the reduced sensitivity of the detector which results from a decreased power out of the fiber. Several analyses (Vali and Shorthill, 1976; Lin and Giallorenzi, 1979) have estimated the optimum fiber length, for existing fibers, to be several kilometers, for which a rotation rate of 10^{-3} deg/h or less could, in theory, be detected. This minimum sensitivity is limited only by the quantum noise of the detector and the attenuation properties of existing fibers. In practice it is very difficult to approach this limit. The variance in the theoretical and experimental sensitivities is due to a number of factors whose nature and experimental resolution will now be discussed.

1. Noise sources in the fiber ring gyro

The noise sources to be discussed in this section are those associated with thermal effects, the need to maintain a single-polarization state in the fiber, beam to fiber coupling, back-scattering, and the optical Kerr effect. In addition there are other noise sources associated with the detection of the phase difference such as $1/f$ noise, dark current noise, amplifier noise, the effect of magnetic fields, and variation of the index of refraction of the fiber, which will not be treated here. These last sources are treated in some detail by Lin and Giallorenzi (1979), Schiffner (1980), and Leeb *et al.* (1979).

a. Thermal noise

The problem of thermally induced nonreciprocities in the round-trip path lengths of the CW and CCW propagating beams is discussed in an article by Shupe (1980). The following discussion is based largely on his paper. The condition which causes thermally induced nonreciprocities is the existence of a time-dependent temperature gradient along the length of the fiber. Now, in the fiber ring interferometer, corresponding wave fronts of the two counter-rotating beams encounter the same region of the fiber at different times and the propagation constant of the fiber, β (which is related to the velocity, v, of light through the fiber by the expression $\beta=\omega/v$, where ω is the frequency of the laser light) is temperature dependent. In this way the CW and CCW propagating beams traverse slightly different effective path lengths and so a spurious phase shift is produced.

The magnitude of this thermally induced nonreciprocal phase delay can be obtained in the following way. Consider the incremental phase delay, $d\varphi$, to both counter-propagating beams produced by each element dl of the fiber's length. The temperature, T, is taken to vary both with time and the position along the fiber. Under these conditions Shupe points out that "The variation of the incremental phase over a period $d\varphi$ at any point along the fiber can be approximated by"

$$d\varphi=\left[\frac{d\beta}{dT}+\beta\alpha\right]\tau\frac{\delta T}{\delta t}dl\ , \tag{2.3}$$

where t is the time, and α is the coefficient of linear expansion of the fiber. This equation is valid over time periods on the order of the time it takes light to make one trip around the fiber coil. Note that the first term in Eq. (2.3) accounts for the variation of the index of refraction with temperature and the second indicates that the scale factor (i.e., length) changes with changing T.

The total thermally induced phase shift induced in a time δt can be calculated by taking the time τ in Eq. (2.3) to be the difference in the time it takes for two wave fronts which enter opposite ends of the fiber at the same time to reach a given point in the fiber which is located at a distance l from one end of the fiber, and then integrating Eq. (2.3) over the length of the fiber,

$$\tau=\frac{\beta}{\omega}(2l-L) \tag{2.4}$$

and performing the integrations gives,

$$\varphi=\left[\frac{d\beta}{dT}+\beta\alpha\right]\frac{\beta}{\omega}\int_0^L(2l-L)[T(t,l)-T(0,l)]dl\,\delta t\ , \tag{2.5}$$

where we have assumed that β and $d\beta/dT$ are time independent and the order of integration over l and t can be interchanged. These are first-order approximations. Furthermore, in order to get a numerical estimate of the apparent rotation due to the thermally induced phase shift, Shupe makes the following assumptions:

$$\beta\simeq kn_c\ , \tag{2.6a}$$

$$\frac{d\beta}{dT}=\frac{kdn_c}{dT}\ , \tag{2.6b}$$

$$T(t,l)-T(0,l)=l\Delta T/L\ , \tag{2.6c}$$

where k is the free-space wave number of the laser light, n_c is the refractive index of the fiber core (the approximation being that $n_c\simeq n$, where n is the refractive index of the fiber cladding), and ΔT is the temperature change across the coil in a time t. Substituting Eqs. (2.6) into (2.5) and equating the resulting phase shift to the right-hand side of Eq. (2.1) in order to get an expression for the thermally induced apparent rotation rate yields

$$\Omega_T=\frac{n_cL^2\Delta T}{24NA}\left[\frac{dn_c}{dT}+n_c\alpha\right]\delta t\ . \tag{2.7}$$

Shupe calculates the temperature change ΔT necessary to produce a shot-noise limited rotation rate in an integration time of 1 h (i.e., $\delta t=1$ h). He uses the shot-noise limited rotation rate calculated by Lin and Giallorenzi (1979) of 0.0078 deg/h for a fiber ring gyro having a fiber coil of radius 10 cm and length 1.56 km, and takes

$$\frac{dn_c}{dT}=10^{-5}/^{\circ}\mathrm{C}\ ,\quad \alpha=5\times10^{-7}/^{\circ}\mathrm{C}\ ,\quad n_c=1.45\ .$$

With these values, Eq. (2.7) yields the result that ΔT need only be $6.7\times10^{-3}/^{\circ}$C before thermally induced nonreciprocities become the limiting factor in the sensitivity of such a fiber ring gyro. In common navigational applications such temperature invariance would be impractical to maintain. Shupe offers two remedies to this problem. The first is to produce fibers with smaller indices of refraction (and smaller values of dn_c/dT). The second suggestion is to wind the fiber coil in such a way that portions of the fiber that are at equal distances from the center of the fiber are beside each other so that they undergo the same temperature fluctuations and the nonreciprocity is eliminated.

b. Polarization and birefringence

All passive, fiber ring gyros make use of so-called single-mode fibers. In practice all real "single-mode" fibers permit the transmission of modes of two orthogonal polarizations through the fiber (in each direction). Disturbances, such as temperature fluctuations and mechanical stresses, cause power to be transferred from one polarization mode to the other. (Normally one of the two modes carries almost all of the power.) Light in one polarization mode has a velocity different from the light which is being propagated in the other polarization mode so that if light from both mode "channels" exists in the output, the interference pattern will consist of two superposed interference patterns with the resulting pattern having less contrast and being shifted with respect to the pattern which would be produced if only the dominant mode were present in the output. Ulrich and Johnson (1979) report just such a blurred and slowly moving fringe pattern which they correlate to the effect described above. They report that a scheme utilizing polarizers and analyzers to suppress the weak polarization mode resulted in a fringe pattern in which the positions of the fringes were perfectly stable, regardless of temperature fluctuations and mechanical disturbances in the fiber which tend to transfer energy from one polarization mode channel to the other. However, as one would expect, the intensity of the fringes varied strongly during these disturbances. For this reason they suggest that detection schemes which respond to the position of the fringes only should be considered.

The noise produced by the transfer of energy between the two modes makes the need for fibers which inhibit this energy transfer clear. One method devised to make single polarization holding fibers is the introduction of high birefringence into the fiber coil (far exceeding the birefringence induced by small temperature fluctuations and mechanical disturbances which are responsible for the undesirable energy transfer). To understand why this high birefringence inhibits the energy transfer consider the birefringence length L (Ramaswary *et al.*, 1978) with

$$L=\frac{2\pi}{\Delta\beta}\ , \tag{2.8}$$

where $\Delta\beta$ is the difference between the propagation constants of the two modes with orthogonal polarizations which the fiber will transmit. The birefringence length is the beat length in which energy is transferred from one mode to the other and then back again. If the manufactured beat length is made smaller than the beat length of any mechanical disturbance which the fiber might undergo, then no energy can be transferred from one polarization mode to the other. The beat lengths of mechanical disturbances are rarely smaller than 10 cm and so coils with inherent beat lengths of 5 cm or less (Rashleigh and Ulrich, 1980) are desirable and obtainable. (Note that for a beat length of 5 cm, $\Delta\beta$ must be approximately 1.26/cm.) Fibers with a high birefringence can be produced by drawing the fibers so that they have an elliptical core or by introducing a highly anisotropic internal stress. In addition winding a typical single-mode fiber under pressure can also produce the necessary high birefringence (Rashleigh and Ulrich, 1980).

c. Beam-to-fiber coupling noise

Another noise source in fiber ring gyros which can be a larger source of error than shot noise results from light which is backscattered when the laser beam is coupled into and out of the fiber. The reflection coefficient at the end face can be approximated by the expression (Ulrich and Rashleigh, 1980)

$$r=\frac{n-1}{n+1}\ , \tag{2.9}$$

where n is the index of refraction on the axis of the fiber. The reflected light can modify the output from the fiber if it interferes with the primary beam. The treatment of the beam-to-fiber coupling noise given here is essentially the same as that of Ulrich and Rashleigh (1980). In a Michelson-type interferometer the reflection-induced phase error can be as large as $|r|$ radians and, for a Mach-Zehnder-type interferometer in which the interference occurs after m coupling reflections as large as $|r|^m$.

Ulrich and Rashleigh state that a reasonable condition for beam-to-fiber coupling to be considered efficient, is that the reflected power which interferes with the primary beam be no larger than the power backscattered by the fiber itself through Rayleigh scattering. For a 1-m-long single-mode fiber an approximate value for the backscattered power is -60 dB so that the power reflected at the input or output beam/fiber interface ($|r_i|^2$, $|r_0|^2$, respectively) should be less than 10^{-6} times the beam power. Using the conditions stated earlier this would result in a phase shift error of 10^{-3} rad or less.

Ulrich and Rashleigh (1980) propose three viable solutions to the problem of beam-to-fiber coupling noise. These are the use of antireflective coatings on the fiber end faces, the use of an immersion cell to reduce the index of refraction step at the beam/fiber interface, and the pro-

duction of fibers with tilted end faces so that little of the reflected light interferes with the primary beam.

The use of antireflective coatings alone does not seem sufficient as these reduce $|r_i|^2$ and $|r_0|^2$ to only about 10^{-3}. However, in conjunction with other remedies, antireflective coatings may reduce the lower limit of beam-to-fiber coupling noise.

The effectiveness of immersion cells is limited by the fact that the indices of refraction vary with temperature. A liquid whose index of refraction, n_l, matches that of the fiber at a given temperature so that

$$r \simeq \frac{n - n_l}{n + n_l} \tag{2.10}$$

is negligible will not provide index matching when the temperature is varied. For a temperature variation of 10°C, $n - n_l$ can be as large as 10^{-2} leading to a power reflection coefficient of as much as 10^{-5}. Careful choice of the immersion liquid and rigid temperature control would of course reduce this coefficient. However, the immersion cell remedy to beam-to-fiber coupling noise is somewhat clumsy in a practical laser gyro and in addition the windows of the immersion cell itself introduce additional reflections.

Currently the favored solution is the use of tilted end faces. In this way, most of the reflected light does not interfere with the primary beam. Ideally one would like to make the angular separation between the geometrical direction of the reflected light and the direction of the primary beam as large as possible. However, one must compromise since as the normal to the end face is made to be at a larger and larger angle to the beam direction, the coupling efficiency is reduced due to the introduction of astigmatic aberrations (which may also lead to nonreciprocal effects). Ulrich and Rashleigh calculate that an angle of 10° between the normal to the end face and the primary beam input direction is necessary to reduce $|r_0|^2$ and $|r_i|^2$ to below 10^{-6}. They caution against using angles much larger than this for the reasons given above. (However the optimum tilt angle, of course, depends largely on the specific experimental setup.)

d. Backscattering

A major source of error to be discussed in this section results from backscattering due to splices in the fiber and Rayleigh backscattering from the fiber itself. In this section we discuss the way in which backscattering contributes to a nonreciprocal phase shift (forward scattering is also thought to contribute but will not be discussed here) in passive devices.

Following Cutler *et al.* (1980) one can make the following estimate of the magnitude of the noise induced by backscattering (Bohm *et al.*, 1981). For simplicity, consider only Rayleigh backscattering. Let α_s be the Rayleigh scattering attenuation coefficient of the fiber so that, taking Rayleigh scattering to be the only loss factor, the power of the primary beam when it exits the fiber after one complete circulation, P_0, is given by

$$P_0 = P_i e^{-\alpha_s L}, \tag{2.11}$$

where P_i is the beam power coupled into the fiber and L is the length of the fiber. In addition, some of the backscattered energy also exits the fiber and mixes with the primary beam. Let $Gz^2/4$ (Bohm *et al.*, 1981) be the fraction of the total scattered power that is transmitted by the fiber core and so mixes with the primary beam in the output. Here G is the scattering directivity along the fiber ($1 \leq G \leq 1.5$) and z is the acceptance angle of the fiber core. The ratio of the power in the backscattered wave to that in the primary wave, after one circulation, is then

$$\frac{P_s}{P_0} = \frac{P_i(1 - e^{-\alpha_s L})Gz^2/4}{P_i e^{-\alpha_s L}}. \tag{2.12}$$

Assuming $\alpha_s L$ to be small so that only terms up to first order in $\alpha_s L$ need be retained yields the approximate result

$$\frac{P_s}{P_0} = \tfrac{1}{4} G z^2 \alpha_s L. \tag{2.13}$$

The magnitude of the phase shift produced by the two counter-rotating waves due to the presence of the secondary backscattering waves is, at most,

$$\varphi_{\max} = 2\left[\frac{P_s}{P_0}\right]^{1/2} = z(G\alpha_s L)^{1/2}. \tag{2.14}$$

This gives rise to an apparent rotation rate of (for circular loops)

$$\Omega_{\max} = \frac{\lambda c z}{4\pi R}\left[\frac{G\alpha_s}{L}\right]^{1/2}, \tag{2.15}$$

where R is the radius of the fiber coil. In order to obtain an order of magnitude estimate of $\Omega_{\max}$ we choose $\lambda = 633$ nm, $L = 1000$ m, $R = 1$ m, $Z = 0.1$ rad, $G = 1.0$, and $\alpha_s = 10^{-4}$/m. Using these values in Eq. (2.15) yields an approximate upper limit to the backscattered-induced rotation rate of 98 deg/h, which is well above the shot-noise limited rotation rate.

Effective techniques have been developed to mitigate the effect of backscattered noise (Cutler *et al.*, 1980; Bohm *et al.*, 1981; Bergh *et al.* 1981a,1981b). One is to construct the components on a single continuous optical fiber (Bergh *et al.*, 1981a) to avoid the backscattering due to the splices. In addition, in order to reduce the effect of the Rayleigh backscattering two techniques are used. The first involves phase modulation which averages out the phase error. The phase modulator introduces the same kind of phase fluctuations as those due to temperature and vibration sensitive Rayleigh backscattering but in a wide frequency band so that the error can be averaged out more easily (Bohm *et al.*, 1981). The second technique reduces the coherence length of the laser source so that only a small portion of the backscattered light is capable

of interfering with the primary beam. Both of these schemes have been tested with good results (see below).

e. Optical Kerr effect

Recently work has been done which indicates that a nonreciprocal phase shift due to the Kerr nature of the fiber cavity is a significant noise source in passive ring laser gyros.

To understand why this is so, a short discussion of the optical Kerr effect will be given here. A Kerr medium (one in which the Kerr effect is operative) is defined as one in which the susceptibility of the medium is given by

$$\varepsilon=\varepsilon_0+\varepsilon_2|E(x)|^2, \tag{2.16}$$

where ε_0 and ε_2 are constants and $E(x)$ is the total electric field at position x in the medium. The presence of the second term in Eq. (2.16) leads to nonreciprocal effects for beams transversing the medium in different directions.

For simplicity we will now specialize this discussion to the case of interest—a fiber ring. Let E_1 and E_2 represent the CW and CCW fields, respectively, propagating through a passive fiber ring gyro so that the total field in the cavity is given by

$$E(x)=E_1(x)e^{iKx}+E_2(x)e^{-iKx}. \tag{2.17}$$

Now, using Eqs. (2.16) and (2.17) we will demonstrate that the CW and CCW beams propagate with different velocities through the fiber due to the nonlinear part of the susceptibility. Recall that the velocity of light through a material medium is given by

$$v=\frac{c}{\sqrt{\varepsilon}}. \tag{2.18}$$

To proceed, then, we find what the effective susceptibility, ε, is for the counterpropagating beams. This can be done by writing the polarization P as

$$P=\varepsilon E. \tag{2.19}$$

Using Eqs. (2.16) and (2.17) in Eq. (2.19) gives (see Kaplan and Meystre, 1981)

$$\begin{aligned}P=&\varepsilon_0[E_1(x)e^{ikx}+E_2(x)e^{-ikx}]\\&+\varepsilon_2E_1(x)e^{ikx}(|E_1|^2+2|E_2|^2)\\&+\varepsilon_2E_2e^{-ikx}(|E_2|^2+2|E_1|^2)+\cdots,\end{aligned} \tag{2.20}$$

where the ellipses represent rapidly varying terms.

The effective susceptibility seen by, say, the CW beam is given by the coefficient of E_1e^{ikx} and that of the CCW beam by the coefficient of E_2e^{-ikx}. Using these susceptibilities in Eq. (2.18) gives, for the propagation velocities of the counterpropagating beams

$$v_{\mathrm{CW}}=\frac{c}{[\varepsilon_0+\varepsilon_2(|E_2|^2+2|E_1|^2)]^{1/2}} \tag{2.21a}$$

and

$$v_{\mathrm{CCW}}=\frac{c}{[\varepsilon_0+\varepsilon_2(|E_2|^2+2|E_1|^2)]^{1/2}}. \tag{2.21b}$$

From Eqs. (2.21) it is evident that if $\varepsilon_2\neq0$ (i.e., the fiber has a Kerr-like nonlinearity) and if $|E_1|^2\neq|E_2|^2$ (i.e., the intensities of the counterpropagating beams are not degenerate) then the velocities of the counterpropagating beams differ and so a nonreciprocal phase shift not caused by the rotation of the ring is induced.

If ε_2 is sufficiently different from zero and the beam splitter does not split the laser beam into equal parts then the nonreciprocal phase shift induced by the optical Kerr effect can become the limiting factor in the sensitivity of the passive ring gyro. Several analyses (Bergh, Lefevre, and Shaw, 1982; Ezekiel, Davis, and Hellwarth, 1982) have shown that for existing fibers and if special care is not taken to ensure the equality of the counterpropagating beams the optical Kerr effect does indeed introduce significant noise into the gyroscope. For example, in the state-of-the-art experimental setup used by Bergh, Lefevre, and Shaw (see Sec. II.A.2), if the ratio of the intensities of the two beams is maintained to 0.5 ± 10^{-4} the apparent rotation rate induced by the Kerr-like nature of the fiber is still 10^{-3} deg/h. Similar results are quoted by Ezekiel *et al.* (1982).

To avoid the Kerr phase shift the two groups mentioned above employ (or suggest) several methods. The most straightforward of these is to simply ensure that the intensities of the counterpropagating beams are degenerate. In this case, as shown by Eqs. (2.21), the velocities of the counterpropagating beams are equal and so there is no spurious phase shift.

Ezekiel *et al.* (1982) offer several possibilities for equalizing the intensities. Among these suggestions are the use of a feedback loop to monitor and control the intensities and the use of a variable waveguide coupler instead of a simple beam splitter (see Sec. II.B).

Bergh *et al.* (1982) suggest using a square wave modulation of the signal so that the weighted average of the intensities of the two beams are equal. That is, the square wave modulation removes the nonreciprocity of the Kerr phase shift. They employed such a technique using an apparatus similar to that discussed in Sec. II.A.2 of this paper and found a significant reduction in noise level (in particular the long-term shift was reduced).

This section has been concerned with the problems in rotation sensing which result from the optical Kerr effect. It is worth mentioning that Kaplan and Meystre (1981, 1982) discuss a technique which used the fact that a Kerr medium in a passive ring laser gyro increases the intensity difference of the counterpropagating waves to enhance the Sagnac effect, i.e., to increase the sensitivity of the device.

In this section we have discussed a number of the error sources present in the fiber ring gyro. In the next section we discuss a state-of-the-art experimental scheme in which these error sources are reduced to a low level. Still this state-of-the-art device has a noise limited capability of measuring a rotation rate of only 0.2 deg/h in a thirty

second integration time. As shown in Sec. VI (see Table I) this is several orders of magnitude above the sensitivity required for practical devices. The limiting technological factor is currently scattering and loss properties of the long optical fibers used in passive phase sensitive optical gyros. Rapid advances are being made in fiber technology which could eventually reduce these problems to a manageable level. However, a more fundamental problem associated with fiber ring gyros is that they are much more susceptible to thermal and mechanical stresses (which result in nonreciprocal effects) than are conventional resonator gyros. Before the passive fiber gyros can become a viable alternative (as practical rotation sensors) to the active ring laser gyros (discussed in Sec. III) the problem of environmental noise will have to be overcome.

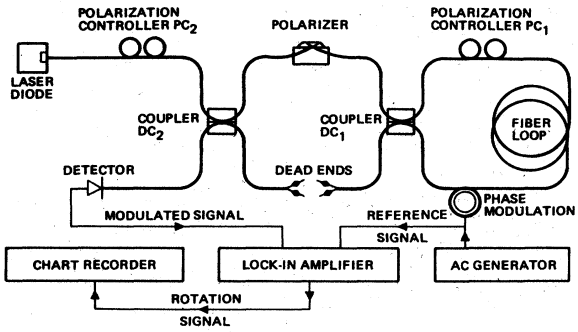

FIG. 4. Schematic of fiber ring gyroscope of Bergh, Lefevre, and Shaw. [Diagram taken from Bergh *et al.* (1981a).]

2. State-of-the-art phase-shift-sensitive fiber ring gyros

To the best of our knowledge the state-of-the-art fiber ring gyroscope which relates a fringe shift to rotation rate is the one developed by Bergh, Lefevre, and Shaw (1981a). A schematic of their system is depicted in Fig. 4.

The salient features of their system are the following. They use a 580-m coil, with a numerical aperture of 0.1 and a core radius of 2 μm wound on a 7-cm-radius spool. All of the components were constructed on a single continuous optical fiber to avoid losses and backscattering due to splices. The four-port coupler (DC_1 in Fig. 4) acts as the beam splitter. The polarizer is designed to select a single polarization state so that there is no birefringence-induced optical path length difference between the counterpropagating beams. PC_1 and PC_2 adjust the input and output polarization states of the beam to ensure efficient passage through the polarizer.

An important feature of this and other highly developed systems is that the signal is biased. This ensures higher sensitivity because for low rotation rates the counterpropagating waves add to nearly a maximum since they have traversed very nearly the same optical path length. At a maximum, the signal is not sensitive to small phase differences and so a phase bias is introduced in order to put the signal in a more sensitive regime. This is accomplished by the phase modulator. The lock-in amplifier is used to measure both the first and second harmonics of the Fourier expansion of the detected signal. The rotation rate is determined from the measurement of the first harmonic and calibrated using information carried by the second harmonic.

The use of a low-loss fiber (13 dB/km between input and detector for a He-Ne source) permits the use of low-power devices without approaching the shot-noise limit. The short-term noise in this system was determined to be due to Rayleigh backscattering. To investigate this noise source a comparison of the phase modulation and reduction of laser coherence length techniques (discussed previously) designed to reduce the backscattered noise was carried out. It was found that the rms value of the phase error [which determines the minimum detectable phase shift which in turn is proportional to the minimum detectable rotation rate via Eq. (1.10)] with a He-Ne laser as the source and no backscattering phase modulation was 1×10^{-3} rad for a 1-sec integration time. This value was reduced to 2×10^{-5} rad when a phase modulator was introduced into the center of the loop. When the He-Ne laser was replaced by a GaAs-diode laser (which has a small coherence length) the phase error was reduced to 5×10^{-5} rad for a 1-sec integration time. This is equivalent to a rotation rate of 0.5 deg/h for the parameters given above. It was found that using a phase modulator in conjunction with the diode laser did not reduce the noise level.

Using an integration time of 30 sec, the minimum detectable rotation rate was found to be 0.2 deg/h, which is well above that obtainable with conventional ring laser gyros (see Sec. III). It should be noted that this minimum detectable rotation rate is a noise equivalent rate. That is, it reflects the size of the noise in the device, and the assumption is made that any rotation rate which exceeds the noise level could be resolved. However, by using a diode laser with a larger spectral width (smaller coherence time) and by lengthening the fiber, Bergh *et al.* hope to increase the sensitivity of their device.

For the description of another highly developed system we refer the reader to the work done by G. Schiffner, in particular, Schiffner, 1980.

TABLE I. Inertial navigation applications.

Gyro resolution (deg/h) and stability	Systems applications
10.0→1.0	Flight control, attitude heading, short-flight devices
1.0×0.1	Some aircraft
0.01	Commercial airliners
0.001→0.000x	Ships, other advanced aircraft
0.000x→0.0000x	Submarines, spacecraft

B. Frequency-sensitive fiber ring gyros

As stated earlier, passive ring resonators can be used to determine rotation rates by measuring the frequency difference between counterpropagating beams whose frequencies are locked to the clockwise (CW) and counterclockwise (CCW) resonant frequencies of the cavity, respectively (Ezekiel and Balsamo, 1977; Davis and Ezekiel, 1981).

Ezekiel and Balsamo (1977) discuss the operating principle of this type of gyro and describe an experimental setup which uses a conventional passive ring resonator (i.e., not a fiber). Currently, the most developed form of this type of laser gyro (which we shall call the frequency-sensitive passive laser gyro) uses an optical fiber as the ring cavity (Davis and Ezekiel, 1981).

A skeletal schematic of the layout of this type of device is depicted in Fig. 5.

Light from a single laser source is split by a beam splitter and then each branch of the beam is frequency shifted by acousto-optic devices so that they become locked to the CW and CCW resonant modes of the cavity (which, of course, are not degenerate when the cavity is rotating), respectively. The frequency difference between the counterpropagating modes is then given by the usual Sagnac-effect formula [Eq. (1.15)],

$$\Delta\omega = \frac{4A\Omega}{\hat{\lambda}P} , \tag{2.22}$$

where, as before, A is the area enclosed by the light path, $\hat{\lambda}$ is the reduced, free space wavelength of the laser light, P is the perimeter of the light path (one loop of the fiber coil), and Ω is the rotation rate of the resonator.

The frequency-sensitive passive gyro has the advantage of a much larger scale factor [as discussed in connection with Eqs. (1.7)—(1.11)] than the phase shift measurement schemes have. This is a particularly important point when conventional cavities (i.e., not fibers) are used. This type of device has the same scale factor as the conventional ring laser gyro but avoids the lock-in problem.

The form of the frequency-sensitive passive gyro that has been given the most attention, however, uses an optical fiber as the resonator. In a comparison with the phase-sensitive fiber devices, the frequency-sensitive device has the advantage of a larger scale factor but this scale factor ($4A/\hat{\lambda}\rho$) does not depend on fiber length as does the scale factor of the phase-sensitive devices. However, Shupe (1981) investigated the shot-noise limit of the frequency-sensitive fiber device and showed that the sensitivity of such a device does indeed depend on the length of the fiber. This dependence can be understood by considering the expression for the shot-noise limited minimum detectable rotation rate of the frequency-sensitive fiber devices. This rotation rate is given approximately by (Shupe, 1981; Ezekiel *et al.*, 1978).

$$\delta\Omega \cong \frac{\lambda P}{4A}\frac{\sqrt{2}\Gamma}{\mathscr{S}} , \tag{2.23}$$

where Γ is the width of the resonant peaks of the fiber and $\mathscr{S}$ denotes the signal-to-noise ratio of the system. Γ and $\mathscr{S}$ depend upon the length of the fiber (see Vali and Shorthill, 1976, for the explicit dependence) and it is through this dependence that $\delta\Omega$ depends on the fiber length. Shupe found that the fiber length which minimizes $\delta\Omega$ is on the order of, but somewhat smaller than, the optimum fiber lengths of phase-sensitive fiber gyros. Using a set of typical laser and fiber parameters Shupe found the shot-noise limited rotation rate to be 2.49×10^{-3} deg/h.

All of the noise sources discussed in Sec. II.A.2 are also present in frequency-sensitive fiber ring gyros. Now a brief description of the state-of-the-art frequency-sensitive passive fiber gyro will be presented. The device to be described here is capable of measuring rotation rates of 0.1 deg/h in a 30-sec integration time. It was developed by Davis and Ezekiel in 1981.

The experimental setup of their device is shown in Fig. 6. (The schematic is taken from Davis and Ezekiel, 1981.)

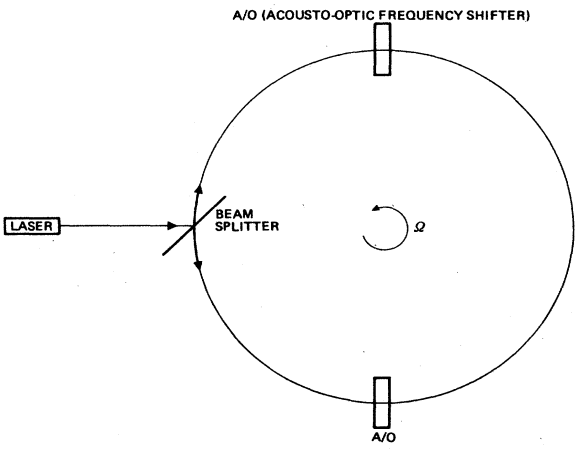

FIG. 5. Schematic of frequency-sensitive passive laser gyro.

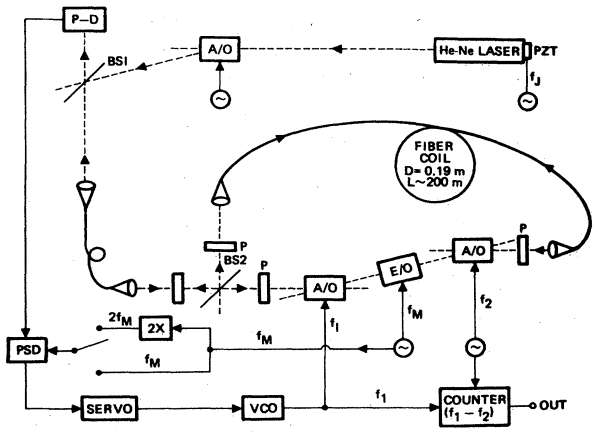

FIG. 6. Experimental setup of fiber-rotation sensor. [Taken from Davis and Ezekiel (1981).]

They used a single-mode fiber coil 200 m long and 19 cm in diameter. The laser source was a 5-mW He-Ne laser. The important features of the setup are two acoustic-optic (A/O) frequency shifters which lock the counterpropagating beams to the CW and CCW resonant frequencies of the fiber, the polarizers (P) which ensure single-mode operation, and the electro-optic (E/O) phase modulator which functions to reduce the Rayleigh backscattering noise. The output is detected by the photodetector (P-D in Fig. 6). The current, $i(t)$, produced in the photodetector by the fiber output is proportional to the square of the sum of the complex amplitudes of the two counterpropagating beams. If the E/O phase modulator is driven to produce phase modulation with amplitude φ_0 and frequency ω_m then the P-D current can be approximated by (Davis and Ezekiel, 1981)

$$i(t)\cong 2I_0\left\{1+J_0\left[2\varphi_0\sin\left[\omega_m\frac{\tau_0}{2}\right]\right]\cos\varphi\right\}+5I_0J_1[2\varphi_0\sin(\omega_m\tau_D/2)]\sin\varphi\cos[\omega_m(t-\tau_D/2)]$$
$$-4I_0J_2[2\varphi_0\sin(\omega_m\tau_D/2)]\cos\varphi\cos[2\omega_m(t-\tau_D/2)]\cdots\,, \tag{2.24}$$

where the ellipses represent higher-order terms, and where τ_D is the round-trip transit time of light in the fiber, φ is the total phase difference between the CW and CW beams due to the rotation of the fiber and any nonreciprocal noise sources, and J_n are the Bessel functions. As given by Eq. (2.1) the rotation-induced phase shift is

$$\varphi_s=\frac{4\pi\Omega L\rho}{\lambda c}\,. \tag{2.25}$$

The usual measurement scheme is to demodulate $i(t)$ at the fundamental frequency, ω_m, by using a phase-sensitive demodulator (PSD in Fig. 6) to obtain an output, y_1, related to φ. From Eq. (2.24) we see that this relationship is

$$y_1\simeq 4I_0J_1[2\varphi_0\sin(\omega_m\tau_0/2)]\sin\varphi\,. \tag{2.26}$$

Davis and Ezekiel found that the best sensitivity could be obtained by operating at a null. That is, the total nonreciprocal phase shift in the coil can be offset, using a feedback loop, by a frequency-induced phase shift produced by shifting the frequencies of the CW and CCW beams with the A/O shifters. In this way, one has

$$\varphi-\frac{2\pi}{c}nL\Delta\nu'=0\,, \tag{2.27}$$

where $\Delta\nu'$ is the net frequency shift of the laser light necessary to offset the nonreciprocal phase shift and nL is the optical path length of the coil. If there were no noise $\Delta\nu'$ would be identical to $\Delta\nu$, the frequency difference between the CW and CCW resonant modes of the cavity. In Ezekiel's setup one of the A/O shifters is operated at a fixed frequency and the other is operated at a variable frequency. This second A/O shifter shifts the frequency of, say, the CW beam whenever the feedback loop indicates that y_1 (and hence φ) is not zero. Equations (2.25) and (2.27) can be combined to give

$$\Delta\nu'=\left[\frac{4A}{\lambda P}\right]\Omega\,, \tag{2.28}$$

which if $\Delta\nu'$ is associated with $\Delta\nu$ is the usual Sagnac effect. So the sensitivity of this device depends upon how nearly $\varphi=\varphi_s$ (that is how nearly $\Delta\nu=\Delta\nu'$), since the rotation rate is determined by monitoring $\Delta\nu'$.

Davis and Ezekiel found that modifying the above procedure by demodulating the output of the second harmonic (and so using $y_2\simeq 4I_0J_2[2\varphi_0\sin(\omega_m\tau_0/2)]\cos\varphi$ as the discriminate in the feedback loop) reduced the noise level. It was with this scheme that they were able to reduce the noise level to a rotation rate equivalent of 0.1 deg/h. Figure 7 compares the rotation rate equivalent noise rate obtained in their experiment when the first and second harmonics of the signal, respectively, were demodulated with the corresponding shot-noise limits. This figure indicates that their setup permits nearly shot-noise limited detection (Fig. 7 again taken from Davis and Ezekiel, 1981). Note that the experimental noise level ceases to decrease

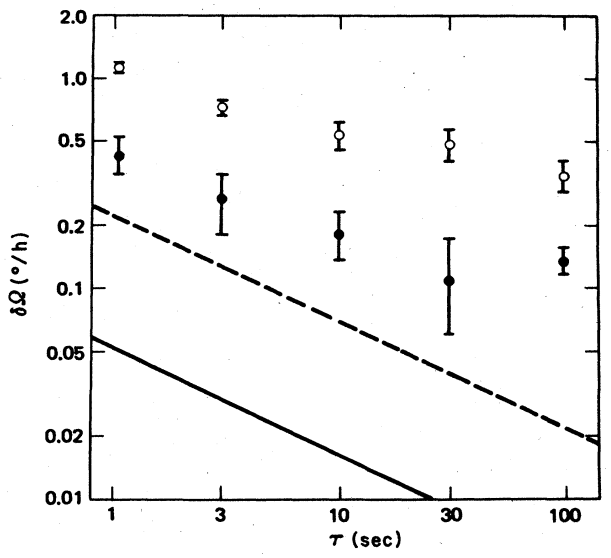

FIG. 7. Measured and theoretical rotation-rate uncertainty $\delta\Omega$ as a function of integration time τ. Open circles denote first harmonic measurement with the solid line being the corresponding shot noise. Filled circles denote second harmonic measurement with the dashed line indicating the corresponding shot-noise limit. [Taken from Davis and Ezekiel (1981).]

after integration times longer than 30 sec. Ezekiel and Davis attribute this to temperature-induced long-term drift.

Ezekiel's device certainly seems to be competitive with phase-sensitive devices but, as yet, its performance does not approach that of the best conventional ring laser gyros.

III. CONVENTIONAL (TWO-MODE) ACTIVE LASER GYRO

A. Readout in the laser gyro

The active laser gyro, whose operating principle has been presented in the preceding section, gives information on the rotation rate in the form of a frequency difference between the counterpropagating waves. A detailed study of this device and of the early state of the art can be found in Aronowitz (1971).

The simplest way to measure the frequency difference is to combine the two beams and observe the beats between them. A way to do this is by means of a combining prism, as shown in Fig. 8.

The beams coming out of the prism will be very nearly colinear. On the surface of the detector they will give rise to a fringe pattern, the intensity of the light being given by

$$I=I_0\left[1+\cos\left[\frac{2\pi\varepsilon x}{\lambda}+2\pi\Delta\nu t+\varphi\right]\right] \tag{3.1}$$

if the intensities of both beams are equal. Here φ is just a constant phase difference and

$$\Delta\mathbf{k}\cdot\mathbf{r}\simeq\frac{2\pi}{\lambda}\varepsilon x\ ,$$

where ε is zero for perfect alignment and x is measured along the surface of the detector. The fringe spacing is given by λ/ε and can typically be of the order of a few millimeters. From the term $2\pi\Delta\nu t$ we see that the fringes will move when the device is rotated (that is, when $\Delta\nu\neq 0$), in a direction which depends on the sense of rotation (through the sign of $\Delta\nu$). A detector set to count the number of intensity maxima that move past it will give an output

$$N=\int_0^t\Delta\nu\,dt=\frac{4A}{\lambda L}\int_0^t\Omega\,dt=\frac{4A\theta}{\lambda L} \tag{3.2}$$

[where use has been made of Eq. (1.15) for the frequency difference]. Here θ is the total angle of rotation of the gyro. To take into account the possibility of $\Delta\nu$ (or, equivalently, Ω) changing sign during the measuring time, one may use a system of two detectors to get information on the direction of motion of the fringes, and a logical circuit to add up "positive" and "negative" counts. In this way the cumulative number of counts is an instantaneous—and "digitalized"—measure of the angle rotated by the device.

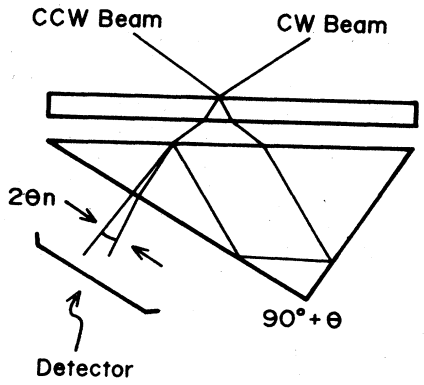

FIG. 8. Readout in the laser gyro. The small deviation of the corner angle of the prism from 90° gives rise to an interference pattern on the detector.

Its use as an actual gyroscope involves three ring cavities assembled in three mutually orthogonal planes. A practical way to do it in a compact package can be seen, for example, in Thomson (1978) and in Aronowitz (1971).

B. Sources of error in the laser gyro

The use of the active laser gyro as a rotation sensor depends crucially on the extent to which the relation Eq. (1.15) is valid. In the ideal laser gyro [that is, one which obeys Eq. (1.15)] the relationship between Ω and $\Delta\nu$ is linear and is shown in Fig. 9(a). There are three main

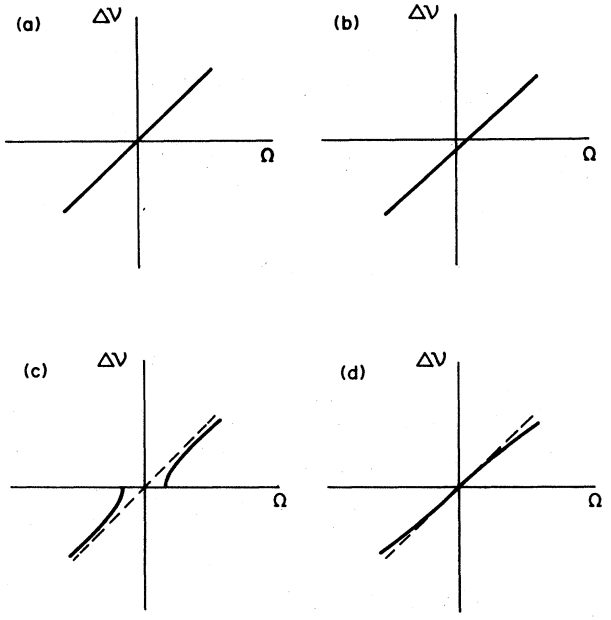

FIG. 9. Beat note vs input rotation rate in a ring laser gyro. (a) The ideal case, a straight line through the origin; (b) a linear relationship with a nonzero null shift; (c) frequency locking; and (d) nonlinearities in the response (variable scale factor).

kinds of error that may cause Eq. (1.15) to be invalid. As shown in Fig. 9, these are the following.

1. Null shift [Fig. 9(b)]. This happens when the frequency difference is "biased," i.e., $\Delta\nu$ is nonzero for zero input rate. It amounts to adding a constant term to the right-hand side of Eq. (1.15), the exact magnitude of which is usually unpredictable. It can arise from any anisotropy in the cavity with respect to radiation traveling in the two directions. If it is constant and repeatable it can be measured once and compensated for in the final output (Aronowitz and Lim, 1978). If it drifts, however, or changes from turn-on to turn-on, it can be a serious problem.

The main cavity anisotropy that gives rise to null shift errors is the so-called Langmuir flow in the active laser medium. It is found that within a dc-excited plasma there is a movement of the neutral atoms which is towards the cathode along the center of the discharge tube, and towards the anode along the walls. Since the laser radiation is along the tube center, it sees a net motion of the medium. This motion introduces an effective anisotropy with respect to the two propagation directions, which leads to a splitting in the frequencies as discussed in Aronowitz (1971).

The usual way to avoid this problem is to make the Langmuir flow reciprocal by using two discharge tubes with opposite polarities, as in Fig. 10. In this way the two "biasing" elements cancel each other. The discharge current has to be the same in both tubes to a rather high accuracy if no null shift is to be observed. In the ring laser discussed in Aronowitz and Lim (1978), an unbalance of 1 μA between the two currents led to an equivalent null shift of 0.0066 deg/h.

There are several other sources of null shifts that can arise in specific cases. Any nonreciprocal loss mechanism in the cavity, for example, will give rise to different mode-pulling coefficients for the two waves, which will again lead to a frequency splitting (at least for nonzero detuning). Power-dependent effects (mode pushing) may also give rise to a frequency difference if the intensities of both waves are not identical (again, this may happen when there are nonreciprocal losses).

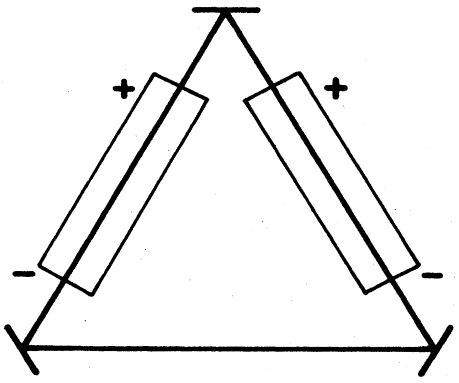

FIG. 10. A scheme to compensate for the null shift due to Langmuir flow. The signs + and − indicate the polarities of the discharge tubes.

Applied external magnetic fields have also been reported to produce null shifts. Here the detailed mechanism is less clear. However, significant correlation between theory and experiment has recently been obtained for the case of the Zeeman laser, on which we will comment below.

2. Mode locking (or "frequency locking"). As shown in Fig. 9(c), this corresponds to the frequency difference $\Delta\nu$ vanishing altogether for small, but nonzero, input rotation rate. All information on the latter is therefore lost. Mode locking is caused by a weak coupling mechanism between the two otherwise independent traveling waves. This is backscattering from one wave into the other, which takes place mostly at the mirrors, due to surface imperfections. Since it is the most important problem that has to be overcome in order to have a working laser gyro, we will discuss it at length in the remainder of this section.

3. Variations in the scale factor as a function of the rotation rate [Fig. 9(d)]. This means that the linearity exhibited by Eq. (1.15) no longer holds. These nonlinear effects may arise by dispersive effects in the laser medium (frequency pulling and pushing). They may also arise, as will be seen later, as a consequence of some of the techniques used to eliminate mode locking, particularly the alternating bias ("dither") method.

C. Mode locking

1. Backscattering and mode locking

Backscattering in the ring laser means that, due to imperfections in the optical path, a small fraction of one of the waves is scattered back in the direction of the oppositely traveling wave. The scattering itself can be expected to be more or less uniform in a solid angle of about 4π steradians; of this, only the part of the light that falls into the solid angle of the counter-rotating beam contributes to coupling the two waves. The resulting coupling coefficient is usually very small, yet it becomes a dominant effect at low rotation rates, as we are about to see.

Here, we want to present an example showing how coupling between the two counter-rotating waves may arise; this example is merely illustrative and does not attempt to describe the actual backscattering process, which is discussed in greater length in Aronowitz (1971).

Assume a very thin piece of a dielectric is placed inside the cavity at a position z_0, with thickness l and index of refraction n,

$$n^2=1+\chi_0\,, \tag{3.3}$$

where χ_0 is the dielectric susceptibility. Reflections off this dielectric slab are supposed to mimic the backscattering at the mirrors mentioned above.

From Lamb's semiclassical laser theory (see Lamb, 1964; Sargent, Scully, and Lamb, 1974, Chap. 8) the two

waves inside the cavity are described by the self-consistency equations

$$\dot{E}_{\pm}+\frac{1}{2}\frac{2\pi\nu}{Q_{\pm}}E_{\pm}=\frac{1}{2}\frac{2\pi\nu}{\varepsilon_0}\mathrm{Im}(\mathscr{P}_{\pm}) , \tag{3.4a}$$

$$2\pi\nu_{\pm}+\dot{\varphi}_{\pm}=2\pi\Omega_{\pm}-\frac{1}{2}\frac{2\pi\nu}{\varepsilon_0}\frac{1}{E_{\pm}}\mathrm{Re}(\mathscr{P}_{\pm}) , \tag{3.4b}$$

where $E_{(\pm)}$ is the electric field amplitude, $\mathscr{P}_{(\pm)}$ the polarization amplitude, and the subindices $+$ and $-$ refer to clockwise and anticlockwise waves, respectively; $\Omega_{(\pm)}$ is the empty cavity frequency, and $\nu_{(\pm)}$ is the frequency that is actually obtained when the dispersive effects of the active medium are taken into account.

The polarization amplitude $\mathscr{P}_{\pm}$ is given by the slowly varying part of the expression

$$2e^{i(2\pi\nu t_{\pm}+\varphi_{\pm})}\frac{1}{L}\int_0^L e^{-ik_{\pm}z}P(z,t)dz , \tag{3.5}$$

where $P(z,t)$ is the total macroscopic polarization

$$\begin{aligned}P(z,t)&=\chi E(z,t)=\chi[E_+(z,t)+E_-(z,t)]\\&=\chi[E_+(t)e^{-i(2\pi\nu_+t+\varphi_+-k_+z)}\\&\quad+E_-(t)e^{-i(2\pi\nu_-t+\varphi_-+k_-z)}] .\end{aligned} \tag{3.6}$$

Equation (3.5) simply gives the projection of $P(z,t)$ onto either of the two counter-rotating modes. Now assume for simplicity that the cavity is empty except for the dielectric slab mentioned above. This results in a susceptibility

$$\chi(z)=\begin{cases}\chi_0 & \text{if } z_0\le z\le z_0+l\\ 0 & \text{otherwise}\end{cases}$$

so that use of (3.6) in (3.5) gives

$$\begin{aligned}\mathscr{P}_+=\frac{\chi_0 l}{L}E_+ &+\frac{\chi_0}{L}e^{-i(k_++k_-)z_0}\left[\frac{e^{-i(k_++k_-)l}-1}{-i(k_+-k_-)}\right]\\&\times e^{2\pi i(\nu_+-\nu_-)t}E_-e^{+i(\varphi_+-\varphi_-)}\end{aligned} \tag{3.7}$$

and an analogous expression for $\mathscr{P}_-$ with the subindices $+$ and $-$ interchanged. If one defines the phase angle difference

$$\psi=2\pi(\nu_+-\nu_-)t+\varphi_+-\varphi_- \tag{3.8}$$

one may write (3.7) as

$$\mathscr{P}_+=\chi_0\frac{l}{L}E_++\chi_0 re^{i\varepsilon}e^{i\psi}E_- \tag{3.9a}$$

and the corresponding equation for $\mathscr{P}_-$ as

$$\mathscr{P}_-=\chi_0\frac{l}{L}E_-+\chi_0 re^{-i\varepsilon}e^{-i\psi}E_+ , \tag{3.9b}$$

where the complex number $re^{i\varepsilon}$ is given by (3.7),

$$re^{i\varepsilon}\equiv\frac{e^{-i(k_++k_-)z_0}}{L}\frac{e^{-i(k_++k_-)l}-1}{-i(k_++k_-)} . \tag{3.10}$$

If now Eqs. (3.9) are used in the frequency determining equation (3.4b) and $E_+=E_-$ is assumed, one gets for the phase angle difference ψ the equation of motion

$$\dot{\psi}=2\pi(\Omega_+-\Omega_-)-\frac{1}{2}\frac{2\pi\nu\chi_0}{\varepsilon_0}r\cos(\psi+\varepsilon) \tag{3.11}$$

which is usually written as

$$\dot{\psi}=S\Omega+b\sin\psi . \tag{3.12}$$

Here Ω is the rotation rate and S the scale factor $[2\pi(\Omega_+-\Omega_-)=S\Omega]$, and ψ has been slightly redefined by adding to it an appropriate constant. The factor $b=(\pi\nu\chi_0 r/\varepsilon_0)$ is called the "backscattering coefficient," and clearly has units of (angular) frequency. Equation (3.11) is indeed the "locking" equation obtained in more sophisticated treatments of backscattering (see, for example, Aronowitz, 1971).

To see how Eq. (3.11) leads to mode locking, note that $\dot{\psi}$ is just the beat note between counter-rotating waves [compare the definition Eq. (3.8)]. Now, inspection of Eq. (3.12) shows that if $S\Omega\gg b$ the phase difference ψ grows essentially as a linear function of time, as it would do in the absence of backscattering. But if $S\Omega\lesssim b$ stationary solutions to (3.12) exist, with $\dot{\psi}=0$, given by

$$\psi\equiv\psi_s=\begin{cases}-\arcsin\dfrac{S\Omega}{b}\\ \pi+\arcsin\dfrac{S\Omega}{b}.\end{cases} \tag{3.13}$$

Of the two solutions given in Eq. (3.13), the second one, having $b\cos\psi_s<0$, is stable: this means that no matter what the initial condition is, the evolution of ψ will eventually bring it arbitrarily close to the value ψ_s, for which the right-hand side of Eq. (3.12) equals zero. That is, eventually (after a time, in fact, of the order of $1/b$) the time derivative of the phase difference ψ [recall the definition, Eq. (3.8)] becomes zero, or, in other words, the frequency difference $\nu_+-\nu_-$ vanishes, in spite of the fact that the rotation rate Ω is nonzero.

When this happens, one says that the two waves have "locked in" at the same frequency. From our (oversimplified, since we assumed $E_+=E_-$ which in practice is not the case) discussion, we can estimate

$$\Omega_{\mathrm{th}}=\frac{b}{S}=\frac{L\lambda}{2\pi 4A}b \tag{3.14}$$

as the threshold for lock-in and hence the minimum detectable rotation rate. Values of b as large as 10^3 rad/sec (100–200 Hz) are not unreasonable; then if $L\sim 30$ cm, $\lambda=6328$ Å, $A\simeq 40$ cm^2, one finds $\Omega_{\mathrm{th}}\simeq 2\times 10^{-3}$ rad/sec$\simeq$400 deg/h. This is an extremely large number, considering that for navigational purposes rotation rates must usually be known with an accuracy of about 0.01 deg/h.

A few remarks may be added about the behavior of ψ in the intermediate region where $S\Omega$ is not much greater than b. In this unlocked regime ψ, as given by Eq. (3.12), is a periodic function of time (modulo 2π). Its period can be used to define an average "frequency difference" as follows; define T as

$$T=\int_0^{2\pi}\frac{d}{S\Omega+b\sin\psi}=\frac{2\pi}{[(S\Omega)^2-b^2]^{1/2}}\ .$$

Then the "average frequency difference" in the unlocked region can be taken to be

$$\Delta\omega_a\equiv\Gamma=[(S\Omega)^2-b^2]^{1/2}\ . \tag{3.15}$$

This is represented in Fig. 11.

Mode locking is clearly the first problem that has to be overcome if one is to have a working laser gyro. Many techniques have been developed to counteract it; the remainder of this section will be devoted to them.

2. Methods for the avoidance of lock-in

a. Constant bias

The most straightforward technique to avoid lock-in and the "dead band" about zero rotation rate is to introduce a constant, externally controlled null shift or "bias," large enough that the laser is always in the unlocked region. The frequency difference will then be

$$\dot{\psi}\simeq S\Omega+\alpha\ , \tag{3.16}$$

where α represents the bias, from which one can recover $S\Omega$ by subtracting the known constant bias. A difficulty is immediately apparent here: the bias has to be a large number (to avoid lock-in) known with very high accuracy,

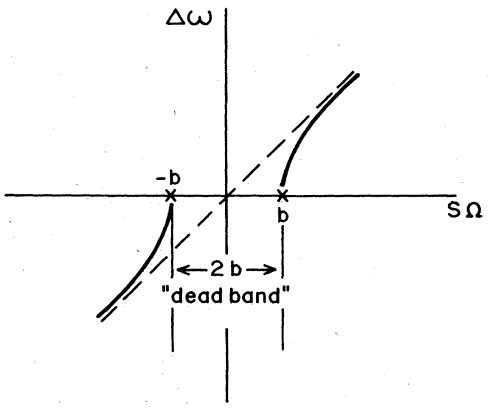

FIG. 11. The average frequency difference given by Eq. (3.15) (solid line) in a laser gyro suffering from mode locking. The dashed line shows the ideal response. The "dead band," or range of input rotation rates for which no frequency difference is observed, extends from $S\Omega=-b$ to $S\Omega=+b$.

so that no significant errors are introduced when subtracting it from the measured frequency difference. For example, to get Ω with an accuracy of 0.1 deg/h, with a bias of 10^5 deg/h, the latter has to be known, and kept constant, to within one part in 10^6. Note that a very large bias is required, not only to overcome locking, but also to be allowed to treat the scale factor as a constant, that is, to linearize Eq. (3.15) to a sufficient accuracy: indeed, we have

$$\langle\dot{\psi}\rangle=[(S\Omega+\alpha)^2-b^2]^{1/2}$$
$$\simeq(S\Omega+\alpha)\left[1-\frac{1}{2}\left[\frac{b}{S\Omega+\alpha}\right]^2\right]$$

which means that a bias on the order of 10^2–10^3 times the lock-in threshold is needed to get scale factor linearities [as assumed in Eq. (3.16)] to an accuracy of 10^{-5}–10^{-6}.

Finally, another reason why a large bias is needed is that $S\Omega$ may have either sign (depending on the sense of rotation), and when its sign is opposite the bias the sum $S\Omega+\alpha$ may become small, and one may again have lock-in and scale factor nonlinearities, only this time around $S\Omega=-\alpha$ rather than around $S\Omega=0$. This effectively imposes a limit on the maximum value of $|\Omega|$ that can be measured, so that one has to choose the bias to be much larger than the maximum expected value of $S|\Omega|$.

Many methods may be used to provide a constant null shift, the most obvious one being to apply a constant rotation of the gyro. In practice all of them suffer from the same problem: the accuracy with which they have to be known and kept stable is simply too high either to attain or to be economically practicable. Of all of them, only the one using the Faraday effect will be briefly considered here, since it is the basis for some other schemes that have proved successful (magnetic dither and DILAG).

The Faraday effect takes place, to some extent, in all isotropic, transparent substances. If a beam of polarized light passes through a medium where a constant, uniform magnetic field is applied along the direction of propagation of the beam, the plane of polarization of the light is rotated through an angle

$$\beta=VBd\ , \tag{3.17}$$

where B is the magnetic flux density, d is the length of medium traversed, and V is the empirically determined *Verdet constant* of the medium. The direction of rotation is always the same with respect to the direction of the magnetic field, irrespective of whether the light propagates parallel or antiparallel to it; therefore the rotation appears to have opposite handedness for counterpropagating waves.

The effect is most easily described in terms of circular polarizations, since for a circularly polarized wave a rotation of the electric vector amounts to multiplication by a phase factor. In a medium with a positive Verdet constant, a wave running parallel to the applied magnetic field will be rotated to the left, so that left-circularly polarized waves are advanced in phase, and right-circularly

polarized waves are retarded, the opposite being the case for waves running antiparallel to B. For simplicity consider right-circularly polarized waves only. It follows from the above discussion that the effect of the Faraday cell is to introduce a nonreciprocal index of refraction

$$n_{\pm}=n\pm\frac{\Delta\varphi}{kd}=n\pm\frac{VB\lambda}{2\pi}\ , \tag{3.18}$$

where the $+$ sign is for the wave running antiparallel to B (which is advanced in phase upon traversing the cell). The consequence of this is that the counterpropagating waves see different optical path lengths, and hence, by the same argument that was presented in Sec. I, their frequencies must be different in order for each to satisfy its own cavity resonance condition. One has

$$|\Delta\nu|=\frac{c\Delta\lambda}{\lambda^2}=\frac{c}{\lambda}\frac{d\Delta n}{L}=2\frac{cVBd}{2\pi L} \tag{3.19}$$

with the wave running parallel to B having the larger frequency (since its index of refraction, n_-, is smaller, it "sees" a shorter cavity). For left-circularly polarized waves, the splitting has the same magnitude but opposite sign (the wave running antiparallel to B having the larger frequency).

A secondary effect of the presence of a Faraday cell in a resonant ring cavity is that only elliptically polarized waves can oscillate, since the polarization vector is rotated in each round trip. To operate it with linear polarizations, the Faraday cell may be inserted between quarter-wave plates that change the linearly polarized light to elliptically polarized and vice versa.

Using this technique, a bias on the order of 10^5–10^6 deg/h can be obtained. To keep it as stable as possible, it has been found convenient to use ferromagnetic or ferrimagnetic materials, with a low saturation magnetization. An external magnetic field is used then to saturate the material, thus making sure the B in Eq. (3.19) is not affected by stray magnetic fields (including the earth's own). There still remains the problem of measuring it with enough accuracy to compensate for it in the output. This can be avoided by the techniques discussed in the following section.

b. Alternating bias

In this scheme, the bias is operated in both the positive and negative rotation rate direction. Over each of these cycles, the net bias averages to zero, so that the output of the gyro, being intrinsically an integrated magnitude, would only reflect the net rotation rate.

The most successful alternating bias technique to date is the mechanical one, in which the gyro is rotated alternately in one direction and the opposite. This process has come to be known as "dithering." It is usually done by mounting the gyro on a rotational spring system which is oscillated by means of a piezoelectric transducer.

The effects of an alternating bias (mechanical or otherwise) that changes sinusoidally in time may by described by the modified lock-in equation [compare Eq. (3.12)],

$$\dot{\psi}=a+b\sin\psi+\alpha\cos(\omega_D t)\ , \tag{3.20}$$

where $a=S\Omega$, and α and ω_D are the amplitude and frequency, respectively, of the oscillating bias (both of them in radians per second). One wants $\alpha\gg b$, as for the static bias discussed previously, and $b\ll\omega_D$ so that the gyro spends most of the time in the unlocked region.

To solve Eq. (3.20) we make the ansatz

$$\psi(t)=at+\frac{\alpha}{\omega_D}\sin(\omega_D t)+\delta(t) \tag{3.21}$$

and find for the unknown function δ at once the following equation

$$\dot{\delta}(t)=b\sin\left[at+\frac{\alpha}{\omega_D}\sin(\omega_D t)+\delta(t)\right]\ . \tag{3.22}$$

Noting the useful Bessel-Fourier expansion (Magnus *et al.*, 1966)

$$e^{ix\sin\beta}=\sum_{m=-\infty}^{\infty}J_m(x)e^{im\beta}\ ,$$

where J_m denotes the mth Bessel function of the first kind, Eq. (3.22) reduces to

$$\dot{\delta}(t)=\sum_{m=-\infty}^{\infty}bJ_m\left[\frac{\alpha}{\omega_D}\right]\sin[(a+m\omega_D)t+\delta(t)]\ . \tag{3.23}$$

This equation is still exact, and to get some insight we now apply a few approximations. Note from Eq. (3.23), that for a rotation rate approximately equal to a multiple of the dither frequency

$$a\cong r\omega_D\ ,$$

where $r=\ldots,-1,0,+1,+2,\ldots$, there is only one term in the sum, which is varying slowly compared to $\omega_D t$, namely $m=-r$. This may be seen as follows. First, notice that the function $\delta(t)$ in the argument of the sine itself is slowly varying, since the magnitude of its time derivative, as given by Eq. (3.22), is $|\dot{\delta}|\sim b\ll\omega_D$. This means that the time dependence of the different terms in the series (3.23) is determined by the frequencies $a+m\omega_D$. Of these, one will be close to zero (namely, if $a\simeq r\omega_D$, the one with $m=-r$), and the others will be of the order of magnitude of ω_D and its harmonics. The gyroscope is averaging over some number of dither periods, so only the slowly varying term survives, which simplifies Eq. (3.23) significantly.

To study this in more detail, we may write the rotation rate a, near a multiple of the dither frequency ω_D, as

$$a=r\omega_D+\tilde{a}\ ,$$

where $|\tilde{a}|\ll\omega_D$. Using this notation we find from Eq. (3.23)

$$\dot{\delta}(t)=bJ_{-r}\left[\frac{\alpha}{\omega_D}\right]\sin[\tilde{a}t+\delta(t)] + \sum_{\substack{m=-\infty \\ m\neq -r}}^{\infty} bJ_m\left[\frac{\alpha}{\omega_D}\right]\sin[(r+m)\omega_D t+\tilde{a}t+\delta(t)] . \tag{3.24}$$

As explained before, the second term on the right-hand side of Eq. (3.24) is at least varying with ω_D because $|\tilde{a}| \ll \omega_D$ and $|\dot{\delta}(t)| \sim b \ll \omega_D$, and therefore averaging over some number of dither periods yields

$$\dot{\delta}(t)=bJ_{-r}\left[\frac{\alpha}{\omega_D}\right]\sin[\tilde{a}t+\delta(t)]$$

which, by the substitution $\varphi=\tilde{a}t+\delta(t)$, can be brought into a more familiar form, namely,

$$\dot{\varphi}=\tilde{a}+bJ_{-r}\left[\frac{\alpha}{\omega_D}\right]\sin\varphi . \tag{3.25}$$

This is the well-known lock-in equation discussed already in Sec. III.C.1, except that the backscattering coefficient now has changed to

$$b \rightarrow bJ_{-r}\left[\frac{\alpha}{\omega_D}\right] .$$

Using the results from Sec. III.C.1, we can at once present the mean beat frequency characteristic using Eq. (3.21),

$$\langle\dot{\psi}\rangle_t=\begin{cases} r\omega_D \quad \text{for } |\tilde{a}| \leq \left|bJ_{-r}\left[\frac{\alpha}{\omega_D}\right]\right| \\ r\omega_D \pm \left\{(\tilde{a})^2-\left[bJ_{-r}\left[\frac{\alpha}{\omega_D}\right]\right]^2\right\}^{1/2} \quad \text{for } \left|bJ_{-r}\left[\frac{\alpha}{\omega_D}\right]\right| \leq |\tilde{a}| \ll \omega_D, \end{cases} \tag{3.26}$$

where $r=\ldots,-2,-1,0,+1,+2,\ldots$.

Due to the nonlinear character of Eq. (3.20) we find additional dead bands centered at multiples of the dither frequency with a width $|bJ_{-r}(\alpha/\omega_D)|$ as indicated in Fig. 12. These steps also arise in the current-voltage characteristic of a driven Josephson junction and were observed for the first time by Shapiro (1963). This phenomenon is not surprising, as the equations describing the phase in a ring laser gyroscope and the current in a Josephson junction are closely related (see, for example, Josephson, 1965). In connection with gyroscopes Killpatrick (1967) integrated Eq. (3.20) numerically (see also Roland and Agrawal, 1981). Hutchings and Stjern (1978) presented approximate analytical results, based on the lines shown above, together with experimental confirmation of these "Shapiro steps" in the mean beat frequency characteristic of a ring laser gyroscope. It is worthwhile to mention that locking at multiples of the driving frequency has been well known to radio physicists since the 1930s, when it was called in German "Mitzieh-Effect" (Erdelyi, 1934).

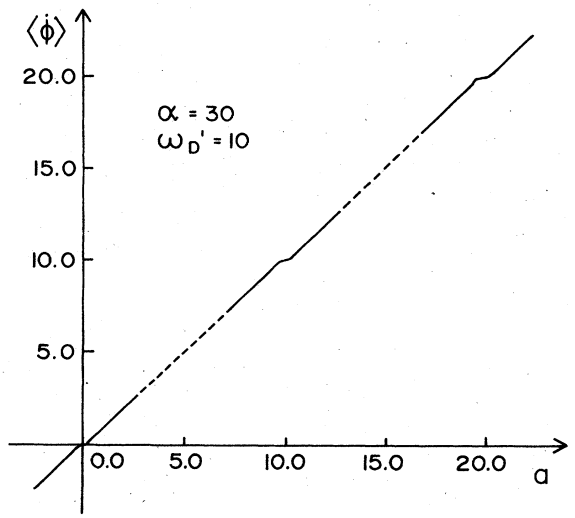

FIG. 12. Average frequency difference for a dithered laser gyro vs input rotation rate. Parameters are given in the text.

Note that especially for $r=0$ the width of the familiar dead band discussed in Sec. III.C.1 is now given by $b\,|J_0(\alpha/\omega_D)|$. Therefore, by choosing α/ω_D equal to a zero point of the zeroth Bessel function ($\alpha/\omega_D=2.40$, etc.) it is possible to make this dead band vanish. This is usually prevented by technical constraints. What can be done is to choose α/ω_D as large as possible, since for large arguments α/ω_D the Bessel function $J_0(\alpha/\omega_D)$ can be written as

$$J_0\left[\frac{\alpha}{\omega_D}\right]=\left[\frac{2}{\pi}\frac{\omega_D}{\alpha}\right]^{1/2}\cos\left[\frac{\alpha}{\omega_D}-\frac{\pi}{4}\right] \tag{3.27}$$

and therefore the width of the dead band goes to zero. In mechanically dithered gyros one may have $\alpha=190$ kHz and $\omega_D=200$ Hz giving $\alpha/\omega_D=950$ and $J_0(\alpha/\omega_D) \leq 0.02$ (Chow *et al.*, 1980).

From Eq. (3.24) we see that as soon as the rotation rate a becomes of the same order as ω_D, more and more terms of the sum contribute and the approximation breaks down. To derive, therefore, an expression for the mean beat frequency between two multiples of the dither frequency we have to apply another technique. From the undithered gyro we know that the mean beat frequency is approximately [see Eq. (3.15)]

$$\Delta\omega_a \equiv \langle\dot{\psi}\rangle_t \cong a\left[1-\frac{1}{2}\left[\frac{b}{a}\right]^2\right] ,$$

i.e., it is the ideal case plus a correction of the order $(b/a)^2$. In order to find this correction in the dithered case and then an approximate analytical expression for $\langle\dot{\psi}\rangle_t$ for this regime we start from the following relation:

$$\frac{d}{dt}\left[-\sum_{m=-\infty}^{\infty}\frac{bJ_m\left[\frac{\alpha}{\omega_D}\right]}{a+m\omega_D}\cos[(a+m\omega_D)t+\delta(t)]\right]-\dot{\delta}(t)\sum_{m=-\infty}^{\infty}\frac{bJ_m\left[\frac{\alpha}{\omega_D}\right]}{a+m\omega_D}\sin[(a+m\omega_D)t+\delta(t)]=\dot{\delta}(t)$$

which can easily be proven by performing the differentiation on the left-hand side, which yields Eq. (3.23). Substituting Eq. (3.23) into the second term on the left-hand side of the above equation we find

$$\dot{\delta}(t)=\frac{d}{dt}\left[-\sum_{m=-\infty}^{\infty}\frac{bJ_m\left[\frac{\alpha}{\omega_D}\right]}{a+m\omega_D}\cos[(a+m\omega_D)t+\delta(t)]\right]-\frac{b^2}{2}\sum_{\substack{m=-\infty\\n=-\infty}}^{\infty}\frac{J_m\left[\frac{\alpha}{\omega_D}\right]J_n\left[\frac{\alpha}{\omega_D}\right]}{a+m\omega_D}\cos[(m-n)\omega_D t]$$

$$+\frac{b^2}{2}\sum_{\substack{m=-\infty\\n=-\infty}}^{\infty}\frac{J_m\left[\frac{\alpha}{\omega_D}\right]J_n\left[\frac{\alpha}{\omega_D}\right]}{a+m\omega_D}\cos 2\left[\left[a+\frac{m+n}{2}\omega_D\right]t+\delta(t)\right].$$

Averaging this equation over time we find

$$\dot{\delta}(t)\cong-\frac{b^2}{2}\sum_{m=-\infty}^{\infty}\frac{J_m^2\left[\frac{\alpha}{\omega_D}\right]}{a+m\omega_D}. \tag{3.28}$$

Note that in deriving Eq. (3.28) we neglected the term varying with twice the frequency.

For $\alpha=0$ (no dither) Eq. (3.28) reduces because of $J_m(0)=\delta_{m,0}$ to Eq. (3.15). Note also that this sum becomes singular at $a=r\omega_D$ ($r=\ldots,-2,-1,0,+1,+2,\ldots$), which is again a manifestation of the Shapiro steps. The sum can be evaluated exactly in terms of Bessel functions (Newberger, 1982) to give together with Eq. (3.21) an approximate result for the mean beat frequency characteristic for rotation rates between two multiples of the dither frequency,

$$\langle\dot{\psi}\rangle_t=a-\frac{b^2}{2}\frac{\pi}{\omega_D}\frac{J_{a/\omega_D}\left[\frac{\alpha}{\omega_D}\right]J_{-a/\omega_D}\left[\frac{\alpha}{\omega_D}\right]}{\sin(a\pi/\omega_D)}. \tag{3.29}$$

Figure 12 shows the lock-in curve of a dither gyro for $b=1$, $\alpha=30$, $\omega_D=10$, where the dashed curve was calculated using Eq. (3.29), whereas at the multiples of ω_D Eq. (3.26) was used.

It turns out that mechanical noise tends to greatly reduce the nonlinearities in the gyro output, smoothing out the lock-in bands in Fig. 12 (see Hutchings and Stjern, 1978; Schleich *et al.*, 1984). To understand how it happens, consider, for example, Eq. (3.25): for large values of α/ω_D, the Bessel function can be written as

$$J_{-r}\left[\frac{\alpha}{\omega_D}\right]\simeq\left[\frac{2\omega_D}{\pi\alpha}\right]^{1/2}\cos\left[\frac{\alpha}{\omega_D}+\tfrac{1}{2}r\pi-\tfrac{1}{4}\pi\right]. \tag{3.30}$$

Now, with α/ω_D of the order of 900, say, it can be seen that small fluctuations in the dither amplitude α may cause the cosine in (3.27) to be "washed away," since an error of less than 1% in α will cause its phase to change by 2π. These errors are sometimes deliberately injected in the dither mechanism; other times the random noise natural to the system itself is enough to ensure that the average of Eq. (3.27) over several dither periods vanishes. Either way, one now has from Eq. (3.25)

$$\langle\dot{\varphi}\rangle=\tilde{a}\Longrightarrow\langle\delta\rangle=0$$

or [from Eq. (3.21)]

$$\langle\psi\rangle=at$$

so that all traces of locking disappear from the output. The phase difference ψ, however, is now a random variable, with a dispersion that grows with time. In other words, the output itself is noisy; its statistics will be calculated in Sec. V.

With mechanical dither it is actually possible (Aronowitz, 1971,1978) to compensate electronically for the oscillating bias in the readout, so that the averaging that was performed in going from Eq. (3.24) to Eq. (3.25) is not really necessary; with this technique, the instantaneous output already equals $at+\delta(t)$, rather than ψ [see Eq. (3.21)].

As mentioned in the preceding section, the Faraday effect can also be used to induce an alternating bias, by periodically reversing the magnetic field applied to the Faraday cell. In addition to the characteristic already mentioned, of having a low saturation magnetization, it is desirable for the magneto-optic material used to have short switching times, again so that the laser spends as little time as possible in the locking region. Most importantly, the inclusion of any external element in the cavity (such as, in this case, the Faraday cell and optionally the quarter-wave plates) may increase the losses and especially the backscattering problems. The magneto-optic element therefore has to be highly transparent, and given a

dielectric coating of high optical quality (see Henry, 1980, and Carter and Inwood, 1981, for technical details). This tends to raise the production costs.

A related technique is that of the so-called "magnetic mirrors" in which the magneto-optic layer is incorporated into one of the mirrors in the cavity. The traveling waves pass through the layer before being reflected (from an ordinary highly reflecting dielectric layer), and this results in a nonreciprocal phase shift as with the usual transmission Faraday element. As an alternative to the Faraday effect, the so-called traverse magneto-optical Kerr effect has been suggested as a means to achieve the bias. The latter affects waves linearly polarized in the plane of incidence and gives a maximum phase shift when the magnetic field B is perpendicular to the direction of propagation of the wave, rather than parallel (or antiparallel) to it, as was the case for the Faraday effect. The magnetic field is therefore applied in the plane of the mirror, and perpendicular to the plane of the cavity. Here also careful coating is necessary, since the "magnetic mirror" has to be of the same high optical quality as the rest of the mirrors (see Henry, 1980, and Carter and Inwood, 1981). For an instance of the performance of a magnetic gyro, see Thomson (1978).

c. Other schemes

We mention here two more methods that have been suggested to minimize or eliminate the problem of lock-in. The "mirror dither" technique involves oscillating one of the mirrors in a shear mode parallel to the plane of the cavity: the idea is to Doppler shift the frequency of the light backscattered from one mode into the counterpropagating one, thereby reducing the coupling between them, and hence the lock-in threshold. The combination of amplitude, direction, frequency, and phasing of the dithering mirror is critical (Coccoli and Lawson, 1970).

Finally, a recently proposed scheme (Diels and McMichael, 1981) would use a phase-conjugation device to couple the counter-rotating waves in such a way as to prevent lock-in. When the coupling due to phase conjugation is larger than the one due to backscattering, computer calculations show the lock-in threshold to be significantly reduced. The technique would also minimize the imbalance between the intensities of the two counter-rotating modes which may occur, for instance, in homogeneously broadened lasers due to strong mode-competition effects.

d. Conclusion

"Conventional" two-mode laser gyros have reached a stage in their development when they are already competitive with purely mechanical gyros for a variety of applications (a review of these can be found in Stowell *et al.*, 1978). Rotation rate sensing capabilities over a range from 10^{-3} to 10^{+4} deg/h have been demonstrated. With respect to cost, on the other hand, their main asset lies in their comparatively inexpensive maintenance.

Of the techniques discussed to avoid mode locking, mechanical body dither is the most widely used in commercial gyros. One of these has been reported (Hammons and Ashby, 1981) to perform under circumstances where the mechanical noise was comparable to the noise arising from purely quantum-mechanical processes (see Sec. V); the random noise diffusion coefficient was of the order of 5×10^{-4} deg/h.

Partly responsible for this development have been the significant advances in mirror technology that have taken place over the past few years; lock-in thresholds as low as 30 deg/h can now be obtained. This implies, as seen from Hammons and Ashby (1981), an important reduction in noise level. (See also Sec. V below.)

In spite of these achievements, there is considerable interest in alternative optical rotation sensors: among these, especially the multioscillator schemes to be discussed in the following section, which can operate without any moving parts (as opposed to dithered gyros) and with less technical complications than the devices discussed so far.

IV. MULTIMODE DEVICES

A. Differential laser gyros

In Sec. III.C it was mentioned that the bias introduced by a Faraday cell in a ring laser gyro [Eq. (3.19)] would have opposite signs for two identical ring lasers, one consisting of two left-circularly polarized, counterpropagating waves, and the other one consisting of right-circularly polarized waves. The differential laser gyro (DILAG) exploits this by using a ring laser with four modes above threshold in a way that is equivalent to having a pair of ring lasers as described above, only sharing the same cavity. Specifically, let us for definiteness number the modes in the following way:

Mode 1, counterclockwise (CCW), right-circularly polarized (RCP);

Mode 2, CCW, left-circularly polarized (LCP);

Mode 3, clockwise, (CW), LCP;

Mode 4, CW, RCP.

Then for the "RCP gyro," made up of Modes 1 and 4, one will have

$$\nu_1-\nu_4=S\Omega+\alpha \tag{4.1a}$$

whereas for the "LCP gyro,"

$$\nu_2-\nu_3=S\Omega-\alpha\ . \tag{4.1b}$$

Here $S\Omega$ is the splitting between the passive cavity frequencies of CCW and CW modes, due to a rotation rate Ω, which is clearly independent of the polarization. The bias is induced by a nonreciprocal device, such as a Faraday cell or a magnetic mirror. Since it is the same device that interacts with Modes 1,4 as with Modes 2,3, the *magnitude* of the bias in Eq. (4.1a) is exactly the same as in Eq. (4.1b).

If beams 1 and 4 are combined on a detector, the beat note $\nu_1-\nu_4$ will be observed, and likewise for $\nu_2-\nu_3$. By

beating the output of the two detectors together, the combination note $\nu_1-\nu_4+\nu_2-\nu_3$ may be observed. But, according to (4.1),

$$\nu_1-\nu_4+\nu_2-\nu_3=2S\Omega\ . \tag{4.2}$$

That is, the differential beat note is independent of the bias, and proportional to the input rotation rate, with a scale factor twice the one for an ordinary two-mode gyro. Any random fluctuations or long-term drifts in the bias cancel in the difference, Eq. (4.2), so that bias stability is no longer a problem, nor is it necessary to know its exact magnitude.

To be sure, Eq. (4.1) will no longer be true if frequency locking occurs. There are clearly three possibilities for mode locking, each with its own mechanism.

(i) Locking of unidirectional waves. This corresponds to the case when $\nu_2=\nu_1$, $\nu_3=\nu_4$. From Eqs. (4.1) it can be seen that there is then no bias, or, rather, that although the resonant frequencies of the empty cavity are biased the active medium overrides it. In fact, what one has in this case are only two counter-rotating linearly polarized waves, like in an ordinary gyro, which nothing will prevent from locking in frequency for low rotation rates (since the effect of the bias has been neutralized).

The mechanism responsible for this may be anisotropy (usually located at the mirrors) that would tend to favor linear over circular polarization. This is the case, for instance, when losses are different for waves polarized along the x and y directions (here, as is customary, z is the laser axis and y is the direction perpendicular to the ring plane). Even more important turn out to be phase anisotropies, which means that the phase shift per cavity round trip is not the same for an x-polarized wave as for a y-polarized wave. Both effects will always be present to some extent, since both the reflection coefficient and the phase shift at the mirrors are polarization dependent for non-normal incidence. They are jointly referred to as "x-y Q and phase anisotropy," and the terms they contribute to the amplitude- and phase-determining equations are of the form

$$(\dot{E}_n)_{xy}=-\left[\frac{c}{L}\frac{\varphi_y-\varphi_x}{2}\sin\psi_{nm}-\frac{c}{L}\frac{l_y-l_x}{2}\cos\psi_{nm}\right]E_m\ , \tag{4.3a}$$

$$(\dot{\psi}_n)_{xy}=\left[\frac{c}{L}\frac{\varphi_y-\varphi_x}{2}\cos\psi_{nm}+\frac{c}{L}\frac{l_y-l_x}{2}\sin\psi_{nm}\right]\frac{E_m}{E_n}\ , \tag{4.3b}$$

where $\psi_{nm}=\psi_n-\psi_m$ (ψ_n is the phase of the nth mode), $n,m=1,2;\ 2,1;\ 3,4;\ 4,3$, φ_x,φ_y are the phase shifts added onto the x- and y-polarized waves per round trip, and l_xE_x,l_yE_y are the losses of the x and y wave per round trip. The origin of the loss term in Eqs. (4.3) can be found, for instance, in Sargent, Scully, and Lamb (1974, Chap. 12). Here we sketch a derivation of both terms.

Consider, for simplicity, Modes 1 and 2. Their polarization vectors are $\hat{\varepsilon}_-$ and $\hat{\varepsilon}_+$, respectively, with

$$\hat{\varepsilon}_\pm=\frac{1}{\sqrt{2}}(\hat{x}\pm i\hat{y})\ .$$

The combined **E** field of these two modes can be written

$$\mathbf{E}_i=\frac{1}{\sqrt{2}}(E_1e^{-i\psi_1}+E_2e^{-i\psi_2})\hat{x}-\frac{i}{\sqrt{2}}(E_1e^{-i\psi_1}-E_2e^{-i\psi_2})\hat{y}\ .$$

With the definitions given above, it is then clear that the **E** field after one round trip will be given by

$$\mathbf{E}_f=\frac{1}{\sqrt{2}}(1-l_x)e^{-i\varphi_x}(E_1e^{-i\psi_1}+E_2e^{-i\psi_2})\hat{x}-\frac{i}{\sqrt{2}}(1-l_y)e^{-i\varphi_y}(E_1e^{-i\psi_1}-E_2e^{-i\psi_2})\hat{y}\ . \tag{4.4}$$

We may separate from Eq. (4.4) the RCP part of forming the dot product with $\hat{\varepsilon}^*_-$; this will give us the effect of losses and phase shifts on Mode 1. We have

$$\mathbf{E}_f\cdot\hat{\varepsilon}^*_-=\{\tfrac{1}{2}[(1-l_x)e^{-i\varphi_x}+(1-l_y)e^{-i\varphi_y}]E_1+\tfrac{1}{2}[(1-l_x)e^{-i\varphi_x}-(1-l_y)e^{-i\varphi_y}]E_2e^{-i(\psi_2-\psi_1)}\}e^{-i\psi_1}\ .$$

All of $l_x,l_y,\varphi_x,\varphi_y$ are very small. Expanding the exponentials, and keeping only terms linear in the above quantities, one finds

$$E_1'e^{i\psi_1'}\equiv\mathbf{E}_f\cdot\hat{\varepsilon}^*_-\simeq\left[E_1\left[1-\frac{l_x+l_y}{2}\right]+\tfrac{1}{2}[(l_y-l_x)+i(\varphi_y-\varphi_x)]E_2e^{-i(\psi_2-\psi_1)}\right]e^{-i\psi_1}\ . \tag{4.5}$$

The first term in Eq. (4.5) simply expresses the effect of the average losses. The second one is clearly the anisotropy term. It can be rewritten as

$$\tfrac{1}{2}[(l_y-l_x)+i(\varphi_y-\varphi_x)]E_2e^{i(\psi_1-\psi_2)}=\left[\tfrac{1}{2}[(l_y-l_x)\cos\psi_{12}-(\varphi_y-\varphi_x)\sin\psi_{12}]+\frac{i}{2}[(l_y-l_x)\sin\psi_{12}+(\varphi_y-\varphi_x)\cos\psi_{12}]\right]E_2\ . \tag{4.6}$$

Again recalling that all terms in Eq. (4.6) are small, it can be seen that, to first order, the real part will contribute to the amplitude E_1', whereas the imaginary part will contribute to the phase ψ_1'. Equations (4.3) then follow (note the factor L/c is the round-trip time, to get the rate of change). Note that from Eq. (4.3b) one can immediately drive the mode-locking equation for Modes 1 and 2:

$$(\dot{\psi}_{12})_{xy} = \frac{c}{L}\frac{\varphi_y-\varphi_x}{2}\left[\frac{E_2}{E_1}-\frac{E_1}{E_2}\right]\cos\psi_{12} + \frac{c}{L}\frac{l_y-l_x}{2}\left[\frac{E_2}{E_1}+\frac{E_1}{E_2}\right]\sin\psi_{12} . \quad (4.7)$$

With average losses of 1%, and a cavity length $L\simeq 30$ cm, a Q anisotropy $l_x/l_y\simeq 0.9$ would give a lock-in coefficient $(c/L)(l_y-l_x)/2\simeq 0.1$ MHz. The phase anisotropy is not as predictable because mirrors from different coating runs exhibit different birefringent behavior for nonnormal incidence. A value of $|\varphi_y-\varphi_x|\simeq 5\times 10^{-2}$ rad/reflection may be considered typical at the state of the art. For a laser with four mirrors, this leads to a phase anisotropy coefficient of $\simeq 16$ MHz. Note, however, that according to Eq. (4.7) its locking effect can be considerably reduced if the amplitudes E_1 and E_2 are approximately equal.

To avoid this form of locking, it is usual practice to introduce a reciprocal bias that splits the frequencies of corotating modes of different polarizations. The most common way to do this is by using an optically active material. A right-handed quartz crystal, for example, placed inside the cavity with its optical axis along the laser axis, will cause all the LCP waves to see a larger index of refraction, and all the RCP to see a smaller one (regardless of in which direction they are traveling); hence Modes 2 and 3 will be downshifted in frequency, and Modes 1 and 4 will be upshifted (by the same amount). The final optical spectrum of the DILAG may then look as in Fig. 13.

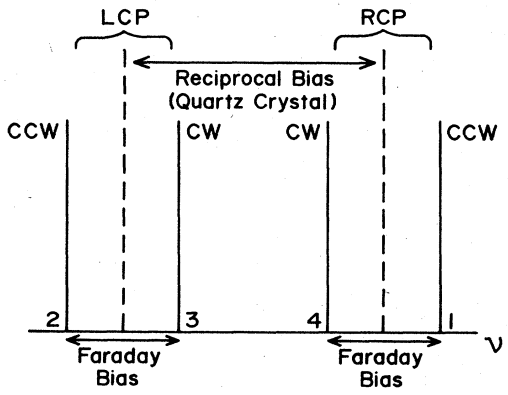

FIG. 13. Mode spectrum of a differential laser gyro (DILAG). The sign of the Faraday bias in this figure assumes that CW waves travel antiparallel to the applied **B** field.

Other schemes use an out-of-plane cavity configuration to reciprocally bias the two polarizations. In this way one does not have to use an additional intracavity element, such as the quartz crystal, which may always be a source of unwanted losses and backscattering. This biasing technique will be discussed at length separately (Sec. IV.A.2).

(ii) Locking of bidirectional waves with opposite polarizations. This would give $\nu_2=\nu_4$, $\nu_3=\nu_1$, and a zero beat note in Eq. (4.2). It corresponds to having standing waves in the cavity, and can be caused by backscattering and localized losses, the same mechanisms responsible for locking in the two-mode gyro. Backscattering couples waves of different polarizations because backscattered right-circularly polarized light becomes left-circularly polarized, and vice versa. Losses that are localized at some particular point in the cavity will clearly favor a standing-wave field configuration with a node at that point.

This kind of locking is prevented by the reciprocal bias introduced above (Fig. 13).

(iii) Locking of bidirectional waves with the same polarization. This corresponds to $\nu_2=\nu_3$ and $\nu_4=\nu_1$. Again one has standing waves, this time linearly polarized. The mechanism again may be localized losses, and backscattering acting together with x-y Q or phase anisotropy. The coefficient corresponding to the latter case would be

$$\frac{b(l_y-l_x)}{2} \quad \text{or} \quad \frac{b(\varphi_y-\varphi_x)}{2} ,$$

where b is the usual backscattering coefficient [see Eq. (3.12)]. This rate is usually 2–3 orders of magnitude smaller than b, which in turn is many orders smaller than the x-y Q or phase coefficient.

This kind of locking is countered by the Faraday bias, which still has to be larger than the maximum expected value of $S|\Omega|$ [see Eqs. (4.1)], as discussed in Sec. III.C.2.

1. The Zeeman laser gyro (ZLAG)

The Zeeman laser gyro is a differential laser gyro in which the Faraday bias is provided by the active laser medium itself; that is, rather than introducing a Faraday cell in the optical cavity, a magnetic field is applied to the laser medium.

Under these conditions, the Faraday bias can itself be calculated from laser theory, in particular from the Zeeman laser theory (Sargent, Scully, and Lamb, 1974, Chap. 20; Hanson and Sargent, 1974; Chow *et al.*, 1979). The mechanism responsible for it can be summarized as follows.

The external magnetic field **B** splits the atomic levels (a,b; see Fig. 13) into sublevels characterized by different values of the magnetic quantum number m (Zeeman effect). Let us designate by a' the values of m associated with the upper level, and by b' those for the lower level, as in Fig. 14. It can be seen (Sargent, Scully, and Lamb, 1974, Chap. 20; Hanson and Sargent, 1974; Chow *et al.*,

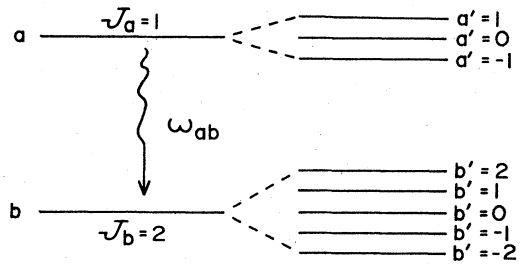

FIG. 14. Level structure for an atom in a magnetic field. Level a has total angular momentum 1, and is split into three sublevels (labeled by a'), while level b has total angular momentum 2 and is split into five sublevels (labeled by b').

1979) that conservation of angular momentum then leads to this selection rule: an LCP wave traveling parallel to **B** (such as Mode 2) or an RCP wave traveling antiparallel to **B** (such as Mode 4) can only induce transitions for which $a'-b'=1$, whereas the other two possible waves (Modes 1 and 3) can only induce transitions for which $a'-b'=-1$. (This discussion assumes again that CW waves traverse the medium in a direction antiparallel to **B**.)

Consider the level scheme in Fig. 14, which corresponds to the 1.15-, 3.39-, and 0.6329-μm Ne lines in the He-Ne laser. For each transition associated (according to the selection rule) with Modes 2 and 4 there is a corresponding transition (having, say, the same a') associated with Modes 1 and 3 and which has an energy larger by twice the splitting between levels,

$$2\hbar\Delta\omega = 2\mu_B Bg \tag{4.8}$$

(where μ_B is the Bohr magneton and g the Landé factor). Hence it is as if the effective atomic line center for Modes 2 and 4 was lower than that for Modes 1 and 3 by an amount $2\Delta\omega$. "Mode pulling" towards these two different atomic frequencies then causes the frequencies ν_2 and ν_4 to split from ν_1 and ν_3. The actual Faraday splitting thus obtained is not nearly as large as $\Delta\omega$ in Eq. (4.8), since the relative importance of mode pulling is given by the ratio between the cavity and the atomic bandwidths, and the former is usually much smaller. In Sanders *et al.* (1978), a Verdet constant for the He-Ne plasma of about 300 Hz/cm G was reported; the experimental result agreed with the one obtained from Zeeman laser theory (see Chow *et al.*, 1980).

In principle the ZLAG can be operated without any intracavity optical elements (by using an out-of-plane cavity for the reciprocal bias, as will be shown) and without any moving parts. Its main problem lies in the fact that mode pulling and pushing effects have been shown, both theoretically and experimentally (Sanders *et al.*, 1978; Chow *et al.*, 1980; Smith and Dorschner, 1980) to give rise to a null shift which depends on the magnetic field intensity and the detuning. Since cavity length fluctuations that lead to detuning variations are unavoidable, it is necessary to look for a ZLAG configuration that minimizes the derivative of the null shift with respect to the detuning. Some important results in this direction were presented in Sanders *et al.* (1978), and suggest that certain optimal combinations of polarization bias and magnetic field may exist. An important factor with respect to future developments is the good correlation found between the experiments and the semiclassical, third-order Zeeman laser theory.

2. Out-of-plane cavity biasing techniques

In essence, all the quartz crystal in a DILAG does is rotate the polarization vectors by a certain angle: the frequency splitting comes from the resonant cavity, since the traveling waves have to adjust their frequencies to compensate for the phase shift per round trip due to that rotation. What the techniques to be discussed here do is perform the rotation of the polarization vectors using an "out-of-plane" configuration of mirrors.

To understand how this is done, consider the system of three orthogonal vectors formed by the propagation vector $\hat{k}$ and the two orthogonal polarizations S and P (P lies in the plane of incidence, while S is perpendicular to it). The relative orientation of these three vectors is preserved upon reflection, except for a 180° phase shift in the S component (space inversion). Then if one uses an even number of mirrors (so that there will be an even number of space inversions, leaving an orthogonal system with the same handedness as the original one) the main factor in determining the effect of successive reflections will be the change in orientation of the plane of incidence itself as the wave travels from one mirror to the next. It is clear that this change has to be of the form of a rotation about the direction of propagation $\hat{k}$ (since this direction is common to both planes of incidence), and can therefore be represented as a rotation of the S and P vectors among themselves.

To help visualize this idea, consider Fig. 15. Here $\hat{n}_1$ and $\hat{n}_2$ are the normals to two consecutive mirrors. The plane of incidence for the first mirror is defined by $\hat{n}_1$ and the incident wave vector $\hat{k}_1$, or equivalently by the normal $\hat{a}_1$ to the plane, given by

$$\hat{a}_1 = \frac{\hat{n}_1 \times \hat{k}_1}{\sin\theta_1} = -\frac{\hat{n}_1 \times \hat{k}_2}{\sin\theta_1} . \tag{4.9}$$

The reflected (unit) wave vector is $\hat{k}_2$, which together with $\hat{n}_2$ defines the normal $\hat{a}_2$ to the second plane of incidence:

$$\hat{a}_2 = \frac{\hat{n}_2 \times \hat{k}_2}{\sin\theta_2} . \tag{4.10}$$

The polarization components S_1 and P_1 refer to the first plane of incidence. To find S_2 and P_2, note that from Eqs. (4.9) and (4.10), both $\hat{a}_1$ and $\hat{a}_2$ are perpendicular to $\hat{k}_2$, so that they both lie in the same plane as S_1 and P_1.

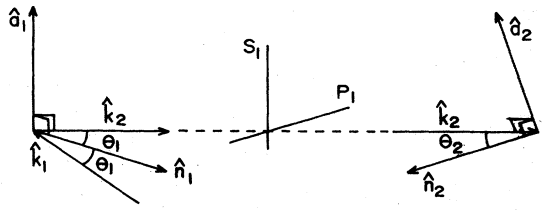

FIG. 15. Geometry of two consecutive reflections: $\hat{n}_1$ and $\hat{n}_2$ are the normals to mirrors 1 and 2, respectively, θ_1 and θ_2 are incidence angles, $\hat{k}_1$ is the unit wave vector of light before the first reflection, and $\hat{k}_2$ is the wave vector after the first reflection. $\hat{a}_1$ and $\hat{a}_2$ are the normals to the two consecutive planes of incidence; S and P refer to the first reflection.

The situation is shown in Fig. 16.

The new S component, S_2, is the projection of the polarization vector along $\hat{a}_2$; in terms of the components S_1 and P_1, and the angle α_{12} between $\hat{a}_1$ and $\hat{a}_2$, it can be written as

$$S_2 = S_1 \cos\alpha_{12} - P_1 \sin\alpha_{12} .$$

Analogously

$$P_2 = P_1 \cos\alpha_{12} + S_1 \sin\alpha_{12} .$$

Defining the rotation matrix

$$R(\alpha_{12}) = \begin{bmatrix} \cos\alpha_{12} & \sin\alpha_{12} \\ -\sin\alpha_{12} & \cos\alpha_{12} \end{bmatrix} \tag{4.11}$$

we have

$$\begin{bmatrix} P_2 \\ S_2 \end{bmatrix} = R(\alpha_{12}) \begin{bmatrix} P_1 \\ S_1 \end{bmatrix} . \tag{4.12}$$

The effect of the mirrors themselves on the P and S components can be represented by the diagonal matrix (Sanders and Anderson, 1981)

$$M_j(\theta_j) = \begin{bmatrix} xie^{i\delta/2} & 0 \\ 0 & -yie^{-i\delta/2} \end{bmatrix} , \tag{4.13}$$

where x and y are the P and S reflectances of mirror j for an angle of incidence θ_j, and δ is the corresponding linear phase birefringence. In terms of the definitions introduced at the beginning of this section, one has $l_x = 1-x$, $l_y = 1-y$, and $\varphi_x - \varphi_y = \delta + \pi$ (as mentioned before, all the π phase shifts effectively cancel in one round trip for an even number of mirrors).

If we have n mirrors, then, the total change in the polarization vector after one round trip is given in terms of the S and P components by the product

$$\begin{bmatrix} P' \\ S' \end{bmatrix} = R(\alpha_{n1}) M_n(\theta_n) \cdots R(\alpha_{23}) M_2(\theta_2) R(\alpha_{12}) M_1(\theta_1) \begin{bmatrix} P \\ S \end{bmatrix} , \tag{4.14}$$

where, as above, α_{ij} is the angle between the planes of incidence of mirrors i and j.

This way of representing the effect of an optical system on polarized light by a succession of 2×2 matrices is of course nothing other than the Jones calculus (see, for instance, Hecht and Zajac, 1974), adapted here to the problem at hand.

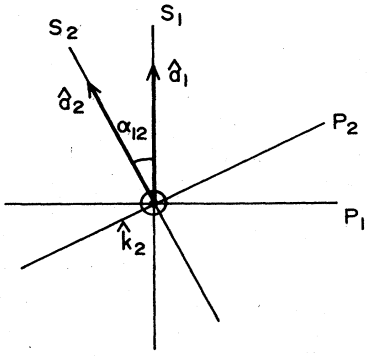

FIG. 16. Rotation of the plane of incidence in two consecutive reflections (see text).

The expression (4.14) can be simplified if one neglects x-y Q and phase anisotropy (that is, set $x = y$ and $\delta = 0$ for all mirrors). Then

$$M_j \equiv \begin{bmatrix} 1 & 0 \\ 0 & -1 \end{bmatrix} (ix_j)$$

and noticing that

$$\begin{bmatrix} 1 & 0 \\ 0 & -1 \end{bmatrix} \begin{bmatrix} \cos\alpha & \sin\alpha \\ -\sin\alpha & \cos\alpha \end{bmatrix} \begin{bmatrix} 1 & 0 \\ 0 & -1 \end{bmatrix} = \begin{bmatrix} \cos\alpha & -\sin\alpha \\ \sin\alpha & \cos\alpha \end{bmatrix}$$

$$= R(-\alpha)$$

the total matrix product in Eq. (4.14) is easily seen to be proportional to a rotation through an angle

$$\alpha_{\text{tot}} = \alpha_{n1} - \alpha_{n,n-1} + \cdots + \alpha_{23} - \alpha_{12} .$$

In fact, one has

$$\begin{bmatrix} P' \\ S' \end{bmatrix} = i^n \left[\prod_{j=1}^{n} x_j \right] R(\alpha_{\text{tot}}) \begin{bmatrix} P \\ S \end{bmatrix} \tag{4.15}$$

which means that the polarization vector is rotated through an angle which is either α_{tot} or $\alpha_{\text{tot}} + \pi$, depend-

ing on whether i^n is $+1$ or -1 (remember that n is even).

Consider the simple case in which Eq. (4.15) reduces to a rotation by 90° (the losses $1-\prod_{j=1}^{n}x_j$ having been balanced by the gain medium). Then after one round trip

$$\begin{bmatrix} P' \\ S' \end{bmatrix} = \begin{bmatrix} 0 & 1 \\ -1 & 0 \end{bmatrix} \begin{bmatrix} P \\ S \end{bmatrix} . \tag{4.16}$$

(For an illustration of how this can be achieved in practice, see Smith and Dorschner, 1980.) It can easily be seen that, with the orientation chosen for S and P (Figs. 16 and 15), right-circularly polarized light will be represented by the Jones vector

$$E_R = \frac{1}{\sqrt{2}} \begin{bmatrix} 1 \\ -i \end{bmatrix} .$$

(This is simply $\hat{\varepsilon}_-$ written in column form; think of P and S as the x and y components of the E field, respectively.) Analogously, LCP light is given by

$$\mathbf{E}_L = \frac{1}{\sqrt{2}} \begin{bmatrix} 1 \\ i \end{bmatrix} .$$

Equation (4.16) then gives

$$\mathbf{E}'_R = \frac{1}{\sqrt{2}} \begin{bmatrix} 0 & 1 \\ -1 & 0 \end{bmatrix} \begin{bmatrix} 1 \\ -i \end{bmatrix} = \begin{bmatrix} -i \\ -1 \end{bmatrix} = -i\mathbf{E}_R$$

$$= e^{-i\pi/2}\mathbf{E}_R ,$$

$$\mathbf{E}'_L = \frac{1}{\sqrt{2}} \begin{bmatrix} 0 & 1 \\ -1 & 0 \end{bmatrix} \begin{bmatrix} 1 \\ -i \end{bmatrix} = \begin{bmatrix} i \\ -1 \end{bmatrix} = i\mathbf{E}_L$$

$$= e^{i\pi/2}\mathbf{E}_L .$$

Hence there is a π phase difference between the RCP and LCP waves in one round trip. To satisfy the resonance condition, the new frequencies will have to be such that

$$\underset{L}{\omega_R}\frac{L}{c} \mp \frac{\pi}{2} = 2\pi m \equiv \frac{\omega_0 L}{c}$$

(where m is the mode number); that is, one has

$$\underset{L}{\omega_R} = \omega_0 \pm \frac{\pi c}{2L} \tag{4.17}$$

and hence the frequency splitting achieved between waves of opposite circular polarizations is

$$\Delta\nu = \frac{\Delta\omega}{2\pi} = \frac{1}{2\pi}(\omega_R - \omega_L) = \frac{c}{L} ,$$

that is, half the intermode spacing.

The reason for the denomination "out of plane" for these techniques is immediate from Eqs. (4.9)–(4.11): if the normals to all the mirrors lie in the same plane, all the vectors $\hat{a}_j$ are parallel and $\alpha_{ij}=0$ for all i,j. It is only by arranging the mirrors so that the plane of incidence actually changes between reflections that a rotation of the polarization can be achieved. This means the optical path cannot lie in one plane as in the usual ring lasers. For these out-of-plane cavities the gyro axis is defined by the general expression

$$\mathbf{G} = \oint \mathbf{r} \times d\mathbf{r} , \tag{4.18}$$

where the line integral runs along the optical path; $\mathbf{r}$ is the position vector and $d\mathbf{r}$ points along the propagation direction at $\mathbf{r}$.

An out-of-plane technique has been suggested (Sanders and Anderson, 1981) to minimize the round trip x-y Q and phase anisotropy. The idea is that mirrors from the same coating run have similar anisotropy characteristics: by arranging such mirrors in pairs, and rotating the polarization by 90° between reflections, anisotropies might ideally be made to cancel; and, at any rate, would be considerably reduced.

B. Self-biased laser gyros

Recently in a number of papers (Scully *et al.*, 1978; Sanders *et al.*, 1978; Anderson *et al.*, 1979,1980) a different multioscillator approach to the problem of mode locking was investigated. Theoretical work led to the conclusion that the presence of an additional pair of modes oscillating in the cavity could significantly reduce the lock-in threshold because of nonlinear coupling effect. In this scheme one would have, for example, the unusual pair of TEM_{00n} counterpropagating modes, and then a pair of (in general weaker) TEM_{01n} modes; or the second pair could have a different longitudinal mode number. An internally generated bias (which eventually could be an alternating bias) was expected to occur when the laser was pumped hard enough that the second pair of modes were brought above threshold. Experiments (Scully *et al.*, 1978; Sanders *et al.*, 1978; Anderson *et al.*, 1979) did indeed show an important reduction of lock-in in these four-mode gyros.

In one particular experiment (Anderson *et al.*, 1980; see also Chow *et al.*, 1980; Anderson, 1981) the lock-in region vanished altogether. A self-induced bias was observed that changed sign when the direction of rotation was changed, as seen in Fig. 17.

The optical spectrum of this laser was as shown in Fig. 18, which also shows the convention used here to number the modes. The "weak" Modes 1 and 4 were TEM_{01n} modes.

The frequency spacing between the strong and weak modes was $\simeq$ 60 MHz. The weak modes were only slightly above threshold; the ratio of intensities I_s/I_w was about 30. Here $I_s=(I_2+I_3)/2$ and $I_w=(I_1+I_4)/2$; these average intensities were observed to be constant in the experiment. It was also observed that the frequency differences $\nu_4-\nu_3$ and $\nu_1-\nu_2$ locked at the same value that is, $\nu_4-\nu_3=\nu_1-\nu_2$, or equivalently $\nu_3-\nu_2=\nu_4-\nu_1$; the gyro output was then $\langle\dot{\varphi}\rangle$, where

$$\varphi \equiv \frac{\psi_{32}+\psi_{41}}{2} . \tag{4.19}$$

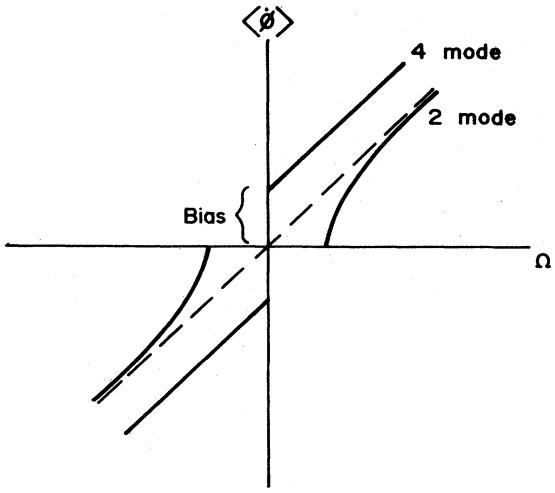

FIG. 17. Beat note vs rotation rate for the four-mode laser gyro demonstrated in Anderson *et al.* (1980). The laser exhibited lock-in when only the usual two counter-rotating modes were above threshold, and a reciprocal bias (and a linear characteristic) when it was operated with four modes.

From the above argument one expects $\dot{\psi}_{32}=\dot{\psi}_{41}$.

In the study of this 2 + 2 laser gyro it is convenient to use the normalized intensity differences

$$i_s=\frac{I_3-I_2}{2I_s},\quad i_w=\frac{I_4-I_1}{2I_w}\ . \tag{4.20}$$

From their definition, they can vary between -1 and $+1$ and in the experiment they were seen to be small. Using all the above information, one can find the following set of equations for the 2 + 2 gyro (obtained in third-order perturbation theory):

$$\frac{di_s}{dt}=-2\alpha_s' i_s+2b_s\sin\varepsilon_s\cos\varphi\ , \tag{4.21a}$$

$$\frac{di_w}{dt}=-2\alpha_w' i_w-2\theta_{sw}I_s i_s-2b_w\sin\varepsilon_w\cos\varphi\ , \tag{4.21b}$$

$$\frac{d\varphi}{dt}=S\Omega+r_w i_w+r_s i_s +[b_s i_s\sin\varepsilon_s-b_w i_w\sin\varepsilon_w]\sin\varphi\ . \tag{4.21c}$$

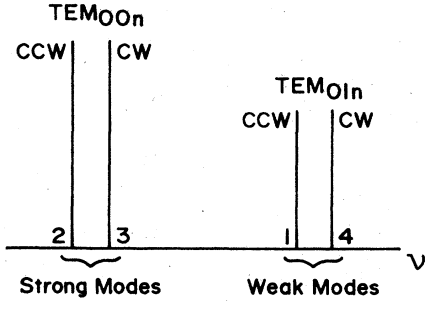

FIG. 18. The spectrum of the 2 + 2 laser gyro.

Here

$$\alpha_s'=(\beta_s-\theta_s)I_s\ ,\qquad \alpha_w'=(\beta_w-\theta_w)I_w\ , \tag{4.22}$$

where β is the third-order self-saturation coefficient, and $\theta_{s(w)}$ is the third-order cross-saturation coefficient for the strong-weak modes; θ_{sw} is a third-order cross-saturation coefficient for the strong-weak pairs; r_w and r_s are (intensity-dependent) cross mode pushing coefficients; b_w and b_s are backscattering coefficients for the weak and strong modes; and ε_s and ε_w are the average backscattering phases

$$\varepsilon_s=\frac{\varepsilon_2+\varepsilon_3}{2},\quad \varepsilon_w=\frac{\varepsilon_1+\varepsilon_4}{2}\ . \tag{4.23}$$

It can be seen that in order for the average intensities I_s and I_w to remain constant (as was observed in the experiment), ε_s and ε_w have to be odd multiples of $\pi/2$.

In Chow *et al.* (1980) and Anderson *et al.* (1980), it was shown how Eqs. (4.21) can lead to a bias (that is, a dc term in the equation for $d\varphi/dt$) under certain hypotheses. Specifically, the mode-pushing terms r_s and r_w were neglected, and the assumptions

$$\alpha_s' \gg \dot{\varphi}\ , \tag{4.24a}$$

$$\alpha_w' \ll \dot{\varphi}\ , \tag{4.24b}$$

were introduced. By virtue of the first one, it is possible to solve Eq. (4.21a) "adiabatically" (see Chow *et al.*, 1980) to get

$$i_s=b_s\frac{\sin\varepsilon_s}{\alpha_s'}\cos\varphi\ . \tag{4.25}$$

Now Eq. (4.25) may be substituted in Eq. (4.21b) to give, together with the additional hypothesis Eq. (4.24b)

$$i_w=-2A\frac{b_w\sin\varepsilon_w}{\dot{\varphi}}\sin\varphi\ , \tag{4.26}$$

where

$$A=1+\frac{b_s\sin\varepsilon_s}{b_w\sin\varepsilon_w}\frac{\theta_{sw}}{\beta_s-\theta_s}\ . \tag{4.27}$$

When Eq. (4.26) is substituted into Eq. (4.21c) one gets the following expression for the 2 + 2 beat note:

$$\dot{\varphi}=S\Omega+A\frac{b_w^2}{\dot{\varphi}}-A\frac{b_w^2}{\dot{\varphi}}\cos2\varphi+\frac{b_s^2}{2\alpha_s'}\sin2\varphi\ . \tag{4.28}$$

To see how this brings about a bias, neglect for the moment the last term in Eq. (4.28): one has then a quadratic equation in $\dot{\varphi}$, with the solution

$$\dot{\varphi}=\tfrac{1}{2}S\Omega\pm\tfrac{1}{2}[(S\Omega)^2+8b_w^2A\sin^2\varphi]^{1/2}\ . \tag{4.29}$$

It is clear that for large positive rotation rate Ω the plus sign gives the right solution, whereas for large negative Ω the minus sign is appropriate. As the rotation rate approaches zero from the positive side, one has

$$\dot{\varphi} \simeq b_w \sqrt{2A}\ |\sin\varphi| \tag{4.30}$$

which shows that $\dot{\varphi}$ has to be either positive or zero. Under these conditions the stationary (locked) solutions $\varphi = n\pi$ have to be unstable, since any small phase fluctuations can only grow. In fact, if one solves the complete equation (4.28) (including the last term) numerically, with an additional small noise term, a nonzero bias is indeed found for all values of the input rotation rate Ω.

Equations (4.21) can also be studied without neglecting the cross-pushing terms r_s and r_w. We make again the assumptions Eqs. (4.24), and write i_s in the form of Eq. (4.25). Now Eqs. (4.21b) and (4.21c) can be rewritten as

$$\frac{di_w}{dt} = -2\alpha'_w i_w - 2b_s A \sin\varepsilon_w \cos\varphi\ , \tag{4.31a}$$

$$\frac{d\varphi}{dt} = S\Omega + r_w i_w - b_w \sin\varepsilon_w i_w \sin\varphi + \frac{r_s b_s}{\alpha'_s}\sin\varepsilon_s \cos\varphi + \frac{b_s^2}{\alpha'_s}\sin\varphi\cos\varphi\ . \tag{4.31b}$$

Note that there is now a term in $\cos\varphi$ in Eq. (4.31b) for $\dot{\varphi}$. An analysis similar to the one carried out in Sec. III.C.2.b [Eqs. (3.21)–(3.24)] leads one to expect a dc term in Eq. (4.31a). In fact, if one assumes

$$i_w = b_0 + a\sin\varphi \tag{4.32}$$

substitution of this form on both sides of Eq. (4.31a) and use of Eq. (4.31b) for $\dot{\varphi}$ on the left-hand side leads (after neglecting small terms) to the result

$$b_0 \simeq \frac{1}{2(r_w + B)}\left[-S\Omega \pm \left[(S\Omega)^2 + 4b_w^2 A + 4b_w^2 A\frac{r_w}{B}\right]^{1/2}\right], \tag{4.33}$$

where

$$B = 2\frac{b_w \sin\varepsilon_w}{b_s \sin\varepsilon_s}\frac{\alpha'_s \alpha'_w}{r_s}\ . \tag{4.34}$$

When Eqs. (4.32) and (4.33) are used in Eq. (4.31b), a bias is obtained that equals $r_w b_0$. To simplify things, assume that $r_w \gg B$, which can be justified as follows: first, calculations show that r_w is larger than the estimated backscattering coefficient $b_w \simeq 10$ kHz; second, the assumption (4.24b) that $\alpha'_w \ll \dot{\varphi}$ entails [compare Eq. (4.31b)] that $\alpha'_w \ll r_s b_s / \alpha'_s$.

Then the dc term in Eq. (4.31b) reads

$$S\Omega + r_w b_0 \simeq \tfrac{1}{2}S\Omega \pm \frac{1}{2}\left[(S\Omega)^2 + 4b_w^2 A + 4b_w^2 A\frac{r_w}{B}\right]^{1/2}. \tag{4.35}$$

In the second term inside the square root one can recognize the term $8b_w^2 A \sin^2\varphi$ in Eq. (4.29), with $\sin^2\varphi$ replaced by its average value $\frac{1}{2}$. In general, the new bias will be much larger than the one obtained previously, since as stated above $r_w/B \gg 1$.

There are several important problems with this approach; some of them may be technical, and some may be of a deeper nature.

First, although α'_s, as calculated from third-order theory, does indeed satisfy Eq. (4.24a) for values of $\dot{\varphi}$ such as those shown in Fig. 16, α'_w does not satisfy Eq. (4.24b) unless a value for I_w is chosen [compare Eq. (4.22)] that has to be much smaller than the experimental values $I_w \simeq I_s/30$. Second, and more important, Eqs. (4.26) and (4.27) show that i_w may be larger than unity, which is impossible by its own definition [what happens of course, is that Eqs. (4.21) were derived assuming that both i_s and i_w were small; they are not valid if either of them is close to ± 1]. In fact, from Eqs. (4.30) and (4.26) it can be seen that, for a rotation rate close to zero,

$$|i_w| \simeq \sqrt{2A}\ . \tag{4.36}$$

From Eq. (4.27) it can be seen that A can be less than 1 if $\sin\varepsilon_s = -\sin\varepsilon_w$; but again the third-order coefficients θ_{sw}, β_s, and θ_s make it hard to get $A < 0.5$ (except if b_w is carefully chosen).

These problems may just be an indication that third-order perturbation theory is not appropriate for this 2 + 2 laser gyro, which, after all, is not surprising, since the two strong modes are operating very far above threshold. A more important objection is as follows: both Eqs. (4.29) and (4.35) give a beat note that tends to $S\Omega$ for large input rotation rate; that is, the bias goes to zero as $\Omega \to \infty$. This contrasts with the constance of the bias exhibited by the experimental results. Also, the choice of a sign in either Eq. (4.29) or (4.35) for small (close to zero) rotation rates is, after all, arbitrary; the solution with the plus sign, say, does not end sharply at $\Omega = 0$: rather, it goes smoothly to zero for large negative Ω. Under these circumstances, one would expect the system to exhibit some hysteresis in the region around $\Omega = 0$: but the experimental results show no trace of this.

A different approach has been presented in Anderson (1981). There the amplitude and phase determining equations (in third-order theory) were solved for the steady state, in the absence of backscattering. The general system has six differential equations, for I_1, I_2, I_3, I_4, $\psi^- \equiv \psi_{32} - \psi_{41}$, and φ; the latter variable is decoupled from the rest, in the absence of backscattering, so that the first five equations could be simultaneously solved.

It was found that there were steady-state solutions having $i_w \neq 0$; from Eq. (4.21c), this implies the existence of a bias $r_w i_w$, which is calculated in Anderson (1981). The assumption is that even in the presence of backscattering, the system remains close enough to the steady-state solution so that the bias term would still be present in Eq. (4.21c), and would, in turn, minimize the effect of backscattering.

The trouble with this theory is that it assumes that the steady-state solutions with $i_w \neq 0$ are stable; in fact, it can be shown that they are unstable with respect to small fluctuations in the phase difference ψ^-. This makes the

validity of the main claim questionable.

Also in Anderson (1981) it was claimed that the locked solutions ($\dot{\varphi}=0$) were unstable. The relevance of this can only be assessed after a numerical study of the six equations shows what the actual behavior of the system is (since all the steady-state solutions are then unstable); one could, for instance, still have $\langle\dot{\varphi}\rangle=0$.

Finally, as with the theory sketched in this section, no definitive explanation for the absence of hysteresis was presented.

In conclusion, the 2 + 2 laser gyro is still far from being clearly understood. Only further investigations (including probably a strong-signal treatment of the strong modes) will clarify the nature of the bias, whether it is "static" in origin, as contended in Anderson (1981) or "dynamic" [meaning that it depends on the backscattering, as evidenced by both Eq. (4.29) and Eq. (4.35)], as proposed in Anderson *et al.* (1980). The interest of the problem, however, is obvious: an understanding of how the self-induced bias arises may lead to the simplest practical laser gyro so far, with no moving parts, no intracavity elements, and no applied external magnetic fields or complicated mirror arrangements.

V. NOISE IN OPTICAL ROTATION SENSORS

A. Quantum noise in ring laser gyroscopes

1. Spectrum of the beat signal and locking in the presence of noise

a. Introduction

Up to now we only considered the ring laser in the framework of Lamb's semiclassical laser theory, which means we treated the laser atoms quantum mechanically, whereas the electric field was considered to be a classical quantity. However, by using the canonical quantization it can become itself an operator. From this point of view the electric field is a superposition of an infinite number of independent (quantum-mechanical) harmonic oscillators described by their creation or destruction operators $a_j^\dagger$ or a_j, respectively, which are quantized in the canonical way (Wentzel, 1949),

$$[a_j,a_k^\dagger]=\delta_{jk} \ . \tag{5.1}$$

This problem was solved in the late 1960s and is here applied to the laser gyro problem (Scully and Lamb, 1967; Sargent *et al.*, 1970). This quantization gives rise to some new effects such as the infinite zero-point energy of the field, the vacuum fluctuations, and spontaneous emission. Due to spontaneous emission the laser field has a random phase and, therefore, the phase of the electric field in the cavity is no longer well determined: it becomes a stochastic quantity. This is crucial, because by using a ring laser as a gyroscope one is measuring, as explained in Sec. I, the phase or frequency difference between the counterpropagating waves. Therefore, the quantum noise influences the output.

The study of the quantum noise is, therefore, extremely important to determine the ultimate sensitivity of ring laser gyroscopes. All other noise sources, as, for example, vibrations of the laser mirrors, can be overcome by some clever technique. But there is no way to get around the quantum noise which stems from the quantization condition (5.1).

In this section we are going to discuss the influence of the quantum noise due to spontaneous emission of laser atoms on two characteristics of the gyroscope, namely the mean beat frequency rotation/rate characteristic and the spectrum of the mean beat signal by summarizing the results presented in Cresser (1982) and Cresser *et al.* (1982a,1982b). For the influence of quantum noise on the locking curve of a dithered gyro, see Schleich *et al.* (1984). In Sec. V.A.2 we will discuss the error introduced by quantum noise into rotation rate measurements.

b. Theory of fluctuations: Langevin and Fokker-Planck methods

Due to spontaneous emission of the laser atoms the phase of the electric field in the cavity is a stochastic variable. The equation of motion for the phase difference between the two counterpropagating waves, Eq. (3.12), now reads

$$\dot{\psi}=a+b\sin\psi+F(t) \ , \tag{5.2}$$

where we feed in the noise by the fluctuating force $F(t)$ which we assume to be Gaussian with mean zero

$$\langle F(t)\rangle=0 \tag{5.3}$$

where $\langle\ \rangle$ denotes the ensemble average. (Here $a=s\Omega$.) This type of problem is well known from the problem of injection locked (symmetry broken) lasers (Chow *et al.*, 1975).

Such stochastic equations are called Langevin equations. A rigorous derivation of Eq. (5.2) can be found in Cresser *et al.* (1982a).

In noise theory one often uses the expressions system and reservoir. The reservoir is coupled to the system and feeds noise in. This causes the system variable to fluctuate around a mean value and according to the fluctuation-dissipation theorem, also causes damping.

In our problem the reservoir is represented by the laser atoms and the system is the laser field in the cavity, the system variable is the phase of the electric field. Comparing the correlation time of the reservoir τ_c (i.e., the decay time of the atoms) with the damping time of the electric field $1/\gamma$ we find

$$\tau_c \ll 1/\gamma \ .$$

Therefore, on the time scale of the electric field we can assume for the two-time correlation function

$$\langle F(t)F(s)\rangle=2D\delta(t-s) \ , \tag{5.4}$$

where

$$D=\frac{\omega}{2Q\langle n\rangle} \tag{5.5}$$

denotes the diffusion constant of this stochastic process ($\langle n\rangle$ is the average number of photons in the field at steady state and Q the quality factor of the cavity). Equation (5.5) is valid only when all angular variables are measured in radians. Its derivation may be found, e.g., in Sargent *et al.* (1974, Sec. 20.3) (it has been assumed that the laser is operating far above threshold; otherwise the expression for D is more complicated).

There are basically two approaches to calculate the average of a function $f(\psi)$ depending on a stochastic variable ψ: the Langevin and the Fokker-Planck methods. In the Langevin approach one solves the equation of motion for ψ in terms of integrals of the fluctuating force F, substitutes this back into $f(\psi)$ and performs the average using Eqs. (5.3) and (5.4) together with the property that $F(t)$ is Gaussian. This approach is difficult in many cases, because one is unable to solve the Langevin equation, which is, at least in the problems of interest, nonlinear; see Eq. (5.2).

A more promising approach is the Fokker-Planck approach, in which one derives a partial differential equation for the conditional probability $P(t,\psi\mid t_0,\psi_0)$—the probability to find at time t the value ψ, given that the value at t_0 was ψ_0—and substitutes this into the familiar expression for an average

$$\langle f(\psi)\rangle=\int d\psi\, P(\psi)f(\psi)\ .$$

This method works fine because in most of the cases one is able to solve the Fokker-Planck equation exactly, in terms of infinite (matrix) continued fractions, a method developed by Risken and co-workers (Risken, 1983).

The Fokker-Planck equation for this problem corresponding to Eq. (5.2)

$$\frac{\partial P}{\partial t}=-\frac{\partial}{\partial\psi}[(a+b\sin\psi)P]+D\frac{\partial^2 P}{\partial\psi^2} \tag{5.6}$$

subject to periodic boundary conditions can be solved approximately in various regions of the rotation rate as well as exactly in terms of infinite continued fractions. In the paper by Cresser *et al.* (1982a) approximate analytical results were obtained for the spectrum of the beat signal in some regions of the rotation rate working in the Fokker-Planck method. These results can also be derived using the Langevin approach (Schleich, 1981). In Cresser *et al.* (1982b) the exact expressions for the spectrum of the beat signal and the mean beat frequency in terms of continued fractions were presented and finally approximate analytical expressions for the spectrum for a certain range of the rotation rate working in the Langevin approach were obtained by Cresser (1982).

c. Spectrum of the laser gyro's beat signal

In Sec. III [see Eq. (3.1)] it was shown that the beat signal is up to a nonessential constant factor given by $\cos\psi(t)$, where the equation of motion for the relative phase ψ between the two counterpropagating waves is Eq. (5.2). Before we proceed to discuss the spectrum of the beat signal in the presence of noise, it is worthwhile to consider the noise-free case (i.e., $F=0$) first.

(i) Noise-free case: $F=0$

As explained in Sec. III.C.1 in the locked zone the phase settles down at steady state to a constant value ψ_s for which $\dot\psi=0$, namely

$$\psi_s=\pi+\arcsin\frac{a}{b}$$

[compare Eq. (3.13)]. The power spectrum of such a constant beat signal is (Champeney, 1971)

$$\begin{aligned}\alpha_{\rm NF}(\omega)&=\int_{-\infty}^{\infty}dt\cos^2\psi_s e^{i\omega t}\\&=2\pi\left[1-\left[\frac{a}{b}\right]^2\right]\delta(\omega)\ .\end{aligned} \tag{5.7}$$

The spectrum therefore consists of a δ function centered at a zero beat frequency and so expresses the existence of a dead band. In the presence of noise the strength of this δ-function component will be diminished as we will see later. In addition a broad background contribution not present in Eq. (5.7) will appear.

Outside the dead band, i.e., for $\mid a\mid > b$, the noise-free spectrum consists of a fundamental at $\Gamma=(a^2-b^2)^{1/2}$, i.e., the mean beat frequency of the gyro [Eq. (3.15)], and higher harmonics at the frequencies $n\Gamma$:

$$\alpha_{\rm NF}=\sum_{\substack{n=-\infty\\ n\neq 0}}^{\infty}w_n\delta(\omega-n\Gamma)\ , \tag{5.8}$$

where the weight w_n of the nth harmonic is

$$w_n=2\pi\left[\frac{\Gamma}{b}\right]^2\left[\frac{\mid a\mid-\Gamma}{b}\right]^{2\mid n\mid}\ .$$

The laser gyro can sustain harmonics because of the nonlinear character of the backscattering. Note also that there is no δ-function contribution at the frequency $\omega=0$, which would indicate a locking behavior.

As we will see later, the higher harmonics appearing in the deterministic problem are also observed in the presence of noise, with the major difference that each component is then broadened instead of being a δ function. In addition we will see the appearance of a δ-function contribution at $\omega=0$, which we have already seen in the locked zone.

(ii) Spectrum in the presence of quantum noise

In order to avoid the complexities associated with the definition of a spectrum for nonstationary processes (Cresser, 1983), we limit our discussions to situations where the laser gyro is allowed to reach steady-state

operating conditions before a measurement is performed. In this case it is found that the beat signal $\cos\psi$ can be represented as a stationary stochastic process, so that we can make use of the Wiener-Khintchine theorem and define the spectrum as

$$\alpha(\omega)=\int_{-\infty}^{\infty} d\tau e^{i\omega\tau}\langle\cos\psi(\tau)\cos\psi(0)\rangle \ . \tag{5.9}$$

The correlation function $\langle\cos\psi(\tau)\cos\psi(0)\rangle$ can be written (Cresser *et al.*, 1982a) as

$$\langle\cos\psi(\tau)\cos\psi(0)\rangle=\int_0^{2\pi} d\psi_1\int_0^{2\pi} d\psi_2\cos\psi_1\cos\psi_2 \times P(\psi_1,\tau\mid\psi_2,0)P_{ss}(\psi_2) \ ,$$

where $P(\psi_1,t\mid\psi_2,0)$ is a solution of the Fokker-Planck equation (5.6) and P_{ss} denotes the steady-state solution of Eq. (5.6).

The procedure to solve Eq. (5.6) and calculate the correlation function $\langle\cos\psi\cos\psi(0)\rangle$ in order to find $\alpha=\alpha(\omega)$ in terms of continued fractions is shown in Cresser *et al.* (1982b), and we quote only the results.

The spectrum is found to be always separable into a "coherent" δ-function contribution at zero frequency, representing the effects of locking and an "incoherent" part of nonzero bandwidth,

$$\alpha(\omega)=\alpha_D\delta(\omega)+\mathscr{B} \ ,$$

where $\mathscr{B}$ represents the broad spectrum. It is instructive to compare the strength of the δ-function contribution α_D to the overall integrated spectrum

$$\alpha_I=\int_{\infty}^{\infty} d\omega\,\alpha(\omega)$$

as a function of rotation rate (see Fig. 19). For laser rotation rates corresponding to the locked zone in the absence of noise, the tendency for locking as measured by the strength of the "coherent" contribution continues to dominate, but this effect rapidly becomes negligibly small outside this zone. Moreover, for rotation rates near the boundary of the locked region, the "incoherent" component starts to give an important contribution. Note that this happens already for rotation rates $a<b$, which indicates that the noise tends to unlock the system.

Now we are going to discuss the behavior of the spectrum $\alpha=\alpha(\omega)$ as the rotation rate decreases from some large value to zero by pointing out analogies to the single mode laser and the laser with injected signal (Chow *et al.*, 1975).

For $a\gg b$, one can essentially neglect the effects of backscattering, i.e., set $b=0$. The two counterpropagating modes are therefore decoupled and the spectrum is that of a single-mode laser. This is not surprising because for $b=0$ Eq. (5.2) reduces to

$$\dot{\psi}=a+F(t) \tag{5.10}$$

which is up to the constant factor a the phase equation for the usual laser (Sargent, Scully, and Lamb, 1974). Therefore, it is not surprising to find

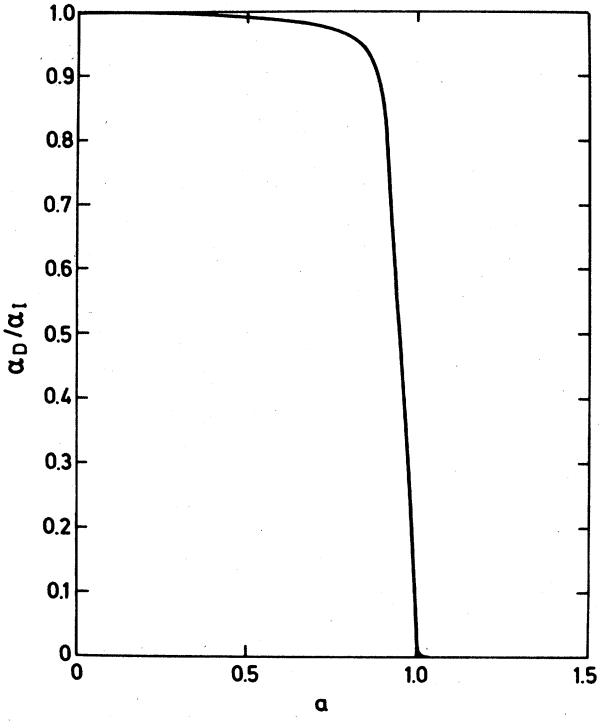

FIG. 19. Area of the δ-function part of the spectrum relative to its total area and as a function of the rotation rate a. $b=1$, $D=10^{-2}$. [Taken from Cresser *et al.* (1982b).]

$$\alpha(\omega)=\frac{1}{2}\left[\frac{D}{(\omega-a)^2+D^2}+\frac{D}{(\omega+a)^2+D^2}\right] , \tag{5.11}$$

i.e., Lorentzians with a width D around the frequencies $\pm a$. The symmetry of the spectrum arises from the fact that due to the heterodyning of the counter-rotating waves the spectrum is given by $\cos\psi$ in contrast to the usual laser, where one measures

$$\langle E^+(\mathbf{r},t')E^-(\mathbf{r},t)\rangle\sim e^{i[\varphi(t')-\varphi(t)]} \ .$$

As the rotation rate $\mid a\mid$ is decreased, the backscattering becomes more important. It brings a nonlinear element to the system and the gyro can sustain higher harmonics, as indicated in Figs. 20(e) and 20(f). An approximate analytical expression for the spectrum was found by Cresser (1982) for $\mid a\mid\gtrsim b$ and for sufficiently weak noise $D\ll b$,

$$\alpha(\omega)=\frac{\pi D^2}{2}\left[\frac{\mid a\mid-\Gamma}{b}\right]^2\left[\frac{\mid a\mid-\Gamma}{\mid\lambda_2\mid^2}-\frac{2\mid a\mid}{\mid\lambda_1\mid^2}\right]^2\delta(\omega) + \left[\frac{\Gamma}{b}\right]^2\sum_{\substack{n=-\infty\\ n\neq 0}}^{\infty}\left[\frac{\mid a\mid-\Gamma}{b}\right]^{2\mid n\mid} \times\frac{2n^2d}{(\omega-n\Gamma)^2+n^4d^2} \ , \tag{5.12}$$

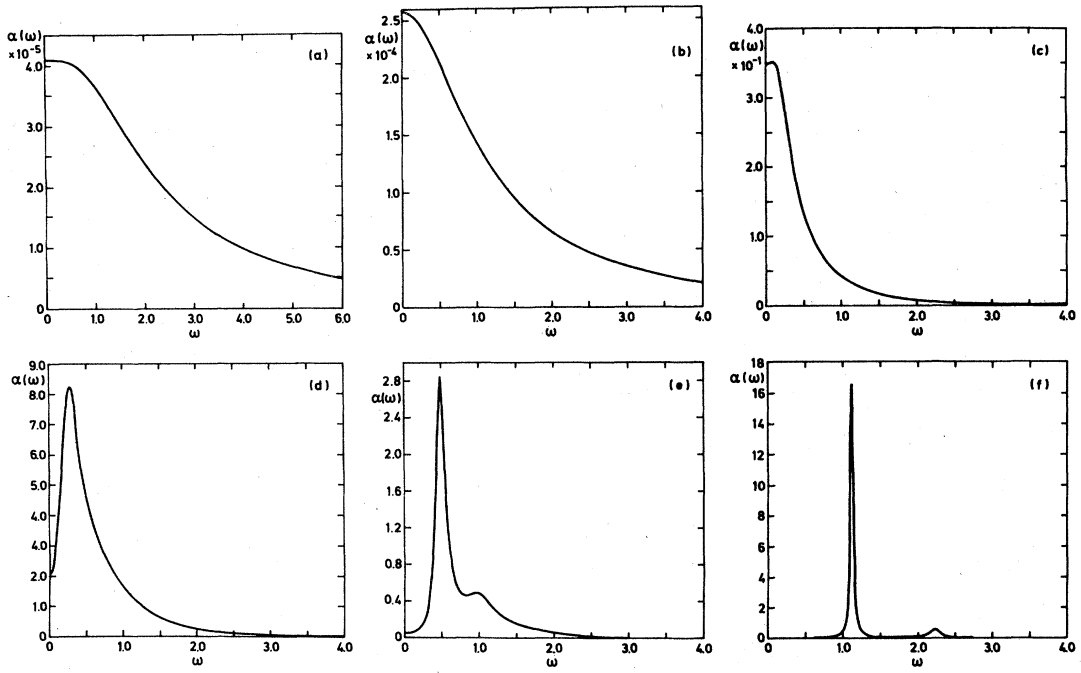

FIG. 20. "Incoherent" part of the beat signal spectrum where $b=1$, $D=10^{-2}$. (a) $a=0$, (b) $a=0.1$, (c) $a=0.95$, (d) $a=1.0$, (e) $a=1.1$, and (f) $a=1.5$. [Taken from Cresser *et al.* (1982b).]

where

$$d\equiv\frac{D(a^2+\frac{1}{2}b^2)}{\Gamma^2}\ ,$$

$$\lambda_n\equiv -in\Gamma+n^2d\ .$$

We notice that the harmonics predicted in the noise-free case [Eq. (5.8)] are now broadened, while the δ-function contribution at $\omega=0$, which we have already seen in the locked zone, has persisted, though diminished. This indicates that the locked region in the presence of noise is not well defined anymore.

For $|a|\lesssim b$ the system, rather than being completely locked as would be the case in the absence of noise, still presents a component of the spectrum centered at a nonzero beat frequency as indicated in Figs. 20(c) and 20(d).

Within the locked zone $|a|<b$, in the absence of noise, the phase ψ is known to settle down to a steady-state value ψ_s. In the presence of noise the phase does not diffuse very far from this value, provided the noise is weak. Under these considerations it is possible to linearize the Langevin equation (5.2). This situation is very similar to that of a laser with an injected signal: the phase of the laser is constrained to a very small range about the injected phase.

The spectrum can be evaluated approximately and consists of a δ function centered at zero frequency, as in the noise-free case, and an "incoherent" part of an infinite sum of Lorentzians all centered at $\omega=0$,

$$\alpha(\omega)=e^{-D/\gamma}\left\{2\pi\left[1-\left[\frac{a}{b}\right]^2\right]\delta(\omega)+2\frac{a^2D}{b^2\gamma}\frac{\gamma}{\omega^2+\gamma^2}+2\left[\frac{D}{\gamma}\right]^2\frac{2\gamma}{\omega^2+(2\gamma)^2}+\cdots\right\}, \tag{5.13}$$

where

$$\gamma\equiv(b^2-a^2)^{1/2}\ . \tag{5.14}$$

Thus the δ-function contribution in Eq. (5.13) represents the tendency for locking to occur even in the presence of noise. However, the strength of this term decreases with increasing rotation rate; that is, the locking effect decreases as one moves away from the center of the locked region.

We also note the presence of two Lorentzians centered at $\omega=0$, the narrowest of which is absent for $a=0$ but which eventually dominates the second broader Lorentzian for increasing a. The exact numerical solution [see Figs. 20(a) and 20(b)] clearly shows a broad background to the δ function which has a width 2γ for $a=0$ but rapidly narrows to have a width of γ for increasing a, as predicted by Eq. (5.13). Finally we note that the parameter γ itself is a decreasing function of a [see Eq. (5.14)] so that as a is increased further, there is a continued decrease in the width of the background spectrum.

d. Mean beat frequency in the presence of noise

As mentioned before due to the quantum noise the dead band of the ring laser gyro is no longer defined. This is

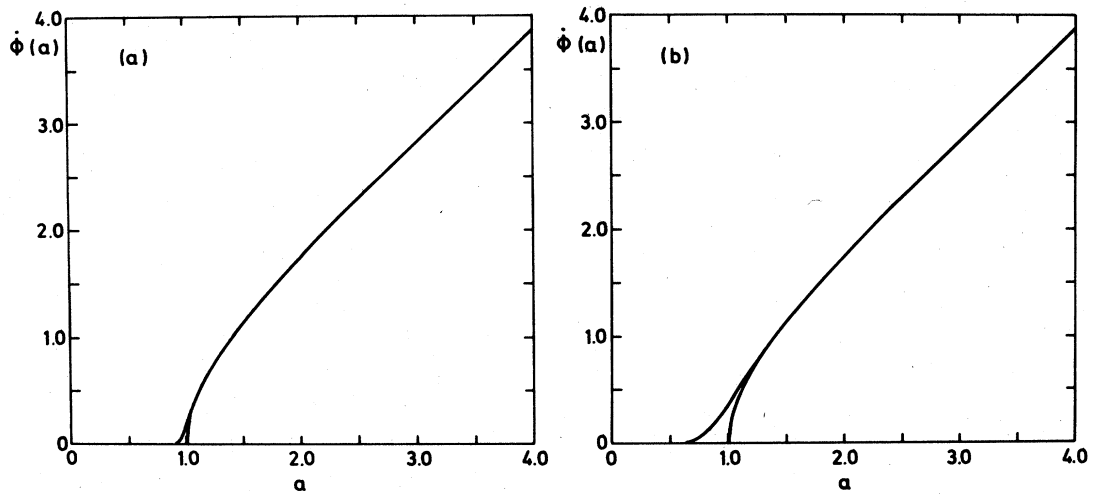

FIG. 21. Mean beat frequency $\langle \dot{\varphi} \rangle$ as a function of the rotation rate a, compared to the noiseless response curve, $b=1$. (a) $D=10^{-2}$ and (b) $D=10^{-1}$. [Taken from Cresser *et al.* (1982b).]

also confirmed by the mean beat frequency (Fig. 21) in which it can clearly be seen that due to the noise unlocking tends to occur at smaller values of a. However, far away from the locking region ($a \gg b$) the curve coincides with the deterministic curve. Therefore, in the laser gyro with noise, there is no sharp boundary as one goes from $|a| < b$ to $|a| > b$. Rather the system goes continuously from a completely locked region to an essentially unlocked region. Where the transition exactly occurs depends on the strength of the random fluctuations as demonstrated for $D=10^{-2}$ and 10^{-1} in Figs. 21(a) and 21(b), respectively. In conclusion we emphasize that the quantum noise plays a useful role in unlocking the laser gyro.

2. Gyro quantum limit

As has been mentioned before, the limit that the quantum noise discussed above imposes on the performance of ring laser gyros has recently become of practical interest. In Hammons and Ashby (1981) and Dorschner *et al.* (1980) operation at this quantum limit has been reported; the device in Hammons and Ashby (1981) was a mechanically dithered gyro, whereas the one in Dorschner *et al.* (1980) was a DILAG.

It is well known that a laser initially prepared in a pure state will evolve into a statistical mixture in time, the evolution being characterized by the exponential decay of the off-diagonal density matrix elements (Sargent, Scully, and Lamb, 1974, Sec. 17.3). In this process, the phase uncertainty grows with time. Since any actual measurement of the phase must extend over a finite time this phase diffusion process has to be considered.

The occurrence of a "randomization of the phase" is a consequence of the existence of a nonzero intrinsic laser linewidth (and vice versa) and the mechanism responsible for it is spontaneous emission. This can be qualitatively understood as follows. The process of stimulated emission alone induces all atoms to emit in exactly the same mode, the one that is above threshold, and with a phase that is driven by the macroscopic field. Hence in the absence of any other mechanism that would cause photons to be emitted in other cavity modes, it would lead to an infinitely sharp spectrum, that is, a vanishing laser linewidth. Spontaneous emission, on the other hand, occurs randomly and with roughly the same probability in every possible mode of the field, and in this way disrupts the monochromaticity (and also the phase coherence) of the lasing process. It is not surprising, therefore, that the laser linewidth [D in Eq. (5.5)] turns out to be inversely proportional to $\langle n \rangle$ since this is the main factor in the ratio of the spontaneous emission rate to the stimulated emission rate.

The connection between phase diffusion and laser linewidth, and their relation to spontaneous emission is worked out in detail in, for example, Sargent, Scully, and Lamb (1974, Sec. 20.3).

We showed above how the coefficient D that appeared in the correlation function (5.4) for the quantum noise coincided with the laser linewidth [in the unlocked regime: see Eq. (5.11)]. It is easy to see how the same coefficient D is related to phase diffusion by starting from Eq. (5.10) for the unlocked regime ($a \gg b$):

$$\dot{\psi} = a + F(t) \tag{5.15}$$

which may be integrated to give

$$\psi(t) = at + \int_0^t F(t')dt' \, . \tag{5.16}$$

Now, using Eq. (5.3), we see that the average value of the phase is still given by at, as it should,

$$\langle \psi(t) \rangle = at + \int_0^t \langle F(t') \rangle dt' = at \tag{5.17}$$

but the fluctuations of $\psi(t)$ about its average value are given by (in rms value)

$$\{\langle[\psi(t)-at]^2\rangle\}^{1/2}=\left[\left\langle\left[\int_0^t F(t')dt'\right]^2\right\rangle\right]^{1/2}$$
$$=\left[\int_0^t dt'\int_0^t dt''\langle F(t')F(t'')\rangle\right]^{1/2}$$
$$=\left[\int_0^t dt'\int_0^t dt''2D\delta(t'-t'')\right]^{1/2}$$
$$=\sqrt{2Dt}\ , \tag{5.18}$$

where use has been made of Eq. (5.4). We may write Eq. (5.18) as

$$\Delta\psi\equiv[\langle(\psi-\langle\psi\rangle)^2\rangle]^{1/2}=\sqrt{2Dt}\ , \tag{5.19}$$

where $\Delta\psi$ is the rms error in the phase difference between counter-rotating waves and t is the measurement time. An error in ψ translates into an error in the determination of the input rotation angle, according to Eq. (3.2), where the proportionality factor is the scale factor S of Eq. (1.15). Hence we have, if θ is the rotation angle,

$$\Delta\theta=\frac{1}{2\pi}\frac{\lambda L}{4A}\Delta\psi=\frac{1}{2\pi}\frac{\lambda L}{4A}\sqrt{2Dt}$$
$$=\frac{1}{2\pi}\frac{\lambda L}{4A}\left[\frac{\omega}{Q\langle n\rangle}\right]^{1/2}\sqrt{t} \tag{5.20}$$

using Eq. (5.5). Here the factor of $(1/2\pi)$ ensures that both $\Delta\psi$ and $\Delta\theta$ are expressed in radians.

The average number of photons can be related to the power loss per mode by the formula

$$P_{\text{loss}}=\frac{\hbar\omega\langle n\rangle}{Q/\omega}\ . \tag{5.21}$$

Hence Eq. (5.20) can be written as

$$\frac{\Delta\theta}{\sqrt{t}}=\frac{1}{2\pi}\frac{\lambda L}{4A}\frac{\omega}{Q}\left[\frac{\hbar\omega}{P_{\text{loss}}}\right]^{1/2}\ . \tag{5.22}$$

Or, introducing a dimensionless parameter l (cf. Hammons and Ashby, 1981) giving the fractional loss per round trip (just as in Sec. IV.A) we can write $P_{\text{loss}}=lP_i$, where P_i is the power per mode inside the cavity, and $\omega/Q=lc/L$, giving

$$\frac{\Delta\theta}{\sqrt{t}}=\frac{1}{2\pi}\frac{\lambda c}{4A}\left[\frac{l\hbar\omega}{P_i}\right]^{1/2}\ . \tag{5.23}$$

The power in the cavity may in turn be related to the output power via the transmission of the output mirror. A factor may be added to Eq. (5.22) or Eq. (5.23) to account for the fact that the lower level is not completely empty, which has a small effect on the linewidth, Eq. (5.5). (See, for example, Dorschner *et al.*, 1980; or Yariv, 1967.)

Equations (5.22) and (5.23) have been written as diffusion coefficients, that is, $\Delta\theta/\sqrt{t}$ has units of rad/$\sqrt{\text{sec}}$. For the four-mode DILAG of Dorschner *et al.* (1980), this diffusion coefficient is smaller by a factor of $\sqrt{2}$, which can be understood as follows. First, the scale factor for a DILAG is twice that for a two-mode gyro of the same characteristics [see Eq. (4.2)], and we divide by the scale factor in Eq. (5.20); second, as Eq. (4.2) shows, in a DILAG one adds four frequencies, not just two; hence the rms error of Eq. (5.19) gets multiplied by $\sqrt{2}$. Hence the overall factor $(1/\sqrt{2})$.

The diffusion coefficient (5.22) was evaluated (Hammons and Ashby, 1981) to be equal to 3×10^{-4} deg/$\sqrt{\text{h}}$ for a He-Ne laser (two mode) with a power loss per mode of 35 μW. This value should be compared with the mechanical "dither noise" for the same laser, given in the following section. In Dorschner *et al.* (1980), where no external noise sources were apparent, the frequency noise measured was in good agreement with the theoretical prediction. Hence the present laser gyro technology may be said to be at the point where purely quantum-mechanical errors (in this case the one due to spontaneous emission, as discussed above) become observable.

So far we have only talked about the error in a measurement of the rotation angle, or equivalently the phase difference. If we are interested in the rotation *rate* instead, it is the uncertainty in the *frequency* difference that we want to consider. Now $\Omega=\theta/t$ (as long as Ω can be considered to be constant); hence the uncertainty in the rotation rate *decreases* with increasing observation time, as $1/\sqrt{t}$.

In terms of the laser frequency difference now, we may think of an experiment in which we measure ψ repeatedly, over a time interval Δt each time. From Eq. (5.18), the rms error in the frequency difference $\omega=\psi/\Delta t$ will be, for each individual measurement

$$\Delta\omega=\frac{\Delta\psi}{\Delta t}=\left[\frac{2D}{\Delta t}\right]^{1/2}\ . \tag{5.24}$$

If we perform N such measurements, the rms error will be decreased by a factor $\sqrt{N}$ (provided ω is constant on the average, that is, provided that we are always measuring the same thing). The final error will be

$$\Delta\omega=\left[\frac{2D}{N\Delta t}\right]^{1/2}=\left[\frac{2D}{T}\right]^{1/2}\ , \tag{5.25}$$

where T is the total observation time. An analogous reasoning applies to the determination of the rotation rate in the laser gyro: for both magnitudes, the statistical uncertainty decreases with longer observation times. The opposite is the case, as we have seen, for the rotation angle.

B. Noise in dithered systems

In Sec. III.C.2 the lock-in equation for a sinusoidally dithered laser gyro was derived [Eq. (3.25)]:

$$\dot{\varphi}=\tilde{a}+bJ_{-r}\left[\frac{\alpha}{\omega_D}\right]\sin\varphi\ . \tag{5.26}$$

It was mentioned there that random mechanical noise could cause the Bessel function J_{-r} in Eq. (5.26) to aver-

age to zero over several dither periods, effectively giving an average beat note free from lock-in effects,

$$\langle\dot{\varphi}\rangle=\tilde{a} \text{ or } \langle\psi\rangle=at \ . \tag{5.27}$$

However, the output δ is now a stochastic variable. In this section we want to calculate its dispersion. Our treatment will essentially follow Hammons and Ashby (1981). We want to point out that what follows can in no way be considered mathematically rigorous. An exact treatment of this problem (which involves multiplicative noise) does not exist in the literature so far (to the best of our knowledge). One can only hope that the treatment presented here yields a useful order-of-magnitude estimate.

We consider $J_{-r}(\alpha/\omega_D)$ to be a random variable in time with zero average. Since α/ω_D is large, we may make use of the asymptotic form

$$J_{-r}\left[\frac{\alpha}{\omega_D}\right]\simeq\left[\frac{2\omega_D}{\pi\alpha}\right]^{1/2}\cos\left[\frac{\alpha}{\omega_D}+\tfrac{1}{2}r\pi-\tfrac{1}{4}\pi\right] . \tag{5.28}$$

Small fluctuations in α do not affect the square root in Eq. (5.28), but they may cause the cosine to "wash out." We may take these fluctuations to be essentially uncorrelated over a time equal to half the dither period,

$$\tau_c=\frac{1}{2}\frac{2\pi}{\omega_D} . \tag{5.29}$$

This can be justified by assuming that random errors are more likely to occur at the times when the bias is reversed (that is, the rotation changes sign) which happens twice in a dither period. Also, the phase of the gyro is particularly sensitive to any small fluctuations at those "switching times," when the bias is momentarily smaller than the backscattering term [see Eq. (3.20)]. All of this leads one to postulate for the random variable $J_{-r}(\alpha/\omega_D)$ a correlation function of the form

$$\left\langle J_{-r}\left[\frac{\alpha}{\omega_D}(t')\right]J_{-r}\left[\frac{\alpha}{\omega}(t'')\right]\right\rangle\sim e^{-|t'-t''|/\tau_c} , \tag{5.30}$$

where a stationary random process has been assumed (i.e., the correlation function depends only on the time difference $t'-t''$). The details of the functional form used in Eq. (5.30) are not really important. To determine the proportionality factor, note that, for $t'=t''$,

$$\left\langle J_{-r}\left[\frac{\alpha}{\omega_D}(t')\right]J_{-r}\left[\frac{\alpha}{\omega_D}(t')\right]\right\rangle \simeq\frac{2\omega_D}{\pi\alpha}\left\langle\cos^2\left[\frac{\alpha}{\omega_D}(t')-\frac{\pi}{4}\right]\right\rangle=\frac{1}{2}\frac{2\omega_D}{\pi\alpha} . \tag{5.31}$$

Hence we may write

$$\left\langle J_{-r}\left[\frac{\alpha}{\omega_D}(t')\right]J_{-r}\left[\frac{\alpha}{D}(t'')\right]\right\rangle=\frac{\omega_D}{\pi\alpha}e^{-|t'-t''|/\tau_c} . \tag{5.32}$$

Now from Eq. (5.26) we have

$$[\varphi-\tilde{a}(t-t_0)]^2=b^2\int_{t_0}^{t}dt'\int_{t_0}^{t}dt''J_{-r}\left[\frac{\alpha}{\omega_D}(t')\right]J_{-r}\left[\frac{\alpha}{\omega_D}(t'')\right]\sin\varphi(t')\sin\varphi(t'') . \tag{5.33}$$

As we did in Sec. III.C.2, we want to look at time intervals $t-t_0$ which are large compared to a dither cycle but small enough that φ does not vary appreciably. Then we can take $\sin\varphi$ outside the double integral. The average value of Eq. (5.33) then [using Eq. (5.32)] may be written as

$$\begin{aligned}\langle[\varphi-\tilde{a}(t-t_0)]^2\rangle&=b^2\sin^2\varphi\frac{\omega_D}{\pi\alpha}\int_{t_0}^{t}dt\int_{t_0}^{t}dt''e^{-|t'-t''|/\tau_c}\\&=b^2\sin^2\varphi\frac{\omega_D}{\pi\alpha}[2\tau_c(t-t_0)-2\tau_c^2(1-e^{-(t-t_0)/\tau_c})] .\end{aligned} \tag{5.34}$$

Again, since we are assuming $t-t_0\gg\tau_c=\pi/\omega_D$, we may approximate Eq. (5.34) by

$$\begin{aligned}\langle[\varphi-\tilde{a}(t-t_0)]\rangle&\simeq b^2\sin^2\varphi\frac{\omega_D}{\pi\alpha}2\tau_c(t-t_0)\\&=b^2\sin^2\varphi\frac{\omega_D}{\pi\alpha}\frac{2\pi}{\omega_D}(t-t_0)\\&=\frac{2b^2}{\alpha}\sin^2\varphi(t-t_0) .\end{aligned} \tag{5.35}$$

Hence if we define the uncertainty in the gyro phase

$$\Delta\psi=\{\langle[\varphi-\tilde{a}(t-t_0)]^2\rangle\}^{1/2} \tag{5.36}$$

we see that it grows as in a diffusion (random walk) process:

$$(\Delta\psi)^2=\frac{2b^2}{\alpha}\sin^2\varphi\,\Delta t . \tag{5.37}$$

When considering the phase diffusion over a time span Δt larger than several periods of the frequency $\tilde{a}$ (that is, $\Delta t\gg2\pi/\tilde{a}$), we may replace $\sin^2\varphi$ by its average value $\frac{1}{2}$. We therefore obtain

$$\Delta\psi=\frac{b}{\sqrt{\alpha}}\sqrt{\Delta t} . \tag{5.38}$$

Note that in Eq. (5.38) the units for b and α are radians per second, those for Δt are seconds, and those for $\Delta\psi$ radians. The equivalent uncertainty in the angle rotated by the gyro can be obtained by dividing Eq. (5.38) by the scale factor S, where, as usual,

$$S=2\pi\frac{4A}{L\lambda}\frac{\text{rad/sec}}{\text{rad/sec}} . \tag{5.39}$$

That is, if θ is the rotation angle in radians

$$\Delta\theta=\frac{b}{S}\left[\frac{\Delta t}{\alpha}\right]^{1/2} . \tag{5.40}$$

In commonly used units, Eq. (5.32) reads (in radians)

$$\Delta\theta=\frac{b'}{S'}\left[\frac{\Delta t}{2\pi\alpha'}\right]^{1/2} , \tag{5.41}$$

where b' and α' are expressed in Hz (that is, $b'=b/2\pi$, $\alpha'=\alpha/2\pi$) and $S'=4A/L\lambda$ (counts/sec)/(radians/sec). [Compare Eq. (3.2).] This coincides with Hammons and Ashby (1981). Still another possible form is (in degrees)

$$\Delta\theta'=\frac{b''}{(2\pi S''\alpha'')^{1/2}}\sqrt{\Delta t} , \tag{5.42}$$

where θ' is in degrees, b'' is the equivalent lock-in rotation rate (i.e., b/S) expressed in degrees per second, α'' is the equivalent rotation rate (α/S) in deg/h, S'' is the scale factor in units of (counts/sec)/(arcsec/sec), and Δt is still in seconds.

As was mentioned before, current mechanically dithered laser gyros may have extremely low random drift errors; the one reported in Hammons and Ashby (1981) had a "diffusion coefficient" $\Delta\theta/\sqrt{\Delta t}$ of the order of 5×10^{-4} deg/$\sqrt{\text{h}}$, the same order of magnitude of the random drift due to quantum noise (i.e., spontaneous emission; see the preceding section). Advances in mirror technology are greatly responsible for this [note Eq. (5.40) is proportional to the backscattering coefficient].

Finally, let us emphasize again that Eq. (5.40) should not be taken too literally, but rather as an order-of-magnitude estimate, on account on the number of assumptions that enter its derivation.

C. Passive systems

A very detailed and complete discussion of the different kinds of noise in passive optical rotation systems, especially in optical fiber interferometers, has been given in Lin and Giallorenzi (1979). That analysis includes the effect of scattering in the fiber, as well as high optical power results. For a detector of bandwidth B they obtain in the shot-noise limited regime

$$(\mathscr{S})_{\text{peak}}\equiv\frac{\langle i_s^2\rangle}{\langle i_N^2\rangle}=\frac{1}{4}\frac{\eta}{h\nu B_0}\frac{P_i^2}{P_i+P_N} . \tag{5.43}$$

Here i_S and i_N are the photocurrents associated with signal and shot noise, respectively; η is the quantum efficiency of the detector; $h\nu$ is the energy per photon; P_i is the optical power (optical intensity times area of the detector) of each of the two counter-rotating beams as they reach the detector; and P_N is the optical power of the scattered (incoherent) light. In Lin and Giallorenzi (1979), P_N is given by a sum of five different scattering contributions: Rayleigh and Brillouin backward and forward scattering and scattering caused by core-cladding interface corrugation. It is also shown there that the effect of P_N cannot in general be neglected for long fibers (a few kilometers long), and it considerably degrades the signal-to-noise (S/N) ratio at short wavelength (in particular, $\lambda=0.633$ μm). Mode stripping was suggested as a way to prevent this degradation and obtain in general large values of S/N.

The shot-noise limited regime is obtained for large signal intensities, so that shot noise becomes a dominant effect over other sources of detector noise, such as dark current, thermal noise, and background noise induced by external light. In this respect, it should be noted that the scattering term P_N clearly increases with input power in the same way as P_i does.

Equation (5.43) shows the S/N ratio to improve with higher input power. The limitation to higher and higher power levels comes from the possibility of giving rise to nonlinear effects in the fiber, in particular to stimulated Raman and Brillouin scattering. Of these two, the second is the dominant. At some critical value of the laser output power, the backscattered stimulated Stokes wave in the Brillouin process would acquire a power level as high as the transmitted power of the beam coming from the other end of the fiber. This is discussed in Lin and Giallorenzi (1979), where it is shown in a numerical example that the (shot-noise limited) sensitivity at the critical power is still appreciably larger than for low powers.

In the absence of scattering noise, the laser power output would still be limited by the possibility of causing damage to the fiber at very high powers.

With the lock-in detection technique proposed by Ezekiel and co-workers, both for ring interferometers (Davis and Ezekiel, 1978) and passive rotation sensors (Ezekiel *et al.*, 1978), the center of the resonance line can be located with an uncertainty given by (Davis and Ezekiel, 1978)

$$\delta f=\frac{\Gamma}{\sqrt{\mathscr{S}}} , \tag{5.44}$$

where $\sqrt{\mathscr{S}}$ is the "amplitude" signal-to-noise [the square root of Eq. (5.43)], and Γ is the full width of the resonance at half power. For the passive cavity resonator, Γ is the cavity bandwidth. For the fiber ring interferometer, the "resonance line" is in fact an interference fringe; its width in radians of phase difference is therefore equal to π, giving

$$\delta\varphi=\frac{\pi}{\sqrt{\mathscr{S}}} . \tag{5.45}$$

Neglecting scattering contributions, the minimum (shot-noise limited) uncertainty in the rotation rate is reported in Davis and Ezekiel (1978) to be, for a fiber interferometer

$$\delta\Omega=\frac{c\lambda_0}{8\pi NA}\delta\varphi\simeq\frac{c\lambda_0}{8\pi nNA}\frac{\pi}{(N_{\rm ph}n\tau)^{1/2}}\ . \tag{5.46}$$

Here n is the index of refraction of the fiber, A the area it encloses, N the number of turns, $N_{\rm ph}$ the number of photons reaching the detector per unit time (related to P_i by $P_i=h\nu N_{\rm ph}$), and τ the detector integration time (related to B_0 by $B_0=1/2\tau$). As an example, they use the values $A=100$ cm^2, $\lambda_0=0.6328$ μm, $N=1000$, $n=1.5$, $N_{\rm ph}=3\times10^{15}$ sec^{-1} (corresponding to 1 mW at the given λ_0), $\eta=0.3$, and $\tau=1$ sec; the uncertainty $\delta\Omega$ is then equal to 5×10^{-8} rad/sec, or 0.01 deg/h. This is consistent with the sensitivity calculated in Lin and Giallorenzi (1979) for a similar case; it was pointed out there, however, that sensitivities as high as 7×10^{-4} deg/h could be achieved (with longer fibers and larger powers, using the 1.1-μm line, for which attenuation is much smaller).

For the passive cavity resonator, the sensitivity reported by Ezekiel *et al.* (1978) based on Eq. (5.44) but with an extra factor of $\sqrt{2}$ to account for the fact that two independently determined frequencies are subtracted, reads

$$\delta\Omega=\frac{\lambda P}{4A}\frac{\sqrt{2}\Gamma}{(N_{\rm ph}\eta\tau)^{1/2}}\ . \tag{5.47}$$

This can be made very small by decreasing the cavity bandwidth Γ, and increasing the power. For geophysical applications, large integration times (in the order of, say, one hour) as well as very large cavities may be considered. To quote from Ezekiel *et al.* (1978) "with a 10 m by 10 m cavity and a 4-watt stabilized argon laser, it should in principle be possible to reach a sensitivity of $10^{-10}\Omega_E$ (Ω_E=earth's rotation rate, 15 deg/hr) in an integration time of 1000 seconds."

VI. RING LASER APPLICATIONS

In this final section we discuss some of the realized and as yet unrealized applications of the ring laser gyroscope. These applications can be divided into two general classes. The first of these is obvious and the purpose for which ring laser gyros were developed in the first place. That is, for use as rotation sensing devices in aircraft and more generally as a replacement for mechanical gyroscopes wherever they are now used. Some of the necessary specifications and particular problems associated with the use of ring laser gyroscopes in this sort of application as well as a discussion of the fabrication of devices currently used in commercial aircraft is given in the next part of this section.

The second class of application of the ring laser is an offshoot of the quest for better and better rotation rate sensitivities. As this quest continues various obstacles to low rotation-rate sensing like those discussed throughout the body of this paper (such as gas flow, lock-in effect, backscattering in fibers, etc.) have been encountered. For the first class of applications these effects are, of course, undesirable. The whole problem can be looked at from the other way around, however. In this new perspective the ring laser gyro is viewed as a device which is capable of measuring these effects heretofore considered only as problems. This perspective (not an unusual scientific viewpoint, of course) is beneficial in that a better understanding of the nonreciprocal effects can help lead to greater sensitivity and also these effects may be interesting (even useful in other spheres) in and of themselves. An exciting example of this sort of use for the ring laser gyro is given in the last part of this section in which an optical test of metric theories of gravitation is discussed.

A. Navigation

The principal proposed use for the ring laser has been, since the early 1960s, that of a navigational gyro. Specifically the ring laser has been suggested and in some cases implemented for use in inertial guidance of aircraft, ships, and missiles, attitude heading and flight control, and gunfire pointing. In addition the ring laser could be used in any situation in which mechanical gyros are now used such as oil field mapping, the pointing of a drill bit, etc. The different navigational applications have a wide range of required gyro sensitivities and stabilities which are tabulated in Table I. In addition, conventional gyro applications require that the gyro operate in a wide range of encountered environmental conditions. The environment, for example, may range from that of the cockpit of a commercial aircraft to the severe heat and sulfur atmosphere (hell fire and brimstone) of an oil well bit to the cold vacuum of deep space encountered by spacecraft to the many thousand g acceleration associated with other kinds of devices. Obviously, the application dictates a considerable influence on the size, shape, design, materials, and packaging of the instrument.

Contrary to tradition, the first major implementation of this new gyro technology has come in the field of commercial passenger carrying aircraft. Both Honeywell and Litton Industries have contracts with Boeing and Airbus Industries, respectively, to supply systems using ring laser gyroscopes for all the functions of navigation of the Boeing 757 and 767 and the Airbus A310, now in production. These systems are required to perform in the traditional one nautical mile per hour range. This requires gyros with bias stabilities and repeatabilities in the neighborhood of 0.01 deg/h and a quantum phase diffusion coefficient [Eq. (5.22)] of approximately 3×10^{-2} deg/h for 100-sec data sample time. These requirements eliminate the possibility of using fiber ring gyros of the type discussed in Sec. II of this paper and, indeed, for nearly all current applications the active ring laser gyro is the only possible choice.

The following is a description of some of the essential design features of the class of ring laser gyros being produced. Figure 22 highlights some of these features. First, the ring laser body is constructed from one of the ultralow thermal expansion glasses such as CerVit or Zerodur. These materials are chosen because they are reasonably transparent, good dielectrics, and provide a stable scale factor, i.e., a stable cavity length over the

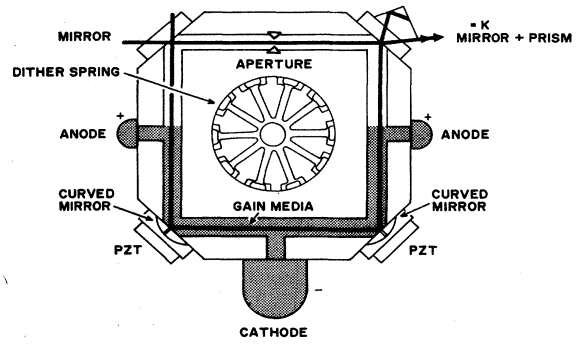

FIG. 22. Schematic of a prototype active ring laser gyro.

range of temperatures of interest. These materials have thermal expansion coefficients on the order of 10^{-8}/°C. The piezo attachments to the backs of two of the mirrors are adequate to compensate for the residual thermal expansion of the blocks. They can maintain a constant cavity perimeter to a few microinches. This is done by an active servo which uses the laser light intensity as the indicator of change in laser cavity length. That is, since the laser gain has a Doppler profile, the laser intensity follows a change in optical frequency which in turn is determined by the cavity length. Thus servoing the laser intensity to a maximum maintains a near constant optical frequency—which is to say a near constant scale factor. Of course, it is also necessary to maintain a single longitudinal mode during operation of the gyro in order to maintain a constant scale factor.

As mentioned above CerVit and Zerodur are "good" dielectrics. What is meant by a "good" dielectric in this context is explained below. A dielectric is needed to maintain the gas discharge. Some dielectrics have the problem that they disassociate in the presence of the gas plasma discharge and condense on the cavity mirrors. This results in a severe degradation of the optical quality of the resonant cavity. CerVit and Zerodur are good dielectrics in that they avoid this complication.

The aperture may be constructed in the glass body or formed on one of the mirrors. Whichever way it is constructed, the aperture should match the beam shape at that point in the cavity. In ring cavities with curved mirrors the beam shape is elliptical. The dimensions of the aperture for such a beam shape can be roughly determined from the beam spot calculation (Rigrod, 1965) and a calculation of the desired diffraction loss (Boyd and Gordon, 1972; Fox and Li, 1972). In practice suppression of the first off-axis modes, i.e., the 01 and 10 modes, such that the finesse of these modes is some ten times less than the finesse of the axial, 00 mode, is desired. The dimension of the elliptical aperture is determined empirically to accomplish this. It is alleged to be important that the position of the aperture be at the beam waist and equidistant from the two gain sections of the cavity (read, for example, Burnashev and Filatov, 1973). The aperture size is typically two or three times the beam waist size.

As emphasized in earlier sections, elimination of nonreciprocal frequency shifts caused by factors other than rotation is central to increasing the sensitivity and reliability of the ring laser gyro. Elimination of a large class of nonreciprocal frequency shifts is accomplished or simplified by constructing the gyro in a symmetric manner. This means ensuring that the gyro is designed so that the two counterpropagating beams encounter the same environmental frequency shifts which then cancel in the output. The light beams traversing a section of the gain medium in which there is a gas flow experience a change in velocity due to the Fresnel-Fizeau effect which results in nondegenerate resonant frequencies for the counterpropagating beams. With the symmetric arrangement of the two equal anodes as shown in Fig. 22, the counterpropagating beams encounter the same gas-flow-induced frequency shift (generated by the plasma current, see Sec. III.B) as long as the current in each gain length is the same. The beat note error caused by a difference in the current is discussed by Aronowitz and Lim (1978). Typical numbers associated with current unbalance in a gyro of the type considered here are a few degrees per hour per milliampere. Another source of gas flow in these instruments is caused by local heating. Again, the symmetric placement of electronic heat sources helps to minimize these effects.

The gain media of popular choice is helium and neon. This is a mixture of ^{3}He, ^{20}Ne, and ^{22}Ne. The dual isotope neon is used to minimize the effects of Bennett hole burning. The undesirability of using a single isotope is discussed by both Aronowitz (1972) and Hutchings *et al.* (1966). In single isotope helium-neon gas the mode competition is so severe that simultaneous stable lasing for both directions around the ring is not possible. Minimum mode competition is obtained by operating the laser at a frequency halfway between the ^{20}Ne and the ^{22}Ne transitions. The 6328-Å ($3S_2 \rightarrow 2P_4$) transition in neon is a popular choice because the holes that are burned in the Doppler-broadened gain curve for this transition, using the dual isotope mixture, do not significantly overlap with each other. This results in a minimum of "pushing" and "pulling" effects on the gyro bias error. For a discussion of Bennett holes and a related analytical technique called the Yntema-Grant diagram, see Chow *et al.* (1980). The typical ratio of helium to neon is around ten to one at a total pressure of somewhere between 3 and 8 Torr. The precise ratios and pressure are determined by the gain required and the plasma current oscillation conditions for the particular gyro design.

Equation (5.22) is an expression for the quantum noise phase diffusion coefficient. From this equation it can be seen that the quantum noise is directly proportional to the ratio of the perimeter L to the area A enclosed by the cavity and is inversely proportional to the cavity Q and the square root of the laser power inside the cavity. So the quantum noise is reduced by using a square rather than a triangle since a square has a smaller ratio of L to A. The laser power (gain) is a function of plasma current, plasma length, bore diameter, and the above-mentioned

gas mixtures. The cavity Q is the most important variable in the expression for the quantum noise phase diffusion coefficient and has its most important dependence on the mirror quality. The mirror quality is important enough to warrant a more extended discussion.

As a matter of fact the mirror quality is undoubtedly the key to being competitive in the commercial ring laser gyro technology. With the new ion beam deposition-coating technology and the current state-of-the-art substrate smoothness, mirrors with total losses of less than one hundred parts per million are now available. At this stage of mirror technology the factor which seems to limit the cavity Q is that the plasma ultraviolet light damages multilayer dielectric mirrors. Exposure to uv radiation from the He-Ne plasma causes an increase in the amount of light absorbed by the exposed mirror. The mirrors least damaged show an increase in absorption of 20 parts per million while for a typical mirror coating produced via the conventional electron beam technology this increasing is about 200 ppm. A second mirror characteristic, which is very important, is the amount of light which it scatters. The light scatter from a mirror affects the cavity Q in that scattered light represents a loss. Perhaps the more detrimental effect of scattered light is that backscattered light is the agent chiefly responsible for the lock-in phenomenon. As more light is backscattered from the cavity mirrors the rotation rate lock-in threshold rises. The scatter quality of current state-of-the-art mirrors is such that the "backscattering coefficient" in Eq. (3.12) is typically around a few "earth rates" (15 deg/h) and the total scatter loss less than 1 ppm. This corresponds to a substrate smoothness of about 1 Å rms roughness and a coating virtually free of microcrystalling growth. The recent progress in the technology behind substrate smoothness and thin film coatings make the ring laser a viable candidate for high accuracy gyro applications.

The device in the center of the prototype gyro depicted by Fig. 22 is the dither spring, which as the name implies, is used to overcome the frequency locking problem. This spring is connected to the glass gyro body and the vehicle (in the navigational application) frame. The glass is mechanically oscillated/dithered about its sensitive axis relative to the vehicle frame. It is just this sort of setup, when the dither is sinusoidal, that is described by Eq. (3.20). Typical values of the peak dither angular velocity amplitude and frequency are about 150 deg/sec and 300 Hz. These values are determined by the mechanical resonance of the driven spring and gyro mass combination.

The gyro output, as given by Eq. (3.20), is a modulated signal and must be demodulated. There are two different techniques used to accomplish this. One involves generating a signal that represents the motion and position of the glass body relative to the vehicle frame. The demodulation is then achieved using this signal in the electronics. The other technique is referred to as "optical demodulation" (Killpatrick, 1968). In this case the combining optics prism is connected to the vehicle frame in a particular fashion and not to the back of the mirror as shown in Fig. 22. In this way the output light from the ring laser is Doppler shifted in such a way that the modulation term in Eq. (3.20) does not show.

A final consideration in the construction of a commercial ring laser gyro is the preparation of the electrodes such that the He-Ne laser will have a long stable life. Typically, the anode is made of copper and the cathode is made of aluminum and both are sealed to the glass body with indium. Preparation of the electron emitter, the cathode, is critical in the production of a long-lived gyro (while preparation of the anode is not). This is because if the cathode size, shape, and oxide layer are not right for the charge emission density, it will sputter. The sputter action of the cathode metal buries the gas atoms in the cathode thus depleting the laser gain media. The techniques for preparing the cathode emitting surface, and choosing the size, geometry, and material of the cathode to ensure long life are part of the art of ring laser gyro construction and so are not published and are kept as company propriety for competitive reasons.

This concludes the discussion of the fabrication of, and requirements associated with, commercial ring laser gyroscopes. It should be emphasized that for most applications the ring laser meets all requirements and in the long run should be cost competitive with conventional mechanical gyros. The next section deals with the other class of applications in which the ring laser gyro is used as a probe of gravitation.

B. Optical test of metric gravitation theories

1. Introduction

To perform experiments in general relativity is extremely difficult. This is due to the "small" gravitational coupling constant

$$G = 6.67 \times 10^{-8} \text{ cm}^3/\text{g sec}^2 .$$

The situation is best summarized by Misner, Thorne, and Wheeler (1973) in their book *Gravitation*: "For the first half century of its life, general relativity was a theorist's paradise but an experimentalist's hell."

Einstein's theory has been tested by only a few (three) crucial tests of general relativity (Ohanian, 1976)—redshift, deflection of starlight by the sun, and perihelion shift of the mercury. As a result of recent laser experiments we now have a "fourth" test—the Nordtvedt effect—using laser lunar ranging experiments (Nordtvedt, 1982). Compare this with the situation in quantum mechanics where we have hundreds of experiments proving its validity. Furthermore there exist alternative theories of relativity; for example, the Brans-Dicke-Jordan theory, Ni's theory and others, which are also viable theories (see, for example, Misner *et al.*, 1973). Thus we are motivated to look for new possible tests of these theories. Now it might seem to be that to decide which

theory is the correct one we would have to do the calculation for a given experiment using all possible theories. But thanks to Will and Nordtvedt (1972a,1972b) this is not necessary. They developed a formalism—the so-called parametrized post Newtonian (PPN) formalism in which it is possible to do the calculation for any gravity experiment only once for all theories. To achieve this, they introduced a set of parameters—the so-called PPN parameters. Each set of parameters corresponds to a different metric theory of gravity, for example, one set gives Einstein's theory and another set gives Brans-Dicke-Jordan's theory. The values of certain PPN parameters are shown in Table II (Will, 1974). The goal of experimentalists is now to determine these PPN parameters as accurately as possible or to design new experiments in which certain parameters can be tested.

But as already mentioned above, experiments in this field are extremely difficult to make. However, thanks to advances in modern optics, especially the development of the laser, new tests of metric gravity are being and will continue to be carried out (see, for example, Barut *et al.*, 1982). In the next section we are going to discuss one of these "laser probes of the macrocosmos" using a ring laser gyroscope (Scully *et al.*, 1980,1981), which will allow one to put tight constraints on certain PPN parameters.

2. Generalized Sagnac effect

In Sec. I.B we derived the Sagnac frequency shift in a ring laser gyroscope for a given metric $g_{\mu\nu}$. Now we are going to apply these results to analyze the influence of the gravitational field of the rotating earth on a ring laser interferometer in an earthbound laboratory.

Consider a ring laser interferometer which is rotating at a rate $\Omega_\oplus$, has a colatitude θ_0 and a distance $\bar{r}=r_\oplus \sin\theta_0$ all relative to the earth's axis ($r_\oplus$ is the radius of the earth). Finally the ring laser is allowed to spin about its own axis at a rate Ω_0; see Fig. 23. For the sake of simplicity we assume the rotation axis of Ω_0 to be parallel to the earth's axis. The case of an arbitrary orientation of the axis was treated by Scully *et al.* (1980,1981).

Transforming the metric for the rotating earth in the PPN formalism into the double rotating frame of the

TABLE II. PPN Parameters in various theories.

Parameter \ Theory	Einstein	Brans-Dicke-Jordan	Ni
γ	1	$\frac{1+\omega}{2+\omega}$	1
Δ_1	1	$\frac{10+7\omega}{14+7\omega}$	$-\frac{1}{7}$
Δ_2	1	1	1
$\alpha_1=7\Delta_1+\Delta_2-4(\gamma+1)$	0	0	-8

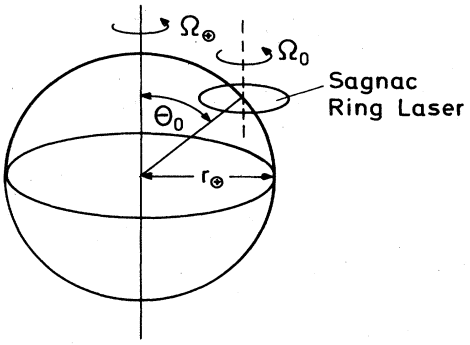

FIG. 23. Sagnac interferometer used to test metric theories of gravity.

gyroscope and substituting into Eq. (1.27) we find after some lengthy algebra (Scully *et al.*, 1981)

$$\Delta\omega=\frac{4A}{\lambda P}[\Omega_0+\Omega_\oplus+\alpha_1 T_{\alpha_1}+\tfrac{1}{2}(\gamma+1)T_\gamma + \tfrac{1}{8}(7\Delta_1+\Delta_2)T_\Delta] , \tag{6.1}$$

where the terms T_{α_1}, T_γ, and T_Δ associated with the so-called preferred frame effect, space curvature effect, and Lense-Thirring effect, respectively, are as follows:

$$T_{\alpha_1}=-\frac{1}{8}\frac{r_s}{r_\oplus}|\mathbf{W}|B(t_s)\sin\theta_0 ,$$
$$T_\gamma=-\frac{r_s}{r_\oplus}\Omega_\oplus\sin^2\theta_0 , \tag{6.2}$$
$$T_\Delta=\frac{1}{10}\frac{r_s}{r_\oplus}\Omega_\oplus(1-3\cos^2\theta_0) ,$$

and $r_s=2GM_\oplus/c^2$ is the Schwarzschild radius and $M_\oplus$ the total mass of the earth. The parameters γ, Δ_1, Δ_2, and α_1 are the PPN parameters, whose values are summarized in Table II. Their physical meaning will become clear when the contributions T_{α_1}, T_γ, T_Δ are discussed. $|\mathbf{W}|$ is the velocity of the earth relative to fixed stars, i.e., relative to the frame in which the cosmic 3-K background radiation is isotropic (Smoot *et al.*, 1977; Smoot and Lubin, 1979) and is of magnitude

$$|\mathbf{W}|=360\pm60 \text{ km/sec} .$$

Further terms appearing above include

$$B(t_s)=\cos\delta\cos\alpha ,$$
$$\delta=6°\pm10° , \tag{6.3}$$
$$\alpha=\Omega_\oplus[t_s-(11\pm0.6)\text{ h}] .$$

With optimized latitude and tilt angles the contribution to $\Delta\omega$ due to the preferred frame term is $1.2\times10^{-7}\alpha_1\Omega_\oplus$. The γ-dependent geodetic rotation rate is $(1.4\times10^{-9})\frac{1}{2}(\gamma+1)\Omega_\oplus$ while that of Lense-Thirring is $(5.6\times10^{-10})\frac{1}{8}(7\Delta_1+\Delta_2)\Omega_\oplus$.

We now turn to a discussion of each of the terms of Eq.

(6.1). The first two terms are purely classical and obviously result from the double rotation of our ring laser, one rotation with the rate Ω_0 about its own axis and one with the earth rotation rate $\Omega_\oplus$ because the gyroscope is fixed on the earth.

The terms T_{α_1}, T_γ, and T_Δ are purely general relativistic effects. To discuss the contributions T_γ and T_Δ we use an analogy between Maxwell's equations and Einstein's field equations in the weak field limit.

The first attempt to explain gravity was made by Heaviside in 1893 (1971). He mentioned that gravitation may obey the same equations as electrodynamics. Therefore, one might expect "electric" and "magnetic" types of gravitational fields. Recently, it was shown by Forward (1961) and Braginsky *et al.* (1977) that indeed such equations follow from Einstein's field equations in the weak field limit. In this analogy the Newtonian field $\mathbf{G}=-\nabla u$ where u is the Newtonian potential, corresponds to the electric field $\mathbf{E}$ and is therefore sometimes called the "gravitoelectric" field. The gravitational potential $\mathbf{h}$ moreover is analogous to the vector potential $\mathbf{A}$ in electrodynamics. Therefore, $\nabla\times\mathbf{h}$ is analogous to the magnetic field $\mathbf{B}$, and might be called the "gravitomagnetic" field. From Eq. (1.27) in Sec. I.B we recognize that the generalized Sagnac shift is proportional to the "gravitomagnetic" field $\nabla\times\mathbf{h}$, and so a magnetic field will produce a Sagnac type of frequency shift. Keeping these ideas in mind it is very easy to understand the T_γ and T_Δ contributions. We start by explaining the so-called geodetic precession T_γ.

It is well known that electric and magnetic fields have no independent existence. A purely electric or magnetic field in one coordinate system will appear as a mixture of electric and magnetic fields in another moving coordinate frame. An observer moving through a purely electric field also sees a magnetic field which is perpendicular to the velocity $\mathbf{v}$ (Jackson, 1965) and is given by

$$\mathbf{B}\sim\mathbf{v}\times\mathbf{E}\ . \tag{6.4}$$

Now let us apply this to the gyroscope problem. The gyroscope is passing through the radial symmetric gravitational field of the earth, $\mathbf{G}\sim(\mathbf{r}/r^3)$ at a radius $r_\oplus$ with a velocity $\mathbf{v}=r_\oplus\Omega_\oplus\sin\theta_0\mathbf{e}_\varphi$, where $\mathbf{e}_\varphi$ is a unit vector in the φ direction which is due to the fact that the gyroscope is fixed on the rotating earth. According to the above discussion this must result in a "gravitomagnetic" field

$$\nabla\times\mathbf{h}\sim\frac{1}{r_\oplus}\Omega_\oplus\sin\theta_0\mathbf{e}_\varphi\times\mathbf{e}_r\ . \tag{6.5}$$

Because the axis is parallel to the z axis, $\mathbf{e}_a=\mathbf{e}_z$, we get

$$(\nabla\times\mathbf{h})\cdot\mathbf{e}_z\sim\frac{\Omega_\oplus}{r_\oplus}\sin^2\theta_0\ . \tag{6.6}$$

This is up to a constant (which can be determined from the exact analogy including all constants) the T_γ contribution. We note that this effect results simply from the presence of matter—the mass of the earth—namely its Newtonian potential. But as Wheeler (1983) phrased it: "Matter tells space how to curve," and the γ parameter expresses the amount of curvature of space by a mass. Similar "curved space" physics leads to the bending of starlight and retardation of radio signals passing by the sun.

The extra rotation term T_Δ is also very easy to understand in terms of the electromagnetic gravitation analogy. It is well known in electrodynamics that a rotating, homogeneously charged sphere of radius a produces not only an electric field $\mathbf{E}$ but also a magnetic field $\mathbf{B}$, which outside of the sphere is given by

$$\mathbf{B}\sim\frac{3\mathbf{r}(\boldsymbol{\Omega}\cdot\mathbf{r})-\boldsymbol{\Omega}(\mathbf{r})^2}{\mathbf{r}^5}a^2\ , \tag{6.7}$$

where $\mathbf{r}$ is the point of observation and $\boldsymbol{\Omega}$ the rotation rate. Therefore, keeping in mind this electrodynamics gravitation analogy, an earthbound gyroscope ($a=r_\oplus$, $\mathbf{r}=r_\oplus\mathbf{e}_r$) will notice a "gravitomagnetic" field

$$\nabla\times\mathbf{h}\sim\frac{3\mathbf{e}_r(\boldsymbol{\Omega}\cdot\mathbf{e}_r)-\boldsymbol{\Omega}}{r_\oplus} \tag{6.8}$$

which will give a

$$(\nabla\times\mathbf{h})\cdot\mathbf{e}_z\sim\frac{\Omega_\oplus}{r_\oplus}(1-3\cos^2\theta_0) \tag{6.9}$$

contribution in the Sagnac frequency shift. Note that this effect is purely due to the rotation of the earth and does not depend on the motion of the gyroscope. The gyroscope is therefore somehow "dragged" by the motion of other masses (here the rotation of the earth). For this reason the PPN parameters Δ_1 and Δ_2 are called frame-dragging parameters and are a measure of to what extent inertial frames are dragged by the motion of masses. This effect is sometimes also called the Lense-Thirring effect (Lense and Thirring, 1918).

The T_{α_1} contribution to the frequency shift arises from the presence or absence of a preferred (rest) frame, which might be thought to be that implied by the 3-K blackbody background. In Einstein's theory of relativity all frames of reference are equivalent and therefore this effect is zero. However, in the Ni cosmology the universe is at rest and the effect is presented not to be zero. The PPN parameter α_2 therefore measures the extent to which preferred frame effects are important in a given theory. Because Einstein predicts such an effect to be zero there exists no electrodynamical analog to this effect and the form of T_{α_1} cannot be derived from simple heuristical arguments.

As we see from Eq. (6.1) the most promising effect for tests would be the preferred frame effect, because of its size. The present limit for α_1 is $|\alpha_1|\leq 0.02$. The proposed experiment should be able to place tight new constraints on the magnitude of α_1. For the details of the experiment we refer to the work of Scully *et al.* (1980,1981).

ACKNOWLEDGMENT

Research for this paper was supported in part by the Air Force Office of Scientific Research.

APPENDIX: DERIVATION OF WAVE EQUATION

Maxwell charge and current-free equations in the metric of Eq. (1.16) are given (Schleich and Scully, 1984) by

$$\nabla\cdot\mathbf{D}=0,\quad \nabla\times\mathbf{E}=-\frac{\partial\mathbf{B}}{\partial t}\ , \tag{1.17}$$

$$\nabla\cdot\mathbf{B}=0,\quad \nabla\times\mathbf{H}=\frac{1}{c^2}\frac{\partial\mathbf{D}}{\partial t}\ , \tag{1.18}$$

together with the material equations

$$\mathbf{D}=\mathbf{E}-c(\mathbf{B}\times\mathbf{h}) \tag{1.19}$$

and

$$\mathbf{B}=\mathbf{H}+\frac{1}{c}(\mathbf{E}\times\mathbf{h})\ . \tag{1.20}$$

We start deriving a wave equation for $\mathbf{E}$ as in ordinary electrodynamics by taking $\nabla\times(\nabla\times\mathbf{E})$ from Eq. (1.17) which yields

$$\nabla\times(\nabla\times\mathbf{E})=\nabla(\nabla\cdot\mathbf{E})-\Delta\mathbf{E}=-\frac{\partial}{\partial t}(\nabla\times\mathbf{B})\ . \tag{A1}$$

Now we have to find expressions for $\nabla\cdot\mathbf{E}$ and $\nabla\times\mathbf{B}$.

From the material equation (1.19) we get, by using standard vector identities,

$$0=\nabla\cdot\mathbf{D}=\nabla\cdot\mathbf{E}-c\mathbf{h}\cdot(\nabla\times\mathbf{B})+c\mathbf{B}\cdot(\nabla\times\mathbf{h})\ .$$

From Eqs. (1.18) together with Eqs. (1.19) and (1.20) follows

$$\nabla\times\mathbf{B}=\frac{1}{c^2}\frac{\partial\mathbf{E}}{\partial t}+O(h)$$

which yields

$$\nabla\cdot\mathbf{E}=\frac{1}{c}\mathbf{h}\cdot\frac{\partial\mathbf{E}}{\partial t}+c(\nabla\times\mathbf{h})\cdot\mathbf{B}+O(h^2)\ ,$$

where we have neglected terms $O(h^2)$. Assuming that the gravitational fields do not vary much over an optical wavelength we can neglect the second term on the right-hand side against the first one. Therefore,

$$\nabla\cdot\mathbf{E}\cong\frac{1}{c}\mathbf{h}\cdot\frac{\partial\mathbf{E}}{\partial t}\ .$$

Now we are able to write using standard vector identities

$$\begin{aligned}\nabla(\nabla\cdot\mathbf{E})&=\frac{1}{c}\nabla\left[\mathbf{h}\cdot\frac{\partial\mathbf{E}}{\partial t}\right]\\&\cong\frac{1}{c}\left[(\mathbf{h}\cdot\nabla)\frac{\partial\mathbf{E}}{\partial t}+\mathbf{h}\times\frac{\partial}{\partial t}(\nabla\times\mathbf{E})\right]\\&=\frac{1}{c}\left[(\mathbf{h}\cdot\nabla)\frac{\partial\mathbf{E}}{\partial t}-\mathbf{h}\times\frac{\partial^2\mathbf{B}}{\partial t^2}\right]\ ,\end{aligned} \tag{A2}$$

where we have again assumed that the gravitational fields vary slowly on an optical wavelength and have made use of Eq. (1.17). In order to derive an expression for $\nabla\times\mathbf{B}$ we use the material equation, Eq. (1.20), to find

$$\begin{aligned}\nabla\times\mathbf{B}&=\nabla\times\mathbf{H}+\frac{1}{c}\nabla\times(\mathbf{E}\times\mathbf{h})\\&=\frac{1}{c^2}\frac{\partial\mathbf{D}}{\partial t}+\frac{1}{c}(\mathbf{h}\cdot\nabla)\mathbf{E}+\mathbf{h}(\nabla\cdot\mathbf{E})\\&\cong\frac{1}{c^2}\frac{\partial\mathbf{E}}{\partial t}-\frac{1}{c}\frac{\partial\mathbf{B}}{\partial t}\times\mathbf{h}+\frac{1}{c}(\mathbf{h}\cdot\nabla)\mathbf{E}+O(h^2)\ ,\end{aligned} \tag{A3}$$

where we have used Eq. (1.18) together with (1.19) and the fact that $\nabla\cdot\mathbf{E}=O(h)$. Substituting the results (A2) and (A3) back into (A1) we get, after minor algebra,

$$\frac{1}{c^2}\frac{\partial^2\mathbf{E}}{\partial t^2}-\Delta\mathbf{E}=-\frac{2}{c}(\mathbf{h}\cdot\nabla)\frac{\partial\mathbf{E}}{\partial t}\ . \tag{1.21}$$

REFERENCES

Anderson, D. Z., 1981, "The four-mode linearly-polarized ring laser gyro," Ph.D. dissertation, University of Arizona (unpublished).

Anderson, D. Z., W. W. Chow, V. E. Sanders, and M. O. Scully, 1979, Appl. Opt. **18**, 941.

Anderson, D. Z., W. W. Chow, M. O. Scully, and V. E. Sanders, 1980, Opt. Lett. **5**, 413.

Aronowitz, F., 1965, Phys. Rev. **139**, A635.

Aronowitz, F., 1971, in *Laser Applications,* edited by M. Ross (Academic, New York), pp. 113–200.

Aronowitz, F., 1972, Appl. Opt. **11**, 405.

Aronowitz, F., 1978, in *Laser Inertial Rotation Sensors,* edited by S. Ezekiel and G. E. Knausenberger (SPIE, Bellingham, Washington), pp. 2–6.

Aronowitz, F., and W. L. Lim, 1978, in *Laser Inertial Rotation Sensors,* edited by S. Ezekiel and G. E. Knausenberger (SPIE, Bellingham, Washington), pp. 7–12.

Barut, A., P. Meystre, and M. O. Scully, 1982, Laser Focus **41**, 49.

Bergh, R. A., H. C. Lefevre, and H. J. Shaw, 1981a, Opt. Lett. **6**, 198.

Bergh, R. A., H. C. Lefevre, and H. J. Shaw, 1981b, Opt. Lett. **6**, 502.

Bergh, R. A., H. C. Lefevre, and H. J. Shaw, 1982, Opt. Lett. **7**, 282.

Bohm, K., P. Russer, E. Weidel, and R. Ulrich, 1981, Opt. Lett. **6**, 64.

Boyd, G. D., and J. P. Gordon, 1972, in *Laser Theory,* edited by F. S. Barnes (IEEE, New York), pp. 489–508.

Braginsky, C. M., C. M. Caves, and K. S. Thorne, 1977, Phys. Rev. D **15**, 2047.

Burnashev, M. N., and Y. V. Filatov, 1973, Opt. Spektrosk. **35**, 992.

Carter, W. S., and R. B. Inwood, 1981, "Magneto-Optical Phase-Modulating Devices," U.S. Patent 4,246,549.

Champeney, D. C., 1971, *Fourier Transforms and Their Physical Applications* (Academic, New York).

Chow, W. W., J. B. Hambenne, D. R. Hanson, M. Sargent III, and M. O. Scully, 1979, IEEE J. Quantum Electron. **QE-15**, 1301.

Chow, W. W., J. B. Hambenne, T. Y. Hutchings, V. Sanders,

M. Sargent III, and M. O. Scully, 1980, IEEE J. Quantum Electron. **QE-16**, 918.
Chow, W. W., M. O. Scully, and E. W. Van Stryland, 1975, Opt. Commun. **15**, 6.
Coccoli, J. D., and J. R. Lawson, 1970, U.S. Patent 3,533,014.
Cresser, J. D., 1982, Phys. Rev. A **26**, 398.
Cresser, J. D., 1983, Phys. Rep. **94**, 47.
Cresser, J. D., W. H. Louisell, P. Meystre, W. Schleich, and M. O. Scully, 1982a, Phys. Rev. A **25**, 2214.
Cresser, J. D., D. Hammons, W. H. Louisell, P. Meystre, and H. Risken, 1982b, Phys. Rev. A **25**, 2226.
Cutler, C. C., S. A. Newton, and H. J. Shaw, 1980, Opt. Lett. **5**, 488.
Davis, J. L., and S. Ezekiel, 1978, SPIE, Vol. 157, pp. 131—136.
Davis, J. L., and S. Ezekiel, 1981, Opt. Lett. **6**, 505.
Diels, J.-C., and I. C. McMichael, 1981, Opt. Lett. **6**, 219.
Dorschner, T. A., H. A. Haus, M. Holz, I. W. Smith, and H. Statz, 1980, IEEE J. Quantum Electron. **QE-16**, 1376.
Erdelyi, A., 1934, Ann. Phys. **19**, 40.
Ezekiel, S., and S. R. Balsamo, 1977, Appl. Phys. Lett. **30**, 478.
Ezekiel, S., J. A. Cole, J. Harrison, and G. Sanders, 1978, in *Laser Inertial Rotation Sensors,* edited by S. Ezekiel and G. E. Knausenberger (SPIE, Bellingham, Washington), p. 68.
Ezekiel, S., J. L. Davis, and R. W. Hellwarth, 1982, Opt. Lett. **1**, 457.
Forward, R. L., 1961, Proc. IRE **49**, 892.
Fox, A. G., and T. Li, 1972, in *Laser Theory,* edited by F. S. Barnes (IEEE, New York).
Gyorffi, G. L., and W. E. Lamb, Jr., 1965, *Theory of a Ring Laser* (Michigan Microfilm, Yale University).
Hammons, S. W., and V. J. Ashby, 1981, *Mechanically Dithered Gyro at the Quantum Limit,* NAECON 1981 (unpublished).
Hanson, D. R., and M. Sargent III, 1974, Phys. Rev. A **9**, 466.
Heaviside, O., 1971, *Electromagnetic Theory* (Chelsea, New York), Appendix A.
Hecht, E., and A. Zajac, 1974, *Optics* (Addison-Wesley, Reading, Mass.), Sect. 8.12.
Henry, R. D., 1980, "Ferrimagnetic Faraday Elements for Ring Lasers," U.S. Patent 4,222,668.
Hutchings, T. J., and D. C. Stjern, 1978, in *Proc. IEEE 1978 Nat'l. Aerospace and Electronic Conf.* (IEEE, New York), p. 549.
Hutchings, T. J., J. Winocur, R. H. Durett, E. D. Jacobs, and W. L. Zingery, 1966, Phys. Rev. **152**, 467.
Jackson, J. D., 1965, *Classical Electrodynamics* (Wiley, New York).
Jacobs, F., and R. Zamoni, 1982, Am. J. Phys. **50**, 659.
Josephson, B. D., 1965, Adv. Phys. **14**, 419.
Kaplan, A. F., and P. Meystre, 1981, Opt. Lett. **6**, 590.
Kaplan, A. F., and P. Meystre, 1982, Opt. Commun. **40**, 229.
Killpatrick, J., 1967, quoted in Aronowitz (1971).
Killpatrick, J. E., 1968, "Laser Angular Rate Sensor," U.S. Patent 3,373,650.
Lamb, W. E., Jr., 1964, Phys. Rev. **134**, A1429.
Lax, M., 1968, *Brandeis University Summer Institute Lectures 1966,* edited by M. Chretien, E. P. Gross, and S. Deser (Gordon and Breach, New York).
Leeb, W. R., G. Schiffner, and E. Scheiterer, 1979, Appl. Opt. **18**, 1293.
Lense, J., and H. Thirring, 1918, Phys. Z. **19**, 156.
Lin, S., and T. G. Giallorenzi, 1979, Appl. Opt. **18**, 915.
Louisell, W. H., 1973, *Quantum Statistical Properties of Radiation* (Wiley, New York).
Magnus, W., F. Oberhettinger, and R. P. Soni, 1966, *Formulas and Theorems for the Special Functions of Mathematical Physics* (Springer, Berlin).
Menegozzi, L. M., and W. E. Lamb, Jr., 1973, Phys. Rev. A **8**, 2103.
Misner, C. W., K. S. Thorne, and J. A. Wheeler, 1973, *Gravitation* (Freeman, San Francisco), p. 571.
Newberger, B. S., 1982, J. Math. Phys. **23**, 1278.
Nordtvedt, K., Jr., 1982, Rep. Prog. Phys. **42**, 631.
Ohanian, H. C., 1976, *Gravitation and Spacetime* (Norton, New York).
Plebanski, J., 1960, Phys. Rev. **118**, 1396.
Post, E. J., 1967, Rev. Mod. Phys. **39**, 475.
Ramaswary, V., W. G. French, and R. D. Stowdley, 1978, Appl. Opt. **17**, 3014.
Rashleigh, S. C., and R. Ulrich, 1980, Opt. Lett. **5**, 354.
Rigrod, W. W., 1965, Bell Sys. Tech. J. **44**, 907.
Risken, H., 1983, *The Fokker-Planck-Equation Methods of Solutions and Applications,* Springer Series in Synergetics, edited by H. Haken (Springer, Berlin).
Roland J. J., and G. P. Agrawal, 1981, Opt. Laser Technol. **13**, 239.
Sagnac, G., 1913a, C. R. Acad. Sci. **157**, 708.
Sagnac, G., 1913b, C. R. Acad. Sci. **157**, 1410.
Sanders, V. E., and D. Z. Anderson, 1981, "Isotropic Nonplanar Ring Laser," U.S. Patent 4,247,832.
Sanders, V., D. Z. Anderson, and M. O. Scully, 1978, in *Laser Inertial Rotation Sensors,* edited by S. Ezekiel and G. E. Knausenberger (SPIE, Bellingham, Washington), pp. 30—33.
Sargent, M., III, M. O. Scully, and W. E. Lamb, Jr., 1970, Opt. Commun. **9**, 2473.
Sargent, M., III, M. O. Scully, and W. E. Lamb, Jr., 1974, *Laser Physics* (Addison-Wesley, Reading, Mass.).
Schiffner, G., 1980, Siemens Forsch. Entwicklungsber. **9**, 15.
Schleich, W., 1981, Quanten-Fluktuationen in Ring-Laser Gyroskopen, Max-Planck Institut für Quantenoptik Report No. 54.
Schleich, W., C.-S. Cha, and J. D. Cresser, 1983, Phys. Rev. Lett. A **29**, 230.
Schleich, W., and M. O. Scully, 1984, in *Modern Trends in Atomic and Molecular Physics, Proceedings of Les Houches Summer School, Session XXXVIII,* edited by R. Stora and G. Grynberg (North-Holland, Amsterdam).
Scully, M. O., and W. E. Lamb, Jr., 1967, Phys. Rev. **159**, 208.
Scully, M. O., V. Sanders, and M. Sargent III, 1978, Opt. Lett. **3**, 43.
Scully, M. O., M. S. Zubairy, and K. Just, 1980, Phys. Lett. **77A**, 88.
Scully, M. O., M. S. Zubairy, and M. P. Haugan, 1981, Phys. Rev. A **24**, 2009.
Shapiro, S., 1963, Phys. Rev. Lett. **11**, 80.
Shupe, D. M., 1980, Appl. Opt. **19**, 654.
Shupe, D. M., 1981, Appl. Opt. **20**, 286.
Simpson, J. H., 1980, in *Proc. IEEE, NAECON 1980* (IEEE, New York), p. 80.
Smith, I. W., and T. A. Dorschner, 1980, "Electromagnetic Wave Ring Resonator," U.S. Patent 4,110,045.
Smoot, G. F., M. V. Gorenstein, and R. A. Muller, 1977, Phys. Rev. Lett. **39**, 898.
Smoot, G. F., and P. M. Lubin, 1979, Astrophys. J. **234**, L83.
Stowell, W. K., R. W. McAdory, and R. Ziernicki, 1978, in *Laser Inertial Rotation Sensors,* edited by S. Ezekiel and G. E. Knausenberger (SPIE, Bellingham, Washington), pp. 166—171.
Thomson, K., 1978, in *Laser Inertial Rotation Sensors,* edited by S. Ezekiel and G. E. Knausenberger (SPIE, Bellingham,

Washington), pp. 13—20.
Ulrich, R., and M. Johnson, 1979, Opt. Lett. **4**, 152.
Ulrich, R., and S. C. Rashleigh, 1980, Appl. Opt. **19**, 2453.
Vali, V., and R. W. Shorthill, 1976, Appl. Opt. **15**, 1099.
Wentzel, G., 1949, *Quantum Theory of Fields* (Interscience, New York), p. 47.
Wheeler, J. A., 1983, in *Quantum Optics, Experimental Gravitation and Measurement Theory,* edited by P. Meystre and M. O. Scully (Plenum, London), p. 4.
Will, C. M., 1974, in *Experimental Gravitation,* edited by B. Bertotti (Academic, New York), p. 15.
Will, C. M., and K. Nordtvedt, Jr., 1972a, Astrophysics **177**, 757.
Will, C. M., and K. Nordtvedt, Jr., 1972b, Astrophysics **177**, 775.
Yariv, A., 1967, *Quantum Electronics* (Wiley, New York), p. 412.